ETH
Eidgenössische Technische Hochschule Zürich
Swiss Federal Institute of Technology Zurich

PAUL SCHERRER INSTITUT
PSI

Matched Distributions in Cyclotrons with Higher Order Moments of the Charge Distribution

Master Thesis

in Computational Science and Engineering CSE

Department of Mathematics

ETH Zurich

written by

BSc ETH CSE
Matthias Frey

supervised by

Dr. A. Adelmann

September 28, 2015

Abstract

A general concept of finding stationary distributions with higher order moments is presented. The external magnetic field and defocussing self-field map are obtained up to any order in a very general way using Lie algebra, implemented with "Truncated-Power-Series-Algebra". In order to achieve better estimates during the iterative process, the Newton-Raphson method is applied with Lagrange multipliers to guarantee physical meaningful results.
The stability of the distribution in the PSI Injector 2 and PSI Ring Cyclotron are analyzed using linear theory. Further, a first simulation with a non-linear term in the charge distribution is performed.

Contents

List of Figures

List of Tables

List of Listings

List of Outputs

1 Introduction

1.1 Scope of Work

The goal of this thesis is the development of the theory and its implementation of finding a non-linear mapping $\mathcal{M}$ and σ_k such that

$$\sigma_k(t) = \mathcal{M} \circ \sigma_k(0) \circ \mathcal{M}^{\mathcal{T}} \text{ and} \tag{1.1}$$

$$\sigma_k = \sigma_k(t) \stackrel{!}{=} \sigma_k(0), \tag{1.2}$$

where $\sigma_k(t)$ are the k-th order moments of a distribution in the six-dimensional phase space and $\circ$, $\mathcal{T}$ represent operations on them. Equation (1.1) basically describes the general transport of moments from the initial state to any state in time t. If the condition (1.2) is fulfilled the system is stationary or, respectively, periodic. In particle physics it's mainly known under the name of matching. The matching of the rms envelopes is for example described in [1] with attention on RF linacs. In [2] the equations are considered in case of beams that are prevailed by space charge. Our work is based on [3] that discusses the matching of second order moments in case of linear focussing and defocussing forces with the fact that the eigenvectors of the stationary distribution are identical to those of the linear transfer map. They are computed by applying transformations with real Dirac matrices as explained in [4].
In order to compute higher order space charge maps we approximate the electric field by power series in each direction. Therefore, we use the scalar potential given in [5, 6] to obtain moments including the electric field.
The correctness of our theory is verified by performing measurements using the linear approximation and by comparing them to the results obtained with the implementation of [7].

1.2 Assumptions

Although this thesis only treats space charge effects due to the self-field interaction of the bunch, we shortly discuss some different types of interactions: Coulomb interaction, collisions and interactions with residual gas [8, p. 363 - 364].
In high intensity machines the strongest impact on the bunch has the Coulomb interaction between the particles inside the bunch itself. They repel each other due to equal charge. Therefore, magnets are not only used to guide the beam, they also counteract the divergent effect. These focussing forces are covered with a linear model in this thesis. Additionally, we assume no collisions among particles.

1.3 Coordinate System

A state of a particle is described by the pair $(\vec{q}, \vec{p})$ where $\vec{q} = (x, y, z)$ are the coordinates and $\vec{p} = (p_x, p_y, p_z)$ the momenta. They are usually denoted by horizontal (x, p_x), vertical (y, p_y) and longitudinal (z, p_z) direction (see e.g. [8, ch. 4.1]). The variables depend on the parameter s (path length) rather than on the time t. The transformation $(t \mapsto s)$ is accomplished by [6, eq. 1.2.1]

$$s = s_0 + \beta ct = \beta ct,$$

where s_0 is the path of the reference particle that is set to zero. The velocity is denoted by [8, eq. 1.5]

$$\beta = \frac{v}{c},$$

with speed of light c. The relativistic factor γ relates to β by [8, eq. 1.10]

$$\gamma = \frac{1}{\sqrt{1 - \beta^2}}. \tag{1.3}$$

Sometimes, the momenta are replaced by (x', y', z') where $' = \frac{\mathrm{d}}{\mathrm{d}s}$ [8, ch. 4.1]. These relate by

$$w' = \frac{p_w}{p_0},$$

where $w \in \{x, y, z\}$ and $p_0 = mc\beta\gamma$ [8, p. 18] is the reference momentum. Hence following relation holds:

$$\frac{\mathrm{d}\tilde{p}_w}{\mathrm{d}t} = \beta c \frac{\mathrm{d}p_w}{\mathrm{d}s} = \beta c p_0 \frac{\mathrm{d}w'}{\mathrm{d}s},$$

where $w \in \{x, y, z\}$ again. The longitudinal direction is sometimes given in (l, δ) where $z = l$ and the quantity z' is proportional to δ, i.e. [8, p. 370]

$$z' \propto \frac{1}{\gamma^2}\delta.$$

1.4 Hamiltonian

A dynamical system is described by a Hamiltonian H where — in our case — it consists of a magnetic H_{mag} and space charge H_{sc} part, i.e.

$$H = H_{mag} + H_{sc}. \tag{1.4}$$

Since we focus on the space charge model in Sec. 4 and Sec. 5, we omit this term for a moment. As already mentioned in Sec. 1.2, we use a linear model to describe the magnetic field of cyclotrons. For this purpose we apply [3, eq. 19] including the vertical direction and neglecting space charge, i.e.

$$H_{mag} = \frac{x'^2}{2} + \frac{k_x}{2}x^2 + \frac{y'^2}{2} + \frac{k_y}{2}y^2 + \frac{\delta^2}{2\gamma^2} - hx\delta, \tag{1.5}$$

where (x, x'), (y, y') and (l, δ) are the canonical pairs, k_x and k_y the focussing strengths, h the inverse bending radius and γ the Lorentz factor as defined in (1.3).

1.5 Matched Distribution Algorithm

This section should give a short overview of the algorithm where the main steps are sketched in Fig. 1.1. Since this thesis relies on an existing program [7] that is based on [3, 4] we don't have to start from the beginning. Nevertheless, several modifications have to be done. The model uses for example linear space charge forces and considers only the matching of the second order moments. All parts that basically don't need to be modified have a green background. On the contrary, the blue boxes represent all elements that have to be replaced or updated in order to handle the non-linearity.
The simulation requires a few numerical and physical input parameters. But, the most interesting

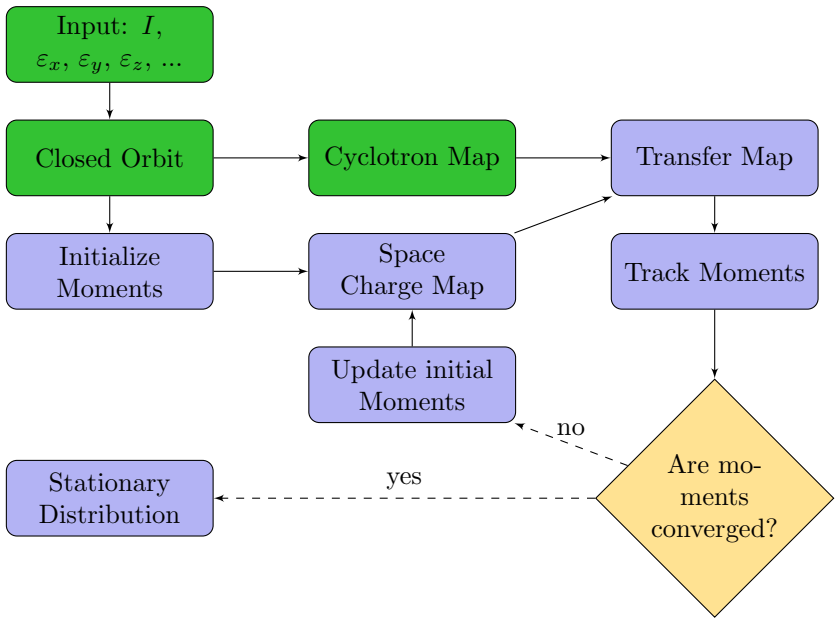

Figure 1.1: Flow chart for finding a matched distribution. All blue parts of the diagram need to be modified whereas the green parts are taken from [7] without change.

parameters for the user are the energy, the intensity and the emittances. It then starts by computing a closed orbit for the given energy. From the equilibrium orbit calculation we get information like tunes, bending radius, etc. that enable the evaluation of the cyclotron maps. Because the magnetic field doesn't depend on the behavior of the bunch, the cyclotron maps have to be computed only once. The equilibrium properties further allow an initial guess of the moments. These are needed to obtain all space charge maps. After the concatenation of the magnetic and space charge maps we track the moments of the initial angle by one turn. In case of stationary moments the simulations stops and prints out the result. Otherwise, we have to get a better estimate of the moments and update all space charge maps.

2 Differential Algebra

The differential algebra (DA) in connection with beam dynamic computations is described by Berz [9] in 1989. It allows a fast and precise differentiation on a computer where it is known as "Truncated-Power-Series-Algebra" (TPSA) (see [10, p. 83 - 85]). The source code for this thesis uses a DA package that was provided by the AMAS group at PSI.
In the following sections we shortly summarize [10, ch. 2.2.1 - 2.2.3] where we use the identical notation in order to make it easier for a more profound reading.

2.1 Univariate Differential Algebra to First Order

When we define a pair of real numbers as (q_0, q_1), the algebra ${}_1D_1$ has subsequent basic operations:

$$\begin{aligned}(q_0, q_1) + (r_0, r_1) &= (q_0 + r_0, q_1 + r_1),\\ t \cdot (q_0, q_1) &= (tq_0, tq_1),\\ (q_0, q_1) \cdot (r_0, r_1) &= (q_0 r_0, q_0 r_1 + q_1 r_0),\end{aligned}$$

where $t \in \mathbb{R}$ and $(r_0, r_1) \in {}_1D_1$. In case of $q_0 \neq 0$ the multiplicative inverse is given by

$$(q_0, q_1)^{-1} = \left(q_0^{-1}, -q_1 q_0^{-2}\right),$$

and for $q_0 > 0$ the root is computed by

$$\sqrt{(q_0, q_1)} = \left(\sqrt{q_0}, \frac{q_1}{2\sqrt{q_0}}\right).$$

Due to the definition of

$$\begin{aligned}&(q_0, q_1) < (r_0, r_1) \text{ if } q_0 < r_0 \text{ or } (q_0 = r_0 \text{ and } q_1 < r_1),\\ &(q_0, q_1) > (r_0, r_1) \text{ if } (r_0, r_1) < (q_0, q_1),\\ &(q_0, q_1) = (r_0, r_1) \text{ if } q_0 = r_0 \text{ and } q_1 = r_1,\end{aligned}$$

the algebra is totally ordered. As a consequence the tuple $d = (0, 1)$ is infinitesimal. Using this property, we're able to make it a DA by introducing the differential operator as

$$\partial(q_0, q_1) = (0, q_1),$$

where q_1 represents the result of the differentiation. That's why it's called the differential part. Through simple algebraic modifications it can be shown that the usual rules of differentiation hold, i.e.

$$\begin{aligned}\partial\{(q_0, q_1) + (r_0, r_1)\} &= \partial(q_0, q_1) + \partial(r_0, r_1),\\ \partial\{(q_0, q_1) \cdot (r_0, r_1)\} &= \{\partial(q_0, q_1)\} \cdot (r_0, r_1) + (q_0, q_1) \cdot \{\partial(r_0, r_1)\}.\end{aligned}$$

For any $x \in \mathbb{R}$ the $[\cdot]$-operator is defined by

$$[x] = (x, 1) = x + d,$$

where d is the infinitesimal element. Consequently,

$$[f(x)] = f([x]) = f(x+d) = (f(x), f'(x)) = f(x) + d \cdot f'(x),$$

for any function $f(x)$ with derivative $f'(x)$. Hence, the DA ${}_1D_1$ of any function represents the linear part of the Taylor series around zero, i.e.

$$[f] = (f(0), f'(0)).$$

2.2 Multivariate Differential Algebra

The DA to order n in ν variables is denoted by ${}_nD_\nu$. All previously defined operations are still valid, i.e.

$$\begin{aligned} [f] + [g] &= [f+g], \\ t \cdot [f] &= [t \cdot f], \\ [f] \cdot [g] &= [f \cdot g], \end{aligned}$$

as well as

$$\begin{aligned} \partial_k([f] + [g]) &= \partial_k[f] + \partial_k[g], \\ \partial_k([f] \cdot [g]) &= [f] \cdot (\partial_k[g]) + (\partial_k[f]) \cdot [g], \end{aligned}$$

where f, g are functions in ${}_nD_\nu$, $t \in \mathbb{R}$ and $k \in [1, \nu]$. Defining $d_k = [x_k]$, the relation to the Taylor series T_f of the function f around zero is now more obvious:

$$\begin{aligned} [f(x_1, \ldots, x_\nu)] = [T_f(x_1, \ldots, x_\nu)] &= \left[\sum_{j_1 + \ldots + j_\nu \le n} c_{j_1, \ldots, j_\nu} \cdot x_1^{j_1} \cdot \ldots \cdot x_\nu^{j_\nu} \right], \\ &= \sum_{j_1 + \ldots + j_\nu \le n} c_{j_1 \ldots, j_\nu} \cdot d_1^{j_1} \cdot \ldots \cdot d_\nu^{j_\nu}, \end{aligned}$$

where the coefficients are given by

$$c_{j_1, \ldots, j_\nu} = \frac{1}{j_1! \cdot \ldots \cdot j_\nu!} \frac{\partial^{j_1 + \ldots + j_\nu}}{\partial x_1^{j_1} \cdot \ldots \cdot \partial x_\nu^{j_\nu}}.$$

Thus, any function that can be expanded as a Taylor series around zero, can be written as a DA vector. Consequently, high order derivatives are obtained fast and accurately.

2.3 Complexity of the Differential Algebra

The number of monomials of ${}_nD_v$ — neglecting the constant — is given in [10, eq. 2.48], i.e.

$$M(n,\nu) = \binom{n+\nu-1}{\nu-1} = \frac{(n+\nu-1)!}{n!\,(\nu-1)!}, \tag{2.1}$$

where $\nu = 6$ in our case. The fast increase of the complexity is illustrated in Fig. 2.1.

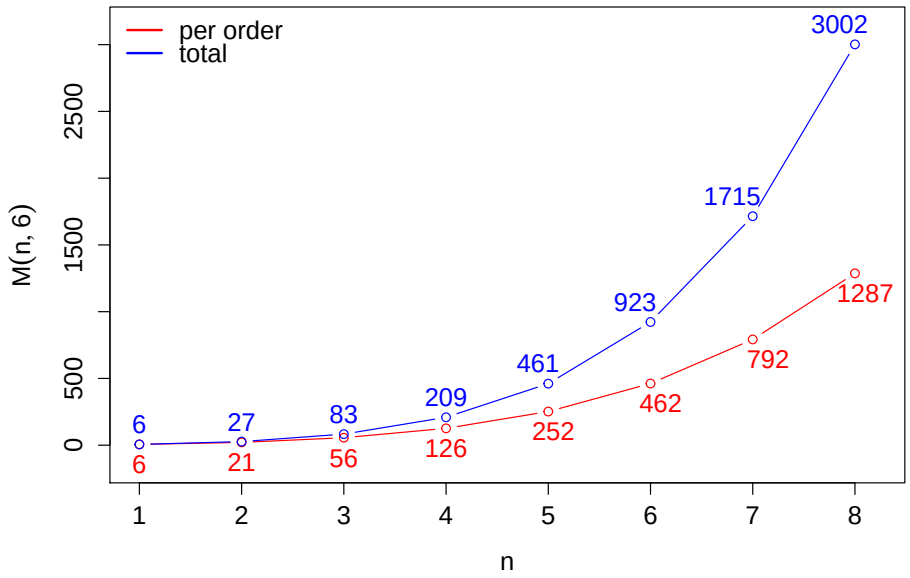

Figure 2.1: The number of monomials up to n-th order in six variables (see Appendix G21).

3 Lie Algebra

3.1 Lie Transformation

This section discusses the Lie transformation which is used to obtain transfer maps. It relies on [11, ch. 5.3 - 5.4] — except to (3.1) — where everything is explained in detail.
Let H be any Hamiltonian in the dynamical variables (x, p_x), (y, p_y) and (z, p_z) that depend without loss of generality on the position s rather than time t. Then the Lie transformation defines the map [11, eq. 29.4.1]

$$\mathcal{M} = \exp\left(-s :H:\right), \tag{3.1}$$

with Lie operator $:H:$ that for a dynamical pair $(\vec{q}, \vec{p})$ is given by

$$:H: = \frac{\partial H}{\partial \vec{q}}\frac{\partial}{\partial \vec{p}} - \frac{\partial H}{\partial \vec{p}}\frac{\partial}{\partial \vec{q}}. \tag{3.2}$$

By truncating the Taylor series expansion of (3.1) at n-th order, i.e.

$$\mathcal{M} = \sum_{j=0}^{\infty} \frac{(-s :H:)^j}{j!} \approx \sum_{j=0}^{n} \frac{(-s :H:)^j}{j!}, \tag{3.3}$$

the Lie operator gets applied n times. Therefore, a n-th order map incorporates the n-th derivative of the Hamiltonian H. In the linear approximation, i.e. $n = 1$, equation (3.3) leads to the well-known 6×6 representation of transfer maps in case of the six-dimensional phase space. In the next section we give a short example using a four-dimensional phase space.

3.1.1 Example: Linear Map

As previously mentioned, a linear map is obtained when truncating the Taylor series expansion of (3.1) at first order, i.e. $n = 1$. We show this with the help of the Hamiltonian

$$H = \frac{x'^2}{2} + \frac{\delta^2}{2\gamma^2} + \frac{k_x - K_x}{2}x^2 - \frac{\gamma^2 K_z}{2}l^2 - hx\delta,$$

stated in [3, eq. 19] with canonical pairs (x, x') and (l, δ), inverse bending radius h, focussing strength k_x, defocussing forces K_x, K_z and relativistic factor γ.
In a first step we apply the Lie operator (3.2) to all variables of the system in order to get the transport equations:

$$\begin{aligned}
:H: x &= \frac{\partial H}{\partial x}\frac{\partial x}{\partial x'} + \frac{\partial H}{\partial l}\frac{\partial x}{\partial \delta} - \frac{\partial H}{\partial x'}\frac{\partial x}{\partial x} - \frac{\partial H}{\partial \delta}\frac{\partial x}{\partial l} = -\frac{\partial H}{\partial x'} = -x', \\
:H: x' &= \frac{\partial H}{\partial x}\frac{\partial x'}{\partial x'} + \frac{\partial H}{\partial l}\frac{\partial x'}{\partial \delta} - \frac{\partial H}{\partial x'}\frac{\partial x'}{\partial x} - \frac{\partial H}{\partial \delta}\frac{\partial x'}{\partial l} = \frac{\partial H}{\partial x} = (k_x - K_x)\, x - h\delta, \\
:H: l &= \frac{\partial H}{\partial x}\frac{\partial l}{\partial x'} + \frac{\partial H}{\partial l}\frac{\partial l}{\partial \delta} - \frac{\partial H}{\partial x'}\frac{\partial l}{\partial x} - \frac{\partial H}{\partial \delta}\frac{\partial l}{\partial l} = -\frac{\partial H}{\partial \delta} = -\frac{1}{\gamma^2}\delta + hx, \\
:H: \delta &= \frac{\partial H}{\partial x}\frac{\partial \delta}{\partial x'} + \frac{\partial H}{\partial l}\frac{\partial \delta}{\partial \delta} - \frac{\partial H}{\partial x'}\frac{\partial \delta}{\partial x} - \frac{\partial H}{\partial \delta}\frac{\partial \delta}{\partial l} = \frac{\partial H}{\partial l} = -\gamma^2 K_z l.
\end{aligned}$$

Therefore, we obtain from (3.3) with the order (x, x', l, δ) and $n = 1$, i.e. $M = I_{4\times4} - :H: s$, the 4×4 transfer matrix:

$$M = I_{4\times4} - \begin{pmatrix} 0 & -1 & 0 & 0 \\ k_x - K_x & 0 & 0 & -h \\ h & 0 & 0 & -\gamma^{-2} \\ 0 & 0 & -\gamma^2 K_z & 0 \end{pmatrix} \cdot s = \begin{pmatrix} 1 & s & 0 & 0 \\ (K_x - k_x)\, s & 1 & 0 & hs \\ -hs & 0 & 1 & \gamma^{-2} s \\ 0 & 0 & \gamma^2 K_z s & 1 \end{pmatrix}.$$

We get exactly the same result when inserting the matrix F of [3, eq. 20]

$$\frac{\mathrm{d}}{\mathrm{d}s} \begin{pmatrix} x \\ x' \\ l \\ \delta \end{pmatrix} = \underbrace{\begin{pmatrix} 0 & 1 & 0 & 0 \\ K_x - k_x & 0 & 0 & h \\ -h & 0 & 0 & \gamma^{-2} \\ 0 & 0 & \gamma^2 K_z & 0 \end{pmatrix}}_{F} \begin{pmatrix} x \\ x' \\ l \\ \delta \end{pmatrix},$$

into [3, eq. 12]

$$M(s) = \exp(Fs) = I_{4\times4} + Fs + \frac{(Fs)^2}{2!} + \frac{(Fs)^3}{3!} + \ldots,$$

and truncating at first order:

$$M(s) = \exp(Fs) \approx I_{4\times4} + Fs = \begin{pmatrix} 1 & s & 0 & 0 \\ (K_x - k_x)\, s & 1 & 0 & hs \\ -hs & 0 & 1 & \gamma^{-2} s \\ 0 & 0 & \gamma^2 K_z s & 1 \end{pmatrix}.$$

Hence, the Lie transformation is a general tool to obtain transfer maps to basically arbitrary order. In combination with the DA of Sec. 2 we also have a numerical tool to obtain maps to any order. The provided DA library already implements this kind of operation.

3.2 Map Factorization

Since our closed orbit of length L is discretized into $N \gg 1$ steps, we have N magnetic maps $\mathcal{M}_{mag}$ as well as N space charge maps $\mathcal{M}_{sc}$. We combine them to the one turn map $\mathcal{M}$ by

$$\mathcal{M} = \mathcal{M}_{sc}(s + (N-1)\Delta s) \circ \cdots \circ \mathcal{M}_{mag}(s + \Delta s) \circ \mathcal{M}_{sc}(s) \circ \mathcal{M}_{mag}(s), \tag{3.4}$$

where $\circ$ defines a concatenation operator and $\Delta s = \frac{L}{N}$ is the trajectory step. During this operation, however, we perform a systematic error due to the "Baker-Campbell-Hausdorff" relation [12, eq. 20 or eq. (21a, 21b)], i.e.

$$\exp(:H_{sc}:)\exp(:H_{cyc}:) = \exp\Big(:H_{sc}: + :H_{cyc}: + \frac{1}{2}:[H_{sc}, H_{cyc}]: + \frac{1}{12}:[H_{sc},[H_{sc}, H_{cyc}]]: + \frac{1}{12}:[H_{cyc},[H_{cyc}, H_{sc}]]: + \ldots\Big),$$

where $[\cdot,\cdot]$ denotes the Poisson bracket that relates to the Lie operator (3.2) by [12, eq. 12]

$$[H_{sc}, H_{cyc}] = :H_{sc}: H_{cyc}.$$

Therefore,

$$\exp(:H_{sc}:)\exp(:H_{cyc}:) \approx \exp(:H_{sc}: + :H_{cyc}:) = \exp(:H_{sc} + H_{cyc}:) \overset{(1.4)}{=} \exp(:H:).$$

3.2.1 Example: Construction of a Transfer Map

On a computer a transfer map $\mathcal{M}$ is stored as a vector of TPSA objects. In the linear case this map is basically a matrix. Thus, the concatenation (3.4) is simply obtained through matrix-matrix multiplications. In order to generalize this operation to arbitrary orders, we need to understand the linear theory first. The principle behind the multiplication is shown with the help of a one-dimensional example. For this purpose suppose a dynamical pair (q, p) where q is the coordinate and p the momentum. Further, assume the mapping

$$M_{cyc}: \quad \begin{array}{l} q \mapsto q - p, \\ p \mapsto q + 3p, \end{array} \tag{3.5}$$

for the focussing part and

$$M_{sc}: \quad \begin{array}{l} q \mapsto q + p, \\ p \mapsto -\frac{1}{2}q + p, \end{array} \tag{3.6}$$

for the defocussing part. The multiplication of the space charge matrix from the left results in

$$M_{sc} \cdot M_{cyc} = \begin{pmatrix} 1 & 1 \\ -\frac{1}{2} & 1 \end{pmatrix} \cdot \begin{pmatrix} 1 & -1 \\ 1 & 3 \end{pmatrix} = \begin{pmatrix} 2 & 2 \\ \frac{1}{2} & \frac{7}{2} \end{pmatrix},$$

which is in polynomial form written as

$$M: \quad \begin{array}{l} q \mapsto 2q + 2p, \\ p \mapsto \frac{1}{2}q + \frac{7}{2}p. \end{array}$$

The same outcome is obtained when inserting the appropriate polynomial of each variable of (3.5) into (3.6):

$$M: \quad \begin{array}{l} q \mapsto q - p + q + 3p = 2q + 2q, \\ p \mapsto -\frac{1}{2}(q - p) + q + 3p = \frac{1}{2}q + \frac{7}{2}p. \end{array}$$

In case of non-linear polynomials, i.e. degree > 1, the procedure is identical. Although the composition might lead to monomials that exceed the global truncation order, it doesn't pose a problem since we implemented the concatenation operation with functions of the DA library that truncate a TPSA object automatically. In the following we demonstrate this behavior with a small numerical example (see Lst. 3.1) where the mappings are given by

$$\mathcal{M}_1: \quad \begin{array}{l} q \mapsto q^3 + p^2, \\ p \mapsto p^2 - \frac{1}{2}q, \end{array} \quad \text{and} \quad \mathcal{M}_2: \quad \begin{array}{l} q \mapsto q - p^3, \\ p \mapsto q + 3p^2. \end{array}$$

The exact solution is

$$\mathcal{M}_1 \circ \mathcal{M}_2 = \begin{pmatrix} q^2 + q^3 + 6qp^2 + 9p^4 - 3q^2p^3 + 3qp^6 - p^9 \\ -0.5q + q^2 + 6qp^2 + 0.5p^3 + 9p^4 \end{pmatrix}.$$

The numerical solution, however, depends on the truncation order as previously mentioned. In Tab. 3.1 all results up to truncation order 9 are shown. The minimal truncation order of this example is 3 due to the initial polynomials. Comparing those outcomes we recognize that the right solution is only obtained if the global truncation order is greater than 9. But, the variable p is already transported correctly at a truncation order of 4.

order	mapping of q	mapping of p
3	$q^2 + q^3 + 6qp^2$	$-0.5q + q^2 + 6qp^2 + 0.5p^3$
4	$q^2 + q^3 + 6qp^2 + 9p^4$	$-0.5q + q^2 + 6qp^2 + 0.5p^3 + 9p^4$
5	$q^2 + q^3 + 6qp^2 + 9p^4 - 3q^2p^3$	$-0.5q + q^2 + 6qp^2 + 0.5p^3 + 9p^4$
6	$q^2 + q^3 + 6qp^2 + 9p^4 - 3q^2p^3$	$-0.5q + q^2 + 6qp^2 + 0.5p^3 + 9p^4$
7	$q^2 + q^3 + 6qp^2 + 9p^4 - 3q^2p^3 + 3qp^6$	$-0.5q + q^2 + 6qp^2 + 0.5p^3 + 9p^4$
8	$q^2 + q^3 + 6qp^2 + 9p^4 - 3q^2p^3 + 3qp^6$	$-0.5q + q^2 + 6qp^2 + 0.5p^3 + 9p^4$
9	$q^2 + q^3 + 6qp^2 + 9p^4 - 3q^2p^3 + 3qp^6 - p^9$	$-0.5q + q^2 + 6qp^2 + 0.5p^3 + 9p^4$

Table 3.1: Results of Lst. 3.1 using different global truncation orders (line 15). Due to third order polynomials the truncation order has to start at three.

```
1  #include <iostream>
2  #include "Utilities/ClassicException.h"
3  #include "FixedAlgebra/FTps.h"
4
5  /// Dimensionality of problem
6  #define DIM 1
7  /// Type of a truncated power series
8  typedef FTps<double,2*DIM> Series;
9  /// Type of a vector of truncated power series
10 typedef FVps<double,2*DIM> Map;
11
12 /// Main function
13 int main(int argc, char** argv) {
14     try {
15         Series::setGlobalTruncOrder(3);
16
17         // define dynamical variables (q,p)
18         Series q = Series::makeVariable(0);
19         Series p = Series::makeVariable(1);
20
21         Map m1;
22         m1.setComponent(0, q * q * q + p * p);
23         m1.setComponent(1, p * p - 0.5 * q);
24
25         Map m2;
26         m2.setComponent(0, q - p * p * p);
27         m2.setComponent(1, q + 3.0 * p * p);
28
29         // combine maps
30         std::cout << m1 * m2 << std::endl;
31
32     } catch(const ClassicException& e) {
33         std::cout << "Function: " << e.where() << std::endl;
34         std::cout << "Problem: " << e.what() << std::endl;
35     }
36     return 0;
37 }
```

Listing 3.1: Example of a map construction. The map is truncated at third order (line 15). The map would be exact when truncating at 9th order. The whole source code is given in Appendix G10.

4 Computation of the Potential

A transfer map $\mathcal{M}$ in particle accelerator simulations consists of focussing and defocussing elements. This chapter focuses on the latter where its Hamiltonian H_{sc} is described through the scalar potential ϕ by

$$H_{sc} = q\phi. \tag{4.1}$$

In the computation of the potential we distinguish in this thesis between *distribution-based* and *particle-based* methods. Depending on the technique we take different assumptions on the behavior of the bunch. This decision is fundamental since both strategies have their limitations and, thus, consequences for the proceeding computations.

4.1 Particle-based Method

The electrostatic potential at $\vec{r}_i$ inside a bunch of particles is essentially given by Coulomb, i.e. [13, eq. 1.48]

$$\phi(\vec{r}_i) = \frac{1}{4\pi\varepsilon_0} \sum_{\substack{j=0 \\ i\neq j}}^{N-1} \frac{q_j}{||\vec{r}_i - \vec{r}_j||_2},$$

where in our case $q_j = q \ \forall j$ and $\vec{r}_i$, $\vec{r}_j$ denote the locations of the particles in Cartesian coordinates. The overall potential energy is consequently [13, eq. 1.50]

$$W = \frac{q^2}{4\pi\varepsilon_0} \sum_{\substack{i,j=0 \\ i\neq j}}^{N-1} \frac{1}{||\vec{r}_i - \vec{r}_j||_2}.$$

Hence, the brute-force evaluation of the potential for every particle takes $O(N^2)$. In 1987, Greengard and Rokhlin [14] introduced a new method called *Fast Multipole Method* (FMM). It allows the computation of a potential at specific locations based on the interactions in a N-body problem in $O(N)$. As explained for example in [15], this method was later enhanced to three dimensions using spherical harmonics to perform the multipole expansions.
In 2011, Zhang and Berz [16] published an article where they describe the computation of the potential with FMM on the basis of the differential algebra (DA). There, they expand the potential basically in terms of

$$d_1 = \frac{1}{r}, \qquad d_2 = \frac{x}{r^2}, \qquad d_3 = \frac{y}{r^2}, \qquad d_4 = \frac{z}{r^2},$$

with $r = \sqrt{x^2 + y^2 + z^2}$. Since our goal is an evaluation of the space charge map up to n-th order on the basis of the dynamical variables, these variables aren't suitable for our purpose. A possible solution could be the expansion in spherical harmonics as previously mentioned. In order to obtain the potential in the canonical variables we would only need to transform back to Cartesian coordinates.

4.2 Distribution-based Method

In contrast to the previously discussed particle-based method the approaches outlined in Sec. 4.2.2 and Sec. 4.2.3 assume a continuous description of the potential which is stated in the following section.

4.2.1 Potential inside an Ellipsoid

The scalar potential ϕ for a charge density $\rho(x, y, z)$ is given by [13, eq. 1.17]

$$\phi(\vec{r}) = \frac{1}{4\pi\varepsilon_0} \int_{\mathbb{R}^3} \frac{\rho(\vec{r}\,')}{||\vec{r} - \vec{r}\,'||_2} \, \mathrm{d}^3\vec{r}\,',$$

with vacuum permittivity ε_0 and positions $\vec{r} = (x, y, z)$, respectively, $\vec{r}\,' = (x', y', z')$. In case of a closed shape with volume V the expression of the potential at an interior point $\vec{r}$ is obtained by [13, eq. 1.23]

$$\phi(\vec{r}) = \frac{1}{4\pi\varepsilon_0} \int_V \frac{\rho(\vec{r}\,')}{||\vec{r} - \vec{r}\,'||_2} \, \mathrm{d}V. \tag{4.2}$$

In [17, ch. 7] Kellogg derived a formula of the potential (4.2) on the assumption of an ellipsoid (see Fig. 4.1) with N homogeneously distributed particles. In 1986, Gluckstern [5] stated a more general expression of the scalar potential where the charge density function $\rho(\omega)$ is assumed to be ellipsoidally symmetric, i.e. [5, eq. 2.1]

$$\omega = \frac{x^2}{a_x^2} + \frac{y^2}{a_y^2} + \frac{z^2}{a_z^2}, \tag{4.3}$$

with semi-principal axes (a_x, a_y, a_z).

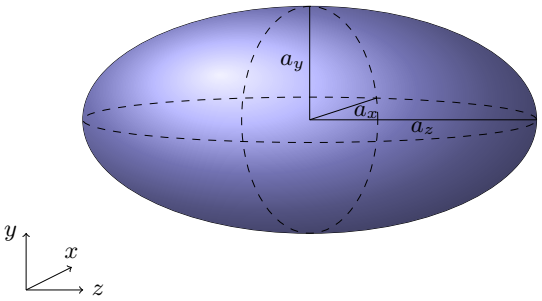

Figure 4.1: Bunch with semi-principal axes a_x, a_y and a_z.

In contrast to Gluckstern's notation, where the charge $Q = qN$ is part of the probability density function f, we write

$$\rho(\omega) = Qf(\omega).$$

Thus, the potential is given by [5, eq. 4.5, 4.19]

$$\phi(x, y, z) = \frac{Qa_x a_y a_z}{4\varepsilon_0} \int_0^\infty \frac{1}{\sqrt{\left(a_x^2 + u\right)\left(a_y^2 + u\right)\left(a_z^2 + u\right)}} \int_{\Omega(u)}^\infty f(\omega) \, \mathrm{d}\omega \, \mathrm{d}u, \tag{4.4}$$

where

$$\Omega(u) = \frac{x^2}{a_x^2 + u} + \frac{y^2}{a_y^2 + u} + \frac{z^2}{a_z^2 + u}. \tag{4.5}$$

4.2.2 Expansion of the Potential

The analytic expression (4.4) could already be taken and expanded in terms of Lie algebra to accomplish a space charge transfer map to arbitrary order. Nevertheless, we have to make an assumption on the distribution, thus, limiting the shape of the bunch.
By the assumption of a Gaussian-shaped bunch we choose the three-dimensional normal distribution where our definition is similar to [5, eq. 5.1]

$$f(\omega) = \frac{1}{(2\pi)^{3/2} a_x a_y a_z} \exp\left(-\frac{\omega}{2}\right), \tag{4.6}$$

which leads to

$$\phi(x,y,z) = \frac{Q}{2^{7/2}\pi^{3/2}\varepsilon_0} \int_0^\infty \frac{1}{\sqrt{\left(a_x^2+u\right)\left(a_y^2+u\right)\left(a_z^2+u\right)}} \int_{\Omega(u)}^\infty \exp\left(-\frac{\omega}{2}\right) \mathrm{d}\omega \, \mathrm{d}u,$$

when inserting into (4.4). The analytical solution of the integral over ω is

$$\int_{\Omega(u)}^\infty \exp\left(-\frac{\omega}{2}\right) \mathrm{d}\omega = -2\exp\left(-\frac{\omega}{2}\right)\Big|_{\omega=\Omega(u)}^{\omega=\infty} = 2\exp\left(-\frac{1}{2}\Omega(u)\right),$$

therefore the potential has following form:

$$\phi(x,y,z) = \frac{Q}{2^{5/2}\pi^{3/2}\varepsilon_0} \int_0^\infty \frac{\exp\left(-\frac{1}{2}\Omega(u)\right)}{\sqrt{\left(a_x^2+u\right)\left(a_y^2+u\right)\left(a_z^2+u\right)}} \mathrm{d}u.$$

Instead of evaluating the potential directly, we make use of the Taylor series expansion of the exponential function [18, eq. 4.2.1], i.e.

$$\exp(w) = \sum_{j=0}^\infty \frac{w^j}{j!}.$$

Though, the potential consists of a sum of integrals:

$$\phi(x,y,z) = \frac{Q}{2^{5/2}\pi^{3/2}\varepsilon_0} \sum_{j=0}^\infty \left[\frac{(-1)^j}{2^j j!} \int_0^\infty \frac{\Omega^j(u)}{\sqrt{\left(a_x^2+u\right)\left(a_y^2+u\right)\left(a_z^2+u\right)}} \mathrm{d}u \right].$$

By considering each integral individually, i.e.

$$\begin{aligned}\phi(x,y,z) = C\int_0^\infty g(u)\,\mathrm{d}u - \frac{C}{2}\int_0^\infty \Omega(u)g(u)\,\mathrm{d}u + \frac{C}{8}\int_0^\infty \Omega^2(u)g(u)\,\mathrm{d}u \\ - \frac{C}{48}\int_0^\infty \Omega^3(u)g(u)\,\mathrm{d}u + \mathcal{O}\left(\Omega^4(u)\right),\end{aligned}$$

where we defined

$$\begin{aligned} g(u) &:= \frac{1}{\sqrt{\left(a_x^2+u\right)\left(a_y^2+u\right)\left(a_z^2+u\right)}}, \\ C &:= \frac{Q}{2^{5/2}\pi^{3/2}\varepsilon_0}, \end{aligned} \tag{4.7}$$

one recognizes that some of them can be rewritten using Carlson's notation of elliptic integrals [19]. Therefore,

$$
\begin{aligned}
\phi(x,y,z) &= 2CR_F(a_x^2,a_y^2,a_z^2) \\
&\quad - \frac{C}{3}\left[x^2R_D(a_y^2,a_z^2,a_x^2) + y^2R_D(a_x^2,a_z^2,a_y^2) + z^2R_D(a_x^2,a_y^2,a_z^2)\right] \\
&\quad + \frac{C}{8}\int_0^\infty \frac{x^4\,\mathrm{d}u}{(a_x^2+u)^{5/2}\left(a_y^2+u\right)^{1/2}(a_z^2+u)^{1/2}} + \frac{C}{4}\int_0^\infty \frac{x^2y^2\,\mathrm{d}u}{(a^2+u)^{3/2}\left(a_y^2+u\right)^{3/2}(a_z^2+u)^{1/2}} \\
&\quad + \frac{C}{8}\int_0^\infty \frac{y^4\,\mathrm{d}u}{(a_x^2+u)^{1/2}\left(a_y^2+u\right)^{5/2}(a_z^2+u)^{1/2}} + \frac{C}{4}\int_0^\infty \frac{x^2z^2\,\mathrm{d}u}{(a_x^2+u)^{3/2}\left(a_y^2+u\right)^{1/2}(a_z^2+u)^{3/2}} \\
&\quad + \frac{C}{4}\int_0^\infty \frac{y^2z^2\,\mathrm{d}u}{(a_x^2+u)^{1/2}\left(a_y^2+u\right)^{3/2}(a_z^2+u)^{3/2}} + \frac{C}{8}\int_0^\infty \frac{z^4\,\mathrm{d}u}{(a_x^2+u)^{1/2}\left(a_y^2+u\right)^{1/2}(a_z^2+u)^{5/2}} \\
&\quad + \mathcal{O}\left(\Omega^3(u)\right).
\end{aligned}
$$

In Appendix B we show all terms up to fifth order. An implementation of Carlson's elliptic integrals can either be found in the Boost C++ Libraries [20] or the GNU Scientific Library (GSL) [21]. In Lst. 4.1 we give a short example of the different function calls. The corresponding numerical results of a varying a_x and fixed a_y, a_z are shown in Fig. 4.2.
All other integrals that can't be expressed in terms of R_F or R_D can be evaluated by a quadrature rule of GSL.
Thanks to the expansion, the potential can be simply stored as a TPSA object where the evaluated integrals represent the coefficients.

```
1 // compute R_{F} and R_{D} using The BOOST C++ Libraries
2 double boost_rf = boost::math::ellint_rf(ax * ax, ay * ay, az * az);
3 double boost_rd = boost::math::ellint_rd(ax * ax, ay * ay, az * az);
4
5 // compute R_{F} and R_{D} using GNU Scientific Library (GSL)
6 double gsl_rf = gsl_sf_ellint_RF(ax * ax, ay * ay, az * az, 1.0e-8);
7 double gsl_rd = gsl_sf_ellint_RD(ax * ax, ay * ay, az * az, 1.0e-8);
```

Listing 4.1: Function calls of Carlson's elliptic integrals using either Boost or GSL.

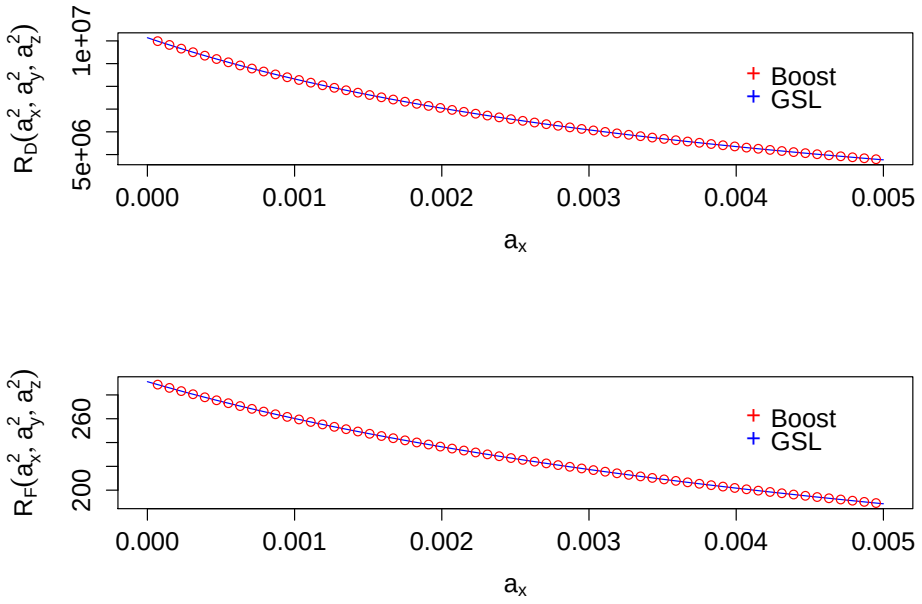

Figure 4.2: Results of evaluating Carlson's elliptic integrals $R_D(a_x^2, a_y^2, a_z^2)$ and $R_F(a_x^2, a_y^2, a_z^2)$ using C++ Boost and GSL, where $a_y = 0.004$ m, $a_z = 0.007$ m and $a_x \in [0, 0.005]$ m. The full source code is given in Appendix G11.

4.2.3 Expansion of the Electric Field

Instead of expanding the scalar potential, we could approximate the electric field generated by the bunch. The electric field $\vec{E} = (E_x, E_y, E_z)$ and the potential $\phi(x, y, z)$ are related by [13, eq. 1.16]

$$\vec{E} = -\nabla\phi. \tag{4.8}$$

Inserting (4.4) into above equation yields subsequent results:

$$\begin{aligned}
E_x &= \frac{Qa_xa_ya_z}{2\varepsilon_0}\int_0^\infty \frac{x}{(a_x^2+u)^{3/2}\sqrt{(a_y^2+u)(a_z^2+u)}} f\left(\frac{x^2}{a_x^2+u}+\frac{y^2}{a_y^2+u}+\frac{z^2}{a_z^2+u}\right)\mathrm{d}u,\\
E_y &= \frac{Qa_xa_ya_z}{2\varepsilon_0}\int_0^\infty \frac{y}{(a_y^2+u)^{3/2}\sqrt{(a_x^2+u)(a_z^2+u)}} f\left(\frac{x^2}{a_x^2+u}+\frac{y^2}{a_y^2+u}+\frac{z^2}{a_z^2+u}\right)\mathrm{d}u,\\
E_z &= \frac{Qa_xa_ya_z}{2\varepsilon_0}\int_0^\infty \frac{z}{(a_z^2+u)^{3/2}\sqrt{(a_x^2+u)(a_y^2+u)}} f\left(\frac{x^2}{a_x^2+u}+\frac{y^2}{a_y^2+u}+\frac{z^2}{a_z^2+u}\right)\mathrm{d}u.
\end{aligned} \tag{4.9}$$

The full derivation is given in Appendix C. In a next step we assume that each component of the field is given by a power series of the form [22, p. 28 - 30]:

$$E_w(w) \approx \sum_{i=0}^{n} c_{i,w} w^i,$$

with coefficients $c_{i,w} \in \mathbb{R}$, truncation order $n \in \mathbb{N}$ and $w \in \{x, y, z\}$. By using the moment definition of Allen [6, eq. 1.2.9], however, without the normalization through the number of particles N, i.e.

$$\langle g \rangle := \int_{\mathbb{R}^6} g f(x, p_x, y, p_y, z, p_z) \, \mathrm{d}x \, \mathrm{d}p_x \, \mathrm{d}y \, \mathrm{d}p_y \, \mathrm{d}z \, \mathrm{d}p_z, \tag{4.10}$$

where g is any function in the dynamical variables, and applying the method of least squares on $\left\langle \left|\left| E_w - \sum_{i=0}^{n} c_{i,w} w^i \right|\right|_2^2 \right\rangle$, we get

$$\begin{aligned}
\frac{\partial}{\partial c_{j,w}} \left[\int_{\mathbb{R}^6} \left(E_w - \sum_{i=0}^{n} c_{i,w} w^i \right)^2 f(\xi) \, \mathrm{d}^6\xi \right] &\overset{!}{=} 0 \quad \forall j \in [0, n], \\
\int_{\mathbb{R}^6} \frac{\partial}{\partial c_{j,w}} \left(E_w - \sum_{i=0}^{n} c_{i,w} w^i \right)^2 f(\xi) \, \mathrm{d}^6\xi &\overset{!}{=} 0 \quad \forall j \in [0, n], \\
-2 \int_{\mathbb{R}^6} \left(E_w - \sum_{i=0}^{n} c_{i,w} w^i \right) w^j f(\xi) \, \mathrm{d}^6\xi &\overset{!}{=} 0 \quad \forall j \in [0, n], \\
\int_{\mathbb{R}^6} E_w w^j f(\xi) \, \mathrm{d}^6\xi - \sum_{i=0}^{n} c_{i,w} \int_{\mathbb{R}^6} w^i w^j f(\xi) \, \mathrm{d}^6\xi &\overset{!}{=} 0 \quad \forall j \in [0, n], \\
\sum_{i=0}^{n} c_{i,w} \left\langle w^i w^j \right\rangle &\overset{!}{=} \left\langle E_w w^j \right\rangle \quad \forall j \in [0, n],
\end{aligned}$$

where we simplified our notation by using ξ to represent the canonical variables (x, p_x, y, p_y, z, p_z). Thus, we end up with a linear system of equations of the form:

$$\begin{pmatrix}
\langle 1 \rangle & \langle w \rangle & \langle w^2 \rangle & \cdots & \langle w^n \rangle \\
\langle w \rangle & \langle w^2 \rangle & \langle w^3 \rangle & \cdots & \langle w^{n+1} \rangle \\
\langle w^2 \rangle & \langle w^3 \rangle & \ddots & & \vdots \\
\vdots & \vdots & & \langle w^{2n-2} \rangle & \langle w^{2n-1} \rangle \\
\langle w^n \rangle & \langle w^{n+1} \rangle & \cdots & \langle w^{2n-1} \rangle & \langle w^{2n} \rangle
\end{pmatrix} \cdot \begin{pmatrix} c_{0,w} \\ c_{1,w} \\ \vdots \\ c_{n-1,w} \\ c_{n,w} \end{pmatrix} = \begin{pmatrix} \langle E_w \rangle \\ \langle E_w w \rangle \\ \vdots \\ \langle E_w w^{n-1} \rangle \\ \langle E_w w^n \rangle \end{pmatrix}. \tag{4.11}$$

After solving equation (4.11) we obtain coefficients that are given by moments of the electric field. Although we expand each direction on its own, the dimensions are coupled through those coefficients due to the moment-based approach.
We omitted the normalization by N in the definition of the moment since we assume normalized distribution functions. Hence, the integral [6, eq. 1.2.8]

$$N = \int_{-\infty}^{\infty} \int_{-\infty}^{\infty} \int_{-\infty}^{\infty} f \left(\frac{x^2}{a_x^2} + \frac{y^2}{a_y^2} + \frac{z^2}{a_z^2} \right) \mathrm{d}x \, \mathrm{d}y \, \mathrm{d}z,$$

is always equal to one.
Since the moments in (4.11) are independent of the momentum space, we perform the computation of (4.10) over the coordinate space only. Therefore, the general expressions are given by

$$
\begin{aligned}
\langle x^n E_x \rangle &= \frac{Q a_x a_y a_z}{2\varepsilon_0} \int_{\mathbb{R}^3} \int_0^\infty \frac{x^{n+1}}{(a_x^2+u)^{3/2}\sqrt{(a_y^2+u)(a_z^2+u)}} f\left(\frac{x^2}{a_x^2+u}+\frac{y^2}{a_y^2+u}+\frac{z^2}{a_z^2+u}\right) \\
&\quad f\left(\frac{x^2}{a_x^2}+\frac{y^2}{a_y^2}+\frac{z^2}{a_z^2}\right) \mathrm{d}u\,\mathrm{d}x\,\mathrm{d}y\,\mathrm{d}z, \\
\langle y^n E_y \rangle &= \frac{Q a_x a_y a_z}{2\varepsilon_0} \int_{\mathbb{R}^3} \int_0^\infty \frac{y^{n+1}}{(a_y^2+u)^{3/2}\sqrt{(a_x^2+u)(a_z^2+u)}} f\left(\frac{x^2}{a_x^2+u}+\frac{y^2}{a_y^2+u}+\frac{z^2}{a_z^2+u}\right) \\
&\quad f\left(\frac{x^2}{a_x^2}+\frac{y^2}{a_y^2}+\frac{z^2}{a_z^2}\right) \mathrm{d}u\,\mathrm{d}x\,\mathrm{d}y\,\mathrm{d}z, \\
\langle z^n E_z \rangle &= \frac{Q a_x a_y a_z}{2\varepsilon_0} \int_{\mathbb{R}^3} \int_0^\infty \frac{z^{n+1}}{(a_z^2+u)^{3/2}\sqrt{(a_x^2+u)(a_y^2+u)}} f\left(\frac{x^2}{a_x^2+u}+\frac{y^2}{a_y^2+u}+\frac{z^2}{a_z^2+u}\right) \\
&\quad f\left(\frac{x^2}{a_x^2}+\frac{y^2}{a_y^2}+\frac{z^2}{a_z^2}\right) \mathrm{d}u\,\mathrm{d}x\,\mathrm{d}y\,\mathrm{d}z.
\end{aligned} \tag{4.12}
$$

The derivation of an explicit form of $\langle x E_x \rangle$, i.e. $n = 1$, for a continuous beam is given in [23] and later recapitulated in [6]. Thanks to this general method, we're basically able to describe the space charge map for any distribution. In case of a Gaussian probability density function f and the transformation in Appendix D, above formulas look like

$$
\begin{aligned}
\langle x^n E_x \rangle &= K \int_{-6a_z}^{6a_z} \int_{-6a_y}^{6a_y} \int_{-6a_x}^{6a_x} \int_0^1 \frac{x^{n+1}}{(a_x^2+\frac{\mu}{1-\mu})^{3/2}\sqrt{(a_y^2+\frac{\mu}{1-\mu})(a_z^2+\frac{\mu}{1-\mu})}} \\
&\quad \exp\left[-\frac{1}{2}\left(\frac{x^2}{\left(a_x^2+\frac{\mu}{1-\mu}\right)}+\frac{y^2}{\left(a_y^2+\frac{\mu}{1-\mu}\right)}+\frac{z}{\left(a_z^2+\frac{\mu}{1-\mu}\right)}\right)\right] \exp\left[-\frac{1}{2}\left(\frac{x^2}{a_x^2}+\frac{y^2}{a_y^2}+\frac{z^2}{a_z^2}\right)\right] \\
&\quad \frac{1}{(1-\mu)^2}\,\mathrm{d}\mu\,\mathrm{d}x\,\mathrm{d}y\,\mathrm{d}z, \\
\langle y^n E_y \rangle &= K \int_{-6a_z}^{6a_z} \int_{-6a_y}^{6a_y} \int_{-6a_x}^{6a_x} \int_0^1 \frac{y^{n+1}}{(a_y^2+\frac{\mu}{1-\mu})^{3/2}\sqrt{(a_x^2+\frac{\mu}{1-\mu})(a_z^2+\frac{\mu}{1-\mu})}} \\
&\quad \exp\left[-\frac{1}{2}\left(\frac{x^2}{\left(a_x^2+\frac{\mu}{1-\mu}\right)}+\frac{y^2}{\left(a_y^2+\frac{\mu}{1-\mu}\right)}+\frac{z^2}{\left(a_z^2+\frac{\mu}{1-\mu}\right)}\right)\right] \exp\left[-\frac{1}{2}\left(\frac{x^2}{a_x^2}+\frac{y^2}{a_y^2}+\frac{z^2}{a_z^2}\right)\right] \\
&\quad \frac{1}{(1-\mu)^2}\,\mathrm{d}\mu\,\mathrm{d}x\,\mathrm{d}y\,\mathrm{d}z, \\
\langle z^n E_z \rangle &= K \int_{-6a_z}^{6a_z} \int_{-6a_y}^{6a_y} \int_{-6a_x}^{6a_x} \int_0^1 \frac{z^{n+1}}{(a_z^2+\frac{\mu}{1-\mu})^{3/2}\sqrt{(a_x^2+\frac{\mu}{1-\mu})(a_y^2+\frac{\mu}{1-\mu})}} \\
&\quad \exp\left[-\frac{1}{2}\left(\frac{x^2}{\left(a_x^2+\frac{\mu}{1-\mu}\right)}+\frac{y^2}{\left(a_y^2+\frac{\mu}{1-\mu}\right)}+\frac{z^2}{\left(a_z^2+\frac{\mu}{1-\mu}\right)}\right)\right] \exp\left[-\frac{1}{2}\left(\frac{x^2}{a_x^2}+\frac{y^2}{a_y^2}+\frac{z^2}{a_z^2}\right)\right] \\
&\quad \frac{1}{(1-\mu)^2}\,\mathrm{d}\mu\,\mathrm{d}x\,\mathrm{d}y\,\mathrm{d}z,
\end{aligned} \tag{4.13}
$$

where we defined

$$K := \frac{Q}{16\pi^3 \varepsilon_0 \operatorname{erf}\left[3\sqrt{2}\right]^3 a_x a_y a_z}, \tag{4.14}$$

with $\operatorname{erf}(\cdot)$ being the error function as specified in [18, eq. 7.1.1] by

$$\operatorname{erf}(z) = \frac{2}{\sqrt{\pi}} \int_0^z \exp(-t^2)\,\mathrm{d}t. \tag{4.15}$$

The single moments, i.e. $\langle w^j \rangle$, are simply obtained by evaluating

$$\begin{aligned}
\langle x^n \rangle &= L \int_{-6a_z}^{6a_z} \int_{-6a_y}^{6a_y} \int_{-6a_x}^{6a_x} x^n \exp\left[-\frac{1}{2}\left(\frac{x^2}{a_x^2} + \frac{y^2}{a_y^2} + \frac{z^2}{a_z^2}\right)\right] \mathrm{d}x\,\mathrm{d}y\,\mathrm{d}z, \\
\langle y^n \rangle &= L \int_{-6a_z}^{6a_z} \int_{-6a_y}^{6a_y} \int_{-6a_x}^{6a_x} y^n \exp\left[-\frac{1}{2}\left(\frac{x^2}{a_x^2} + \frac{y^2}{a_y^2} + \frac{z^2}{a_z^2}\right)\right] \mathrm{d}x\,\mathrm{d}y\,\mathrm{d}z, \\
\langle z^n \rangle &= L \int_{-6a_z}^{6a_z} \int_{-6a_y}^{6a_y} \int_{-6a_x}^{6a_x} z^n \exp\left[-\frac{1}{2}\left(\frac{x^2}{a_x^2} + \frac{y^2}{a_y^2} + \frac{z^2}{a_z^2}\right)\right] \mathrm{d}x\,\mathrm{d}y\,\mathrm{d}z,
\end{aligned}$$

with

$$L := \frac{1}{(2\pi)^{3/2} \operatorname{erf}\left[3\sqrt{2}\right]^3 a_x a_y a_z}.$$

Through truncating the bunch at 6σ we introduce a systematic error because all particles that are further away aren't considered anymore. For a one-dimensional normal distribution $\mathcal{N}(0,1)$ this error is $1.973175 \cdot 10^{-9}$. A comparison of various truncation values is shown in Fig. 4.3. The corresponding source code can be found in Appendix G22.

4.2.3.1 Integration Method

The choice of the integration scheme is important. First of all, we need highly accurate results. Secondly, the time to evaluate those integrals shouldn't take too long, since we have to compute them several times during the calculation of a matched distribution.
A numerical integration can either be performed using a quadrature rule or a stochastic method (e.g. Vegas Monte Carlo). The GNU Scientific Library (GSL) [21] provides both of them. Those quadrature rules, however, consider only the one-dimensional case. We would have to combine them or develop our own code in order to evaluate the multidimensional moment integrals. A more sophisticated solution is the application of the GSL extension Cubature (version 1.0.2) that is developed by Johnson [24]. It uses adaptive methods and allows parallelization.
A comparison of the GSL Vegas Monte Carlo implementation and Cubature is shown in Fig. 4.4. There, we measured the time of computing (4.13) with $n = 1$ while ignoring the normalization factor (4.14).
Although it's not a proper comparison we took the number of sample points of the Monte Carlo integration equal to the relative tolerance used in Cubature. In order to obtain an error of the same magnitude the number of samples would have to be squared, i.e. a relative error of e.g. 10^{-8} is approximately achieved with 10^{16} samples.
The green curve in Fig. 4.4a belongs to a simple use of OpenMP using 16 threads. It's about 8 - 11 times faster than the single core execution (see Tab. 4.1).
The measurements clearly indicate that Cubature yields better results than Vegas Monte Carlo in approximately equal amount of time. Nevertheless, a fast parallel version of Monte Carlo on GPUs might be still a possible option.

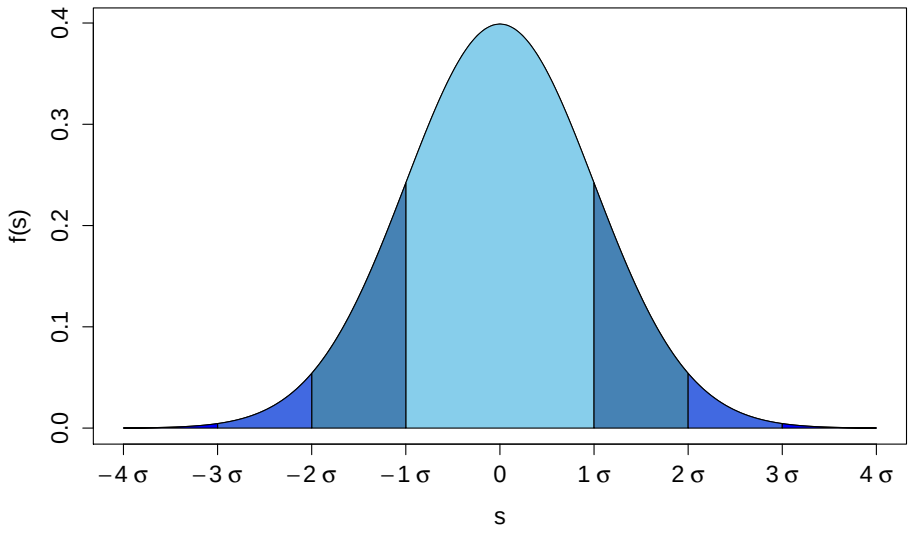

(a) One-dimensional normal distribution $\mathcal{N}(0, 1)$.

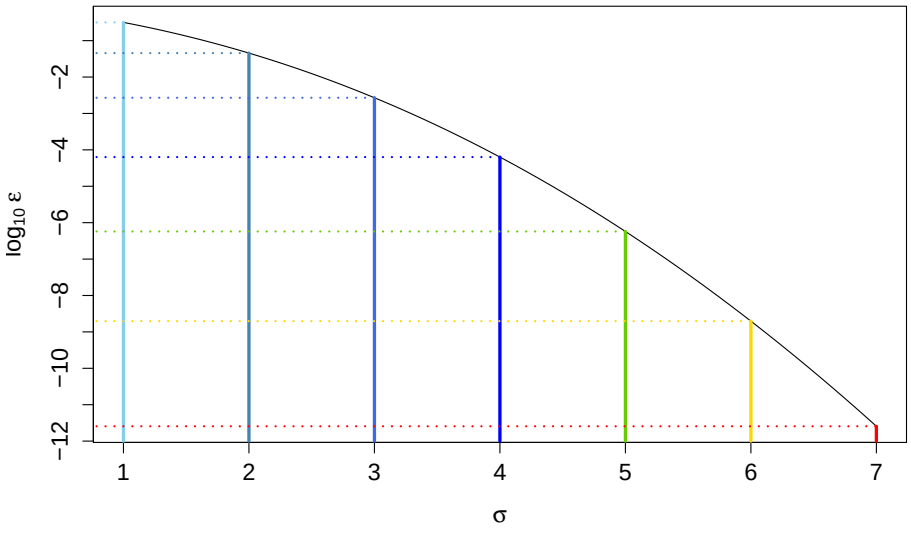

(b) Integration error ε when truncating the Gaussian at 1σ, $2\sigma, \ldots, 7\sigma$.

Figure 4.3: Normal distribution and truncation error.

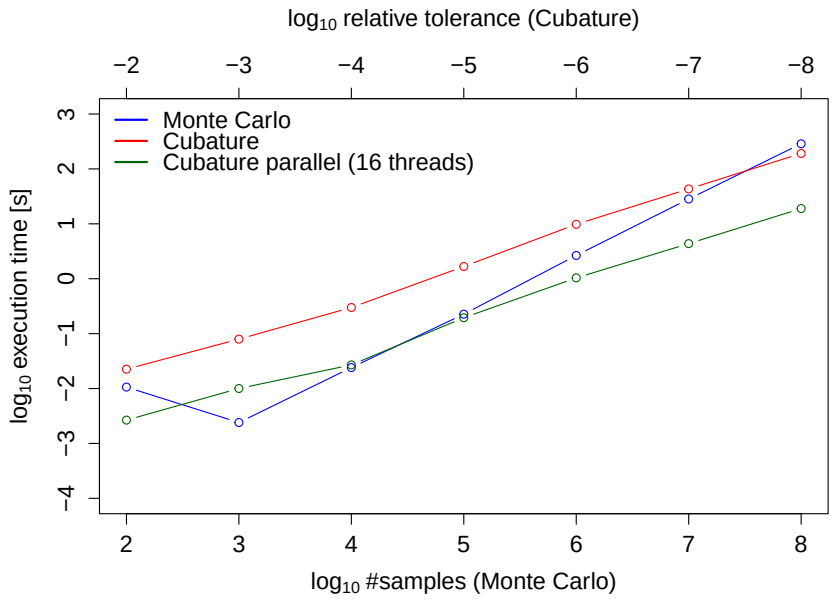

(a) Runtime of Vegas Monte Carlo vs. Cubature.

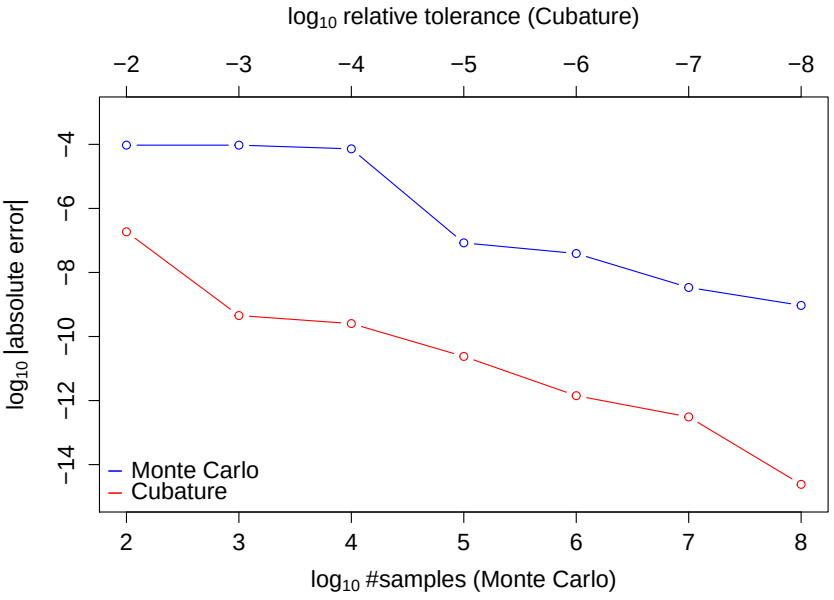

(b) Absolute error of Vegas Monte Carlo vs. Cubature. Reference solution: Cubature with relative tolerance of 10^{-9}.

Figure 4.4: Comparison between Monte Carlo integration [21] and Cubature [24]. The moment $\langle xE_x \rangle$ without prefactor (4.14) got evaluated. Both axes are in logarithmic scale. The x-axis is either the number of samples or the required relative tolerance. The semi-principal axes were set to $a_x = 0.005$ m, $a_y = 0.004$ m and $a_z = 0.007$ m. The source codes are in Appendix G12 and Appendix G13.

rel. tol.	single [µs]	parallel [µs]	speedup
10^{-2}	22 507	2659	8.4645
10^{-3}	79 407	10 013	7.9304
10^{-4}	299 179	26 938	11.1062
10^{-5}	1 669 853	194 690	8.5770
10^{-6}	9 802 970	1 035 953	9.4628
10^{-7}	43 183 540	4 356 089	9.9134
10^{-8}	191 400 164	18 958 266	10.0959

Table 4.1: Comparison of execution time of Cubature with decreasing relative tolerance. The parallel version was run with 16 threads on Merlin4 [25].

4.2.3.2 Verification of Integrals

Allen [6] computed analytical expressions of the moments in case of a continuous beam in longitudinal direction, hence, we can check the correctness of our numerical integration. The general representation of some quantities is [6, p. 26 - 29]

$$N_{cs} = \pi a_x a_y \int_0^\infty f(s)\,\mathrm{d}s, \qquad \left\langle x^2 \right\rangle = \frac{\pi a_x^3 a_y}{2N_{cs}} \int_0^\infty s f(s)\,\mathrm{d}s,$$
$$\left\langle y^2 \right\rangle = \frac{\pi a_x a_y^3}{2N_{cs}} \int_0^\infty s f(s)\,\mathrm{d}s, \qquad \langle x E_x \rangle = \frac{Q N_{cs}}{4\pi\varepsilon_0} \frac{a_x}{a_x + a_y},$$

where N_{sc} is the amount of particles of a cross section [6, p. 26]. In case of a two-dimensional Gaussian distribution (4.6), i.e.

$$f(s) = \frac{1}{2\pi a_x a_y} \exp\left[-\frac{s}{2}\right],$$

beam size $a_x = 0.005$ m, $a_y = 0.006$ m and 10^9 particles ($Q = qN$), we get following results with *Mathematica* [26] (see Appendix G2):

$$N_{cs} = 1, \qquad \left\langle x^2 \right\rangle = 2.5 \cdot 10^{-5}\ \mathrm{m}^2,$$
$$\left\langle y^2 \right\rangle = 3.6 \cdot 10^{-5}\ \mathrm{m}^2, \qquad \langle x E_x \rangle = 0.654529\ \mathrm{V\,m}.$$

We obtain identical results in C++ when for example setting the relative tolerance to 10^{-6} and the maximum number of function evaluations to 10^8. The source code is given in Appendix G14.

4.2.3.3 Charge Distribution

Using Gauss's law [13, eq. 1.13]

$$\nabla \cdot \vec{E} = \frac{\rho}{\varepsilon_0}, \tag{4.16}$$

we're able to recompute the charge distribution. The expansion of the electric field simplifies this task since each direction is expanded independently, i.e.

$$\begin{aligned}
\rho(x,y,z) = \varepsilon_0 \nabla \cdot \vec{E} &= \varepsilon_0 \left(\frac{\mathrm{d}E_x(x)}{\mathrm{d}x} + \frac{\mathrm{d}E_y(y)}{\mathrm{d}y} + \frac{\mathrm{d}E_z(z)}{\mathrm{d}z} \right) \\
&= \varepsilon_0 \left(\frac{\mathrm{d}}{\mathrm{d}x} \sum_{k=0}^{n} c_{k,x} x^k + \frac{\mathrm{d}}{\mathrm{d}y} \sum_{k=0}^{n} c_{k,y} y^k + \frac{\mathrm{d}}{\mathrm{d}z} \sum_{k=0}^{n} c_{k,z} z^k \right) \\
&= \varepsilon_0 \left(\sum_{k=1}^{n} k c_{k,x} x^{k-1} + \sum_{k=1}^{n} k c_{k,y} y^{k-1} + \sum_{k=1}^{n} k c_{k,z} z^{k-1} \right) \\
&= \varepsilon_0 \sum_{k=1}^{n} k \left(c_{k,x} x^{k-1} + c_{k,y} y^{k-1} + c_{k,z} z^{k-1} \right).
\end{aligned}$$

In the following we show some examples of the charge distribution evaluated with various truncation orders n. The simulations were performed assuming a bunch of 10^9 particles and $a_x = a_y = a_z = 0.005$ m. The exact result with the uniform probability density function that we define by

$$f(\omega) = \begin{cases} \frac{1}{8 a_x a_y a_z} & \omega < 1, \\ 0 & \omega > 1, \end{cases} \tag{4.17}$$

is given by

$$\rho = \frac{Q}{8 a_x a_y a_z} = \frac{10^9}{8 \cdot 0.005^3} \text{ e/m}^3 = 10^{15} \text{ e/m}^3.$$

The series expansion yields the results given in Fig. 4.5 where the distributions are plotted with $z = 0$. The source code is in Appendix G15. The numerical result agrees with the analytical solution. However, with increasing number of expansion terms the support restricts to $\approx 1\sigma$ due to our bounds of integration (see Appendix D.2). Another characteristic is the different behavior on the border depending on the truncation order. The value either decreases (Fig. 4.5c) or increases (Fig. 4.5d) because of the alternating signs of the power series coefficients.
In Fig. 4.6 are the results with the Gaussian distribution. The shape of the Gaussian seems to be correct only for a truncation order of $n = 3$. The highest magnitude of (4.6) with $\rho(x,y,z) = Qf(x,y,z)$ is

$$\rho(0,0,0) = \frac{Q}{(2\pi)^{3/2} a_x a_y a_z} = \frac{10^9}{(2\pi)^{3/2} \cdot 0.005^3} \text{ e/m}^3 \approx 5.0795 \cdot 10^{14} \text{ e/m}^3.$$

The numerical solution is slightly lower (e.g. $\rho_{max} \approx 2.6040 \cdot 10^{14}$ for $n = 3$). But with increasing order it seems to converge to the analytical value (e.g. $\rho_{max} \approx 3.2067 \cdot 10^{14}$ for $n = 9$) .

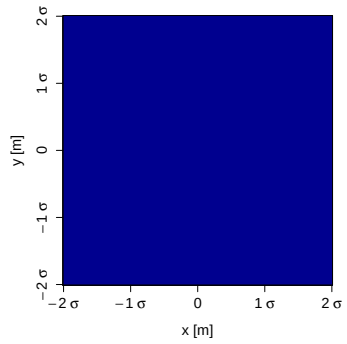

(a) Truncation at order 3. $\rho = 10^{15}$ e/m^3.

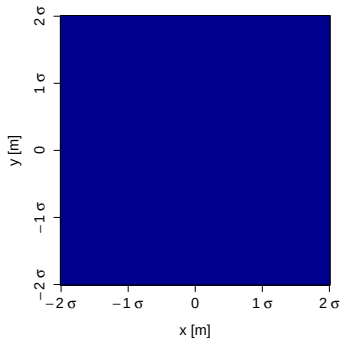

(b) Truncation at order 5. $\rho = 10^{15}$ e/m^3.

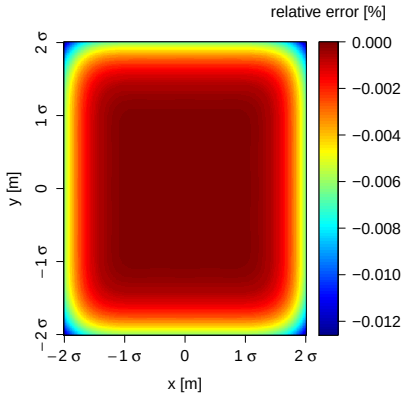

(c) Truncation at order 7.

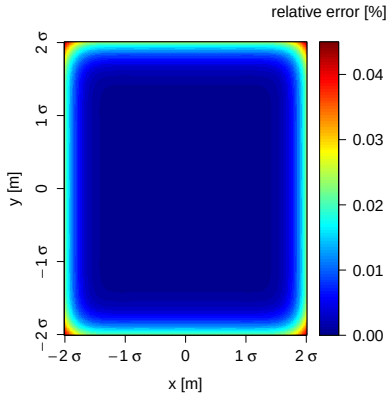

(d) Truncation at order 9.

Figure 4.5: Uniform charge distribution (plotted with $z = 0$) obtained with semi-principal axes $\sigma = a_x = a_y = a_z = 0.005$ m and (4.17). A relative tolerance of 10^{-6} and a maximum number of function evaluations 10^8 were applied.

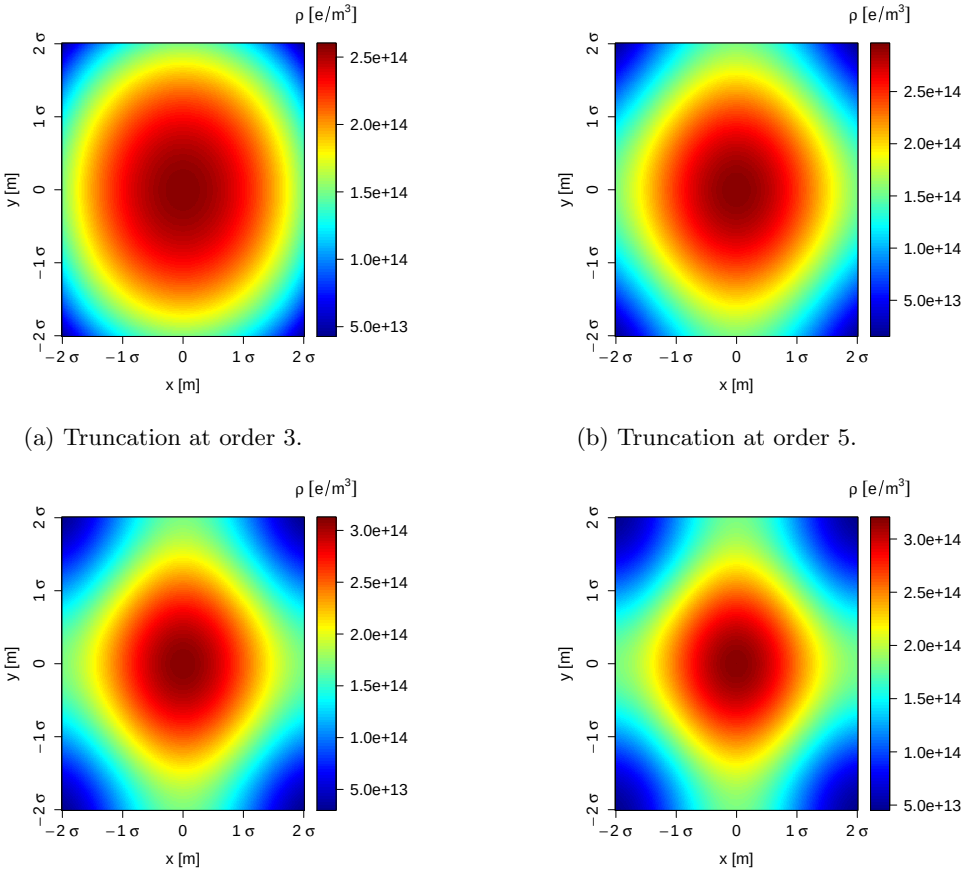

(a) Truncation at order 3.

(b) Truncation at order 5.

(c) Truncation at order 7.

(d) Truncation at order 9.

Figure 4.6: Gaussian charge distribution (plotted with $z = 0$) obtained with semi-principal axes $\sigma = a_x = a_y = a_z = 0.005$ m. A relative tolerance of 10^{-6} and a maximum number of function evaluations 10^8 were applied.

4.2.3.4 Electric Field

Due to the poor result using the Gaussian charge distribution in the previous section we analyze the electric field approximation. The analytical result can be obtained by applying Gauss's law of (4.16) in spherical coordinates

$$\frac{1}{r^2}\frac{\partial}{\partial r}\left(r^2 E_r\right) + \frac{1}{r\sin(\vartheta)}\frac{\partial}{\partial \vartheta}\left(\sin(\vartheta)E_\vartheta\right) + \frac{1}{r\sin(\vartheta)}\frac{\partial}{\partial \varphi}E_\varphi = \frac{\rho}{\varepsilon_0}, \tag{4.18}$$

with $\vec{E} = (E_r, E_\vartheta, E_\varphi)$ and [27, p. 511]. Then, the charge density of the spherical Gaussian (see Appendix E.1)

$$\rho(r) = Qf(r) = \frac{Q}{(2\pi)^{3/2}a^3}\exp\left[-\frac{r^2}{2a^2}\right],$$

yields

$$\frac{\partial}{\partial r}\left(r^2 E_r\right) = \frac{Qr^2}{(2\pi)^{3/2}a^3\varepsilon_0}\exp\left[-\frac{r^2}{2a^2}\right],$$

with solution (see Appendix G3):

$$E_r(r) = \frac{Q}{2\sqrt{2}\pi^{3/2}r^2\varepsilon_0 a^3}\left(\sqrt{\frac{\pi}{2}}a^3\operatorname{erf}\left[\frac{r}{\sqrt{2}a}\right] - a^2 r\exp\left[-\frac{r^2}{2a^2}\right]\right), \tag{4.19}$$

where $\operatorname{erf}(\cdot)$ is the error function given in (4.15). A plot of the electric field in the range of $r \in [0, 6\sigma]$ is shown in Fig. 4.7.
On the other hand, the integration of (4.9) with (4.6) and $a = a_x = a_y = a_z$ (see Appendix G3) results in

$$E_w = \frac{Qw}{4\sqrt{2}\pi^{3/2}\varepsilon_0}\left(\frac{\sqrt{2\pi}\operatorname{erf}\left[\frac{1}{\sqrt{2}a}\sqrt{x^2+y^2+z^2}\right]}{\left(x^2+y^2+z^2\right)^{3/2}} - \frac{2\exp\left[-\frac{1}{2a^2}\left(x^2+y^2+z^2\right)\right]}{a\left(x^2+y^2+z^2\right)}\right), \tag{4.20}$$

where $w \in \{x, y, z\}$. Although it's not directly obvious, we can show that the l_2-norm of (4.19) and (4.20) with $w \in \{x, y, z\}$ are equivalent. By substituting (E.1) into (4.20), we get:

$$\begin{aligned}
E_w &= \frac{Qw}{4\sqrt{2}\pi^{3/2}\varepsilon_0}\left(\frac{\sqrt{2\pi}\operatorname{erf}\left[\frac{r}{\sqrt{2}a}\right]}{r^3} - \frac{2\exp\left[-\frac{r^2}{2a^2}\right]}{ar^2}\right) \\
&= \frac{Qw}{4\sqrt{2}\pi^{3/2}r^3\varepsilon_0 a^3}\left(\sqrt{2\pi}a^3\operatorname{erf}\left[\frac{r}{\sqrt{2}a}\right] - 2a^2 r\exp\left[-\frac{r^2}{2a^2}\right]\right) \\
&= \frac{Qw}{2\sqrt{2}\pi^{3/2}r^3\varepsilon_0 a^3}\left(\sqrt{\frac{\pi}{2}}a^3\operatorname{erf}\left[\frac{r}{\sqrt{2}a}\right] - a^2 r\exp\left[-\frac{r^2}{2a^2}\right]\right) \\
&= \underbrace{\frac{Q}{2\sqrt{2}\pi^{3/2}r^2\varepsilon_0 a^3}\left(\sqrt{\frac{\pi}{2}}a^3\operatorname{erf}\left[\frac{r}{\sqrt{2}a}\right] - a^2 r\exp\left[-\frac{r^2}{2a^2}\right]\right)}_{(4.19)}\frac{w}{r}.
\end{aligned}$$

Therefore, the electric field components are given by

$$\begin{aligned}
E_x &= E_r(r)\frac{r\sin(\vartheta)\cos(\varphi)}{r} = E_r(r)\sin(\vartheta)\cos(\varphi), \\
E_y &= E_r(r)\frac{r\sin(\vartheta)\sin(\varphi)}{r} = E_r(r)\sin(\vartheta)\sin(\varphi), \\
E_z &= E_r(r)\frac{r\cos(\vartheta)}{r} = E_r(r)\cos(\vartheta),
\end{aligned}$$

with a squared l_2-norm of

$$\begin{aligned} E_x^2 + E_y^2 + E_z^2 &= \left[E_r(r)\sin(\vartheta)\cos(\varphi)\right]^2 + \left[E_r(r)\sin(\vartheta)\sin(\varphi)\right]^2 + \left[E_r(r)\cos(\vartheta)\right]^2 \\ &= E_r^2(r)\left[\sin^2(\vartheta)\cos^2(\varphi) + \sin^2(\vartheta)\sin^2(\varphi) + \cos^2(\vartheta)\right] \\ &= E_r^2(r)\left[\sin^2(\vartheta) + \cos^2(\vartheta)\right] \\ &= E_r^2(r). \end{aligned}$$

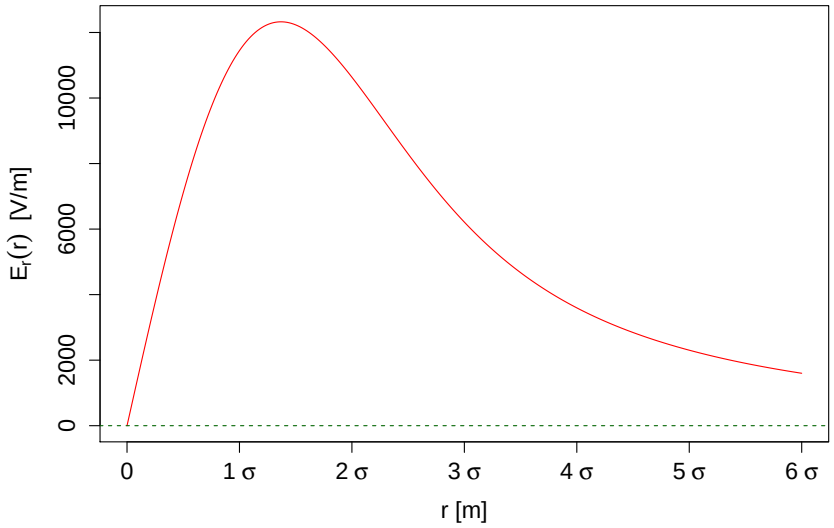

Figure 4.7: Electric field of a sphere using a Gaussian charge distribution with $\sigma = a = a_x = a_y = a_z = 0.005$ m. The x-axis represents the distance from the center of the sphere.

In Fig. 4.8 are electric field approximations with various truncation orders. It confirms the poor behavior that we have already observed in Sec. 4.2.3.3. The curve indicates a peak as in Fig. 4.7 but it's shifted by approximately 1σ. The analytic solution (see Appendix G3) has the maximum at $r \approx 0.0068$ m with $E_{max} \approx 12\,326.0476$ V/m. The peak position and its value seem to slowly converge to the right value as shown in Tab. 4.2.

order	peak at r [m]	peak value [V/m]	abs. error	rel. error [%]
3	0.0151	15578.9	3252.8524	26.3901
5	0.0133	14692.1	2366.0524	19.1955
7	0.0127	14328.0	2001.9524	16.2416
9	0.0126	14166.6	1840.5524	14.9322

Table 4.2: The peak of the electric field for various truncation orders. The last two columns indicate the absolute and relative error with respect to the true peak of $E_{max} \approx 12\,326.0476$ V/m at $r \approx 0.0068$ m.

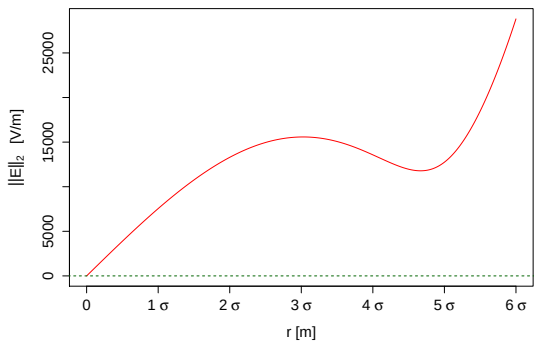

(a) Truncation at degree 3.

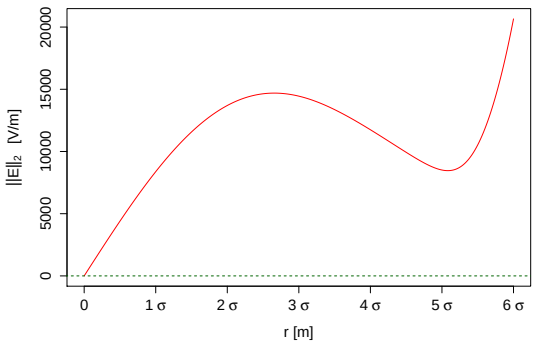

(b) Truncation at degree 5.

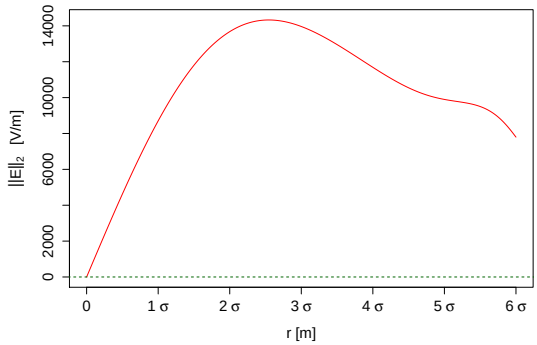

(c) Truncation at degree 7.

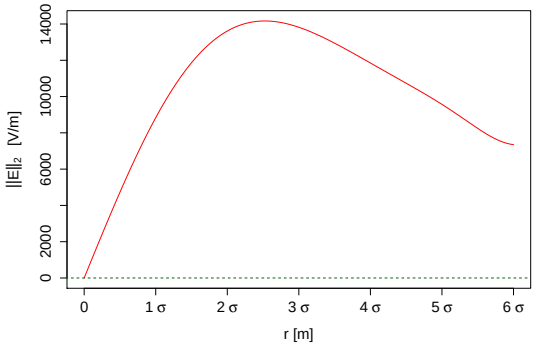

(d) Truncation at degree 9.

Figure 4.8: Electric field $||\vec{E}(r, \vartheta, \varphi)||_2$ at $\vartheta = \varphi = \frac{\pi}{4}$ using a Gaussian charge distribution with $\sigma = a_x = a_y = a_z = 0.005$ m. The x-axis represents the distance from the center of the sphere. The Cartesian coordinates are transformed by (E.1). Relative tolerance of moment computation was set to 10^{-6} with maximum number of function evaluations 10^8. The corresponding source code is given in Appendix G16.

4.2.3.5 Electric Field Density

The total energy is [13, eq. 6.112]

$$W_e = \frac{\varepsilon_0}{2} \int_V \left(\vec{E}^2 + c^2 \vec{B}^2 \right) \mathrm{d}V,$$

with volume V, electric field $\vec{E}$ and magnetic field $\vec{B}$. The magnetic field is zero because we assume a bunch with velocity $v = 0$. Additionally, we consider a sphere of radius R, thus, above formula simplifies to

$$W_e = \frac{\varepsilon_0}{2} \int_V \vec{E}^2 \, \mathrm{d}V = \frac{\varepsilon_0}{2} \int_0^{2\pi} \int_0^{\pi} \int_0^{R} \vec{E}^2 r^2 \sin(\vartheta) \, \mathrm{d}r \, \mathrm{d}\vartheta \, \mathrm{d}\varphi,$$

where the transformation to spherical coordinates is given in Appendix E. As we approximate the electric field in each direction through a power series, the equation can be rewritten as

$$W_e = \frac{\varepsilon_0}{2} \int_0^{2\pi} \int_0^{\pi} \int_0^{R} \left[E_x^2(x) + E_y^2(y) + E_z^2(z)\right] r^2 \sin(\vartheta)\, \mathrm{d}r\, \mathrm{d}\vartheta\, \mathrm{d}\varphi, \tag{4.21}$$

where the coordinates have to be substituted by (E.1) during the computation.
A spherical bunch of N particles homogeneously distributed have a charge distribution (4.17) of

$$\rho = \frac{Q}{8R^3},$$

where $Q = qN$. By applying Gauss's law (4.16) in spherical coordinates (4.18) we obtain the electric field

$$E_r(r) = \frac{Q}{24\varepsilon_0 R^3} r,$$

where the independence of ϑ and φ simplifies the calculation. In this case the computation of (4.21) is given by

$$W_e = \frac{\varepsilon_0}{2} \int_0^{2\pi} \int_0^{\pi} \int_0^{R} E_r^2(r) r^2 \sin(\vartheta)\, \mathrm{d}r\, \mathrm{d}\vartheta\, \mathrm{d}\varphi,$$

which can be analytically solved assuming the uniform distribution (see Appendix G4):

$$W_{e,unif} = \frac{Q^2 \pi}{1440\varepsilon_0 R}. \tag{4.22}$$

In Fig. 4.9 and Tab. 4.3 is a comparison of (4.22) with the approach of expanding the electric field where we have chosen $N = 10^9$ and $R = 0.005$ m. The analytical result (4.22) with this configuration yields

$$W_{e,unif} \approx 7.8955 \cdot 10^9 \text{ eV},$$

or, respectively, ≈ 7.8955 eV/particle.
When requiring a relative error of 10^{-9} and maximum number of function evaluations of 10^8 for the numerical integrations, the expansion agrees with the reference solution up to truncation order 13. Then, the numerical issue kicks in.
Thanks to the spherical symmetry we only need to compute the moments in one direction. Additionally, all integrals of odd integrands are zero:

$$\langle w^p \rangle = 0 \quad \forall p \in \{2n+1 \mid n \in \mathbb{N}_0\} \quad \text{and} \quad \langle w^p E_w \rangle = 0 \quad \forall p \in \{2n \mid n \in \mathbb{N}_0\},$$

where $w \in \{x, y, z\}$.

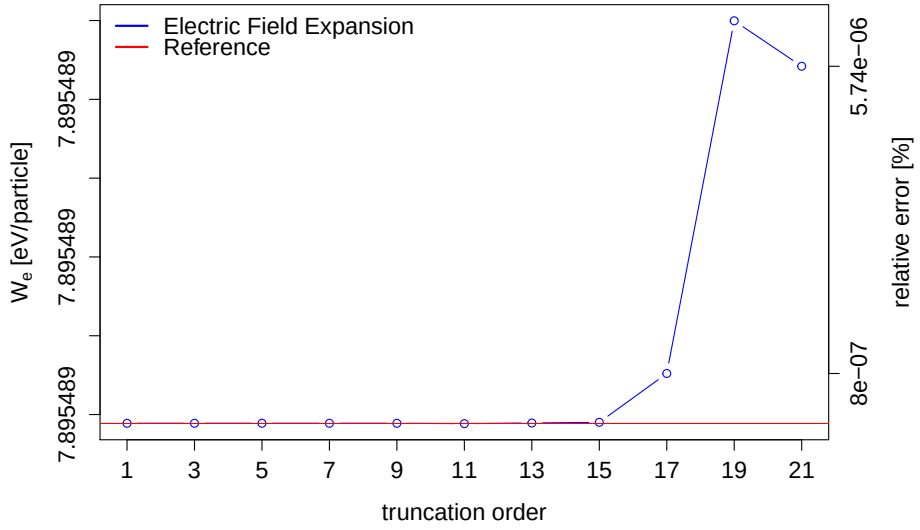

Figure 4.9: Electric field energy of a spherical bunch with $R = a_x = a_y = a_z = 0.005$ m and uniform charge distribution. The relative error is computed by $(n/r - 1) \cdot 100$ where n represents the numerical value and r the reference value. The C++ code is in Appendix G17.

order	field energy [MeV]	relative error [%]
1	7 895.488 788 908 594	$2.249 \cdot 10^{-10}$
3	7 895.488 788 914 006	$2.935 \cdot 10^{-10}$
5	7 895.488 788 914 002	$2.934 \cdot 10^{-10}$
7	7 895.488 788 913 866	$2.917 \cdot 10^{-10}$
9	7 895.488 788 918 492	$3.503 \cdot 10^{-10}$
11	7 895.488 788 442 384	$-5.680 \cdot 10^{-9}$
13	7 895.488 789 249 182	$4.539 \cdot 10^{-9}$
15	7 895.488 790 126 233	$1.565 \cdot 10^{-8}$
17	7 895.488 852 108 553	$8.007 \cdot 10^{-7}$
19	7 895.489 299 672 355	$6.469 \cdot 10^{-6}$
21	7 895.489 241 960 982	$5.738 \cdot 10^{-6}$

Table 4.3: Numerical values of the field energy for various truncation orders based on the uniform probability density function (4.17). The last column represents the relative deviation in percent from the reference solution (see Appendix G4), i.e. 7 895.488 788 890 838 MeV.

4.2.4 Distribution with Higher Order Terms

Up to now we haven't applied any higher order terms in the charge distribution. In [28] they describe the usage of such additional terms as part of the Gaussian distribution, i.e. [28, eq. 12]

$$f(\vec{x}, \sigma_2) = A_0 \exp\left[-\frac{1}{2}\vec{x}^\top \sigma_2^{-1}\vec{x} - g(\vec{x})\right],$$

where A_0 is some prefactor, $\vec{x} = (x, p_x, y, p_y, z, p_z)$ and $g(\vec{x})$ represents a function of higher order terms. However, they do not specify how this function looks like.

4.3 Discussion of Methods

In this section we shortly compare all previously described methods and give a motivation of our choice.
A limitation of the distribution-based methods is their assumption of a charge distribution. We basically prescribe a charge distribution that, however, might be a bad approximation over time. A possible solution might be the use of methods that estimate the probability density function based on moments. Such methods normally depend on basis functions like Laguerre or Hermite polynomials. [29]
The huge benefit of distribution-based methods is the fact that we don't need to track particles, i.e. everything can be described by moments.
The particle-based method, on the other hand, allows any kind of distribution and moment tracking shouldn't represent a problem. But since we require for each trajectory a space charge map, we would need to resample particles from the moments or simply track single particles. This requires more memory and is more complex — especially when want to resample particles based on higher order moments.
Additionally, it wasn't really clear to us how one should obtain a space charge map from FMM, although it's claimed in [16].
All these disadvantages and uncertainties of the particle-based method finally convinced us to apply one of those distribution-based models where we decided to implement the approach of expanding the electric field since it is more general.

5 Non-Linear Space Charge Map

5.1 General Form

In order to obtain higher order space charge maps, we have to expand (3.1) with the space charge Hamiltonian (4.1). Applying the series expansion (3.3) leads to

$$\mathcal{M}_{sc} = \sum_{j=0}^{\infty} \frac{(-s:H_{sc}:)^j}{j!} = 1 - s:H_{sc}: + \frac{s^2:H_{sc}:^2}{2!} - \frac{s^3:H_{sc}:^3}{3!} \pm \dots,$$

where the repeated application of the Lie operator includes higher order derivatives. Due to (4.1) above formula is rewritten as

$$\mathcal{M}_{sc} = 1 - sq:\phi: + \frac{(sq)^2:\phi:^2}{2!} - \frac{(sq)^3:\phi:^3}{3!} \pm \dots. \tag{5.1}$$

In the dynamical variables the Lie operator in (3.2) is given by

$$:\phi: = \frac{\partial\phi}{\partial x}\frac{\partial}{\partial p_x} + \frac{\partial\phi}{\partial y}\frac{\partial}{\partial p_y} + \frac{\partial\phi}{\partial z}\frac{\partial}{\partial p_z} - \underbrace{\frac{\partial\phi}{\partial p_x}}_{0}\frac{\partial}{\partial x} - \underbrace{\frac{\partial\phi}{\partial p_y}}_{0}\frac{\partial}{\partial y} - \underbrace{\frac{\partial\phi}{\partial p_z}}_{0}\frac{\partial}{\partial z},$$

where all derivatives of the potential $\phi(x, y, z)$ with respect to the momenta are zero. Using the relation (4.8) then yields

$$:\phi: = -E_x\frac{\partial}{\partial p_x} - E_y\frac{\partial}{\partial p_y} - E_z\frac{\partial}{\partial p_z}.$$

Therefore, the evaluation of above equation in e.g. horizontal direction (x, p_x) gives

$$\begin{aligned}
:\phi:x &= -E_x\underbrace{\frac{\partial x}{\partial p_x}}_{0} - E_y\underbrace{\frac{\partial x}{\partial p_y}}_{0} - E_z\underbrace{\frac{\partial x}{\partial p_z}}_{0} = 0,\\
:\phi:p_x &= -E_x\underbrace{\frac{\partial p_x}{\partial p_x}}_{1} - E_y\underbrace{\frac{\partial p_x}{\partial p_y}}_{0} - E_z\underbrace{\frac{\partial p_z}{\partial p_z}}_{0} = -E_x,
\end{aligned}$$

where the same holds for the vertical and longitudinal direction. Because the electric field is independent of the momenta, the second term in the series expansion (5.1) vanishes, i.e.

$$\begin{aligned}
:\phi:^2x &= :\phi:0 = 0,\\
:\phi:^2p_x &= -:\phi:E_x = E_x\underbrace{\frac{\partial E_x}{\partial p_x}}_{0} + E_y\underbrace{\frac{\partial E_x}{\partial p_y}}_{0} + E_z\underbrace{\frac{\partial E_x}{\partial p_z}}_{0} = 0,
\end{aligned}$$

where we exploited [11, eq. 5.3.4], i.e. $:\phi:^2 = :\phi::\phi:$. Consequently, all terms

$$\begin{aligned}
:\phi:^j w &= 0 \quad \forall j \geq 1,\\
:\phi:^j p_w &= 0 \quad \forall j > 1,
\end{aligned}$$

with $w \in \{x, y, z\}$ vanish which reduces (5.1) to

$$\mathcal{M}_{sc} = 1 - sq :\phi: .$$

The space charge map for each canonical variable is therefore given by

$$\mathcal{M}_{sc} = \begin{pmatrix} 1 \\ 1 + sqE_x \\ 1 \\ 1 + sqE_y \\ 1 \\ 1 + sqE_z \end{pmatrix},$$

where we ordered the variables according to (x, p_x, y, p_y, z, p_z). By inserting the model of expanding the electric field of Sec. 4.2.3 we obtain

$$\mathcal{M}_{sc} \approx \begin{pmatrix} 1 \\ 1 + sq \sum_{i=0}^{n} c_{i,x} x^i \\ 1 \\ 1 + sq \sum_{i=0}^{n} c_{i,y} y^i \\ 1 \\ 1 + sq \sum_{i=0}^{n} c_{i,z} z^i \end{pmatrix},$$

with coefficients $c_{i,x}$, $c_{i,y}$ and $c_{i,z}$ that are obtained by solving (4.11). Since the source code is based on the variables $(x, x', y, y', z, \delta)$ instead of (x, p_x, y, p_y, z, p_z), we have to apply the transformations explained in Sec. 1.3. Therefore, the space charge map is finally given by

$$\mathcal{M}_{sc} \approx \begin{pmatrix} 1 \\ 1 + \frac{sq}{m\beta^2 c^2 \gamma} \sum_{i=0}^{n} c_{i,x} x^i \\ 1 \\ 1 + \frac{sq}{m\beta^2 c^2 \gamma} \sum_{i=0}^{n} c_{i,y} y^i \\ 1 \\ 1 + \gamma^2 \frac{sq}{m\beta^2 c^2 \gamma} \sum_{i=0}^{n} c_{i,z} z^i \end{pmatrix}.$$

5.2 Linear Approximation of the Electric Field

Since the linear space charge map is known, we can verify above theory by making a linear approximation of the electric field in all directions, i.e. $E_w = c_0 + c_1 w$ with $w \in \{x, y, z\}$. Assuming a centered beam that is $\langle w \rangle = 0$, the general result of (4.11) is

$$\begin{pmatrix} 1 & 0 \\ 0 & \langle w^2 \rangle \end{pmatrix} \cdot \begin{pmatrix} c_{0,w} \\ c_{1,w} \end{pmatrix} = \begin{pmatrix} 0 \\ \langle E_w w \rangle \end{pmatrix} \Longrightarrow E_w \approx \frac{\langle w E_w \rangle}{\langle w^2 \rangle} w,$$

with $w \in \{x, y, z\}$ again. Though, the 6×6 space charge matrix in $(x, x', y, y', z, \delta)$ is

$$M_{sc}(s) = \begin{pmatrix} 1 & 0 & 0 & 0 & 0 & 0 \\ \frac{q}{m\beta^2 c^2 \gamma} \frac{\langle x E_x \rangle}{\langle x^2 \rangle} s & 1 & 0 & 0 & 0 & 0 \\ 0 & 0 & 1 & 0 & 0 & 0 \\ 0 & 0 & \frac{q}{m\beta^2 c^2 \gamma} \frac{\langle y E_y \rangle}{\langle y^2 \rangle} s & 1 & 0 & 0 \\ 0 & 0 & 0 & 0 & 1 & 0 \\ 0 & 0 & 0 & 0 & \frac{q}{m\beta^2 c^2 \gamma} \frac{\langle z E_z \rangle}{\langle z^2 \rangle} \gamma^2 s & 1 \end{pmatrix}. \tag{5.2}$$

This is exactly the same matrix compared to [7, ch. 2.5.2],

$$M_{sc}(s) = \begin{pmatrix} 1 & 0 & 0 & 0 & 0 & 0 \\ K_x s & 1 & 0 & 0 & 0 & 0 \\ 0 & 0 & 1 & 0 & 0 & 0 \\ 0 & 0 & K_y s & 1 & 0 & 0 \\ 0 & 0 & 0 & 0 & 1 & 0 \\ 0 & 0 & 0 & 0 & K_z \gamma^2 s & 1 \end{pmatrix}, \tag{5.3}$$

which is based on the theory of [8, ch. 11.4.] with $(x, x', y, y', l, \delta)$. The strengths of the space charge forces K_x, K_y and K_z are defined in [3, eq. 21] by

$$K_x = \frac{K_3\,[1 - f(s)]}{(\sigma_x + \sigma_y)\sigma_x\sigma_z}, \qquad K_y = \frac{K_3\,[1 - f(s)]}{(\sigma_x + \sigma_y)\sigma_y\sigma_z}, \qquad K_z = \frac{K_3 f(s)}{\sigma_x\sigma_y\sigma_z},$$

with [8, eq. 11.35]

$$f \approx \frac{\sqrt{\sigma_x\sigma_y}}{3\gamma\sigma_z},$$

and [8, eq. 11.36]

$$K_3 = \frac{3qI\lambda}{20\sqrt{5}\pi\varepsilon_0 mc^3\beta^2\gamma^3}. \tag{5.4}$$

where λ is the wavelength.

5.2.1 Dimensional Analysis

In this section we compare the dimensions of (5.2) and (5.3). For this purpose we abbreviate the units in a more general way, i.e. length L, mass M, time T and charge Q. Therefore, the units of the quantities in the previous section are expressed by

$$[I] = \mathrm{T}^{-1}\,\mathrm{Q}, \qquad [\varepsilon_0] = \mathrm{L}^{-3}\,\mathrm{M}^{-1}\,\mathrm{T}^{2}\,\mathrm{Q}^{2}, \qquad [c] = \mathrm{L}\,\mathrm{T}^{-1}, \qquad [E_x] = [E_y] = [E_z] = \mathrm{L}\,\mathrm{M}\,\mathrm{T}^{-2}\,\mathrm{Q}^{-1},$$
$$[m] = M, \qquad [q] = Q, \qquad [\beta] = 1, \qquad [\gamma] = 1.$$

The SI unit of (5.4) is then given by

$$[K_3] = \frac{\mathrm{L}\,\mathrm{T}^{-1}\,\mathrm{Q}^2}{\mathrm{L}^3\,\mathrm{L}^{-3}\,\mathrm{M}\,\mathrm{M}^{-1}\,\mathrm{T}^2\,\mathrm{T}^{-3}\,\mathrm{Q}^2} = \frac{\mathrm{L}\,\mathrm{T}^{-1}\,\mathrm{Q}^2}{\mathrm{T}^{-1}\,\mathrm{Q}^2} = \mathrm{L}.$$

Consequently, the space charge strengths have units of

$$[K_x] = [K_y] = [K_z] = \frac{\mathrm{L}}{\mathrm{L}^3} = \mathrm{L}^{-2}.$$

Since the subdiagonal entries of (5.2) have units of

$$\left[\frac{q}{m\beta^2c^2\gamma}\frac{\langle xE_x\rangle}{\langle x^2\rangle}\right] = \left[\frac{q}{m\beta^2c^2\gamma}\frac{\langle yE_y\rangle}{\langle y^2\rangle}\right] = \left[\frac{q\gamma^2}{m\beta^2c^2\gamma}\frac{\langle zE_z\rangle}{\langle z^2\rangle}\right] = \frac{\mathrm{L}\,\mathrm{L}\,\mathrm{M}\,\mathrm{T}^{-2}\,\mathrm{Q}\,\mathrm{Q}^{-1}}{\mathrm{L}^2\,\mathrm{L}^2\,\mathrm{M}\,\mathrm{T}^{-2}} = \mathrm{L}^{-2},$$

the dimensions of (5.2) and (5.3) agree.

6 Moment Tracking

In the following sections we discuss the theory of tracking moments by higher order transfer maps. This kind of transport is also explained in [12, ch. 5.2].
But before illustrating the theory of non-linear moment tracking, we have to understand the linear case. For this purpose we study the second order moment tracking and make an example in the one-dimensional phase space.

6.1 Linear Mapping of Second Order Moments

On the assumption of a linear transfer map $M \in \mathbb{R}^{6\times 6}$ the second moment matrix [8, eq. 4.134] defined in the dynamical variables (x, p_x), (y, p_y) and (z, p_z), i.e.

$$\sigma_2 = \begin{pmatrix} \langle x^2\rangle & \langle xp_x\rangle & \langle xy\rangle & \langle xp_y\rangle & \langle xz\rangle & \langle xp_z\rangle \\ \langle p_x x\rangle & \langle p_x^2\rangle & \langle p_x y\rangle & \langle p_x p_y\rangle & \langle p_x z\rangle & \langle p_x p_z\rangle \\ \langle yx\rangle & \langle yp_x\rangle & \langle y^2\rangle & \langle yp_y\rangle & \langle yz\rangle & \langle yp_z\rangle \\ \langle p_y x\rangle & \langle p_y p_x\rangle & \langle p_y y\rangle & \langle p_y^2\rangle & \langle p_y z\rangle & \langle p_y p_z\rangle \\ \langle zx\rangle & \langle zp_x\rangle & \langle zy\rangle & \langle zp_y\rangle & \langle z^2\rangle & \langle zp_z\rangle \\ \langle p_z x\rangle & \langle p_z p_x\rangle & \langle p_z y\rangle & \langle p_z p_y\rangle & \langle p_z z\rangle & \langle p_z^2\rangle \end{pmatrix}, \tag{6.1}$$

is transported on the path s by [8, eq. 4.141]

$$\sigma_2(s) = M\sigma_2(0)M^\top. \tag{6.2}$$

Based on above notation we define the general formula of mapping the k-th order tensor of moments by

$$\sigma_k(s) = \mathcal{M} \circ \sigma_k(0) \circ \mathcal{M}^{\mathcal{T}}, \tag{6.3}$$

where $\mathcal{M}$ is the k-th order map. Since the simple matrix operations applied in (6.2) aren't valid anymore, we denote those new operations by $\circ$ and $\mathcal{T}$. In the next section we try to understand (6.2) by an example.

6.1.1 Example

Assume the one-dimensional phase space with the canonical pair (q, p) and covariance matrix

$$\sigma = \begin{pmatrix} \langle q^2\rangle & \langle qp\rangle \\ \langle qp\rangle & \langle p^2\rangle \end{pmatrix}. \tag{6.4}$$

Further, suppose that the variable q is mapped linearly by

$$q \mapsto \lambda_0 q + \lambda_1 p, \tag{6.5}$$

with λ_0, $\lambda_1 \in \mathbb{C}$. Hence, the transfer map is given by

$$M = \begin{pmatrix} \lambda_0 & \lambda_1 \\ \bullet & \bullet \end{pmatrix}, \tag{6.6}$$

where $\bullet$ represents a placeholder for the coefficients of the linear polynomial for the momentum. Therefore, inserting (6.4) and (6.6) into (6.2) yields following result:

$$\overbrace{\begin{pmatrix} \langle q^2 \rangle_f & \langle qp \rangle_f \\ \langle qp \rangle_f & \langle p^2 \rangle_f \end{pmatrix}}^{\sigma_f} = \overbrace{\begin{pmatrix} \lambda_0 & \lambda_1 \\ \bullet & \bullet \end{pmatrix}}^{M} \overbrace{\begin{pmatrix} \langle q^2 \rangle_i & \langle qp \rangle_i \\ \langle qp \rangle_i & \langle p^2 \rangle_i \end{pmatrix}}^{\sigma_i} \overbrace{\begin{pmatrix} \lambda_0 & \bullet \\ \lambda_1 & \bullet \end{pmatrix}}^{M^\top} = \begin{pmatrix} \lambda_0 & \lambda_1 \\ \bullet & \bullet \end{pmatrix} \begin{pmatrix} \lambda_0 \langle q^2 \rangle_i + \lambda_1 \langle qp \rangle_i & \star \\ \lambda_0 \langle qp \rangle_i + \lambda_1 \langle p^2 \rangle_i & \star \end{pmatrix}$$
$$= \begin{pmatrix} \lambda_0^2 \langle q^2 \rangle_i + 2\lambda_0\lambda_1 \langle qp \rangle_i + \lambda_1^2 \langle p^2 \rangle_i & * \\ * & * \end{pmatrix},$$

where $\star$ and $*$ symbolize modified entries and the subscripts i, f indicate *initial*, respectively, *final* state. Thus, the moment $\langle q^2 \rangle$ is mapped by a linear combination of $\langle qp \rangle$, $\langle p^2 \rangle$ and $\langle q^2 \rangle$ itself. We obtain the identical result when squaring (6.5) and computing the moment of it, i.e.

$$\begin{aligned} \langle q^2 \rangle_f &= \int_{\mathbb{R}^2} (\lambda_0 q_i + \lambda_1 p_i)^2 f(q,p) \,\mathrm{d}q \,\mathrm{d}p = \int_{\mathbb{R}^2} \left(\lambda_0^2 q_i^2 + 2\lambda_0\lambda_1 q_i p_i + \lambda_1^2 p_i^2\right) f(q,p) \,\mathrm{d}q \,\mathrm{d}p \\ &= \lambda_0^2 \int_{\mathbb{R}^2} q_i^2 f(q,p) \,\mathrm{d}q \,\mathrm{d}p + 2\lambda_0\lambda_1 \int_{\mathbb{R}^2} q_i p_i f(q,p) \,\mathrm{d}q \,\mathrm{d}p + \lambda_1^2 \int_{\mathbb{R}^2} p_i^2 f(q,p) \,\mathrm{d}q \,\mathrm{d}p \\ &= \lambda_0^2 \langle q^2 \rangle_i + 2\lambda_0\lambda_1 \langle qp \rangle_i + \lambda_1^2 \langle p^2 \rangle_i , \end{aligned}$$

with probability density function $f(q,p)$. In the next section we discuss this property in connection with arbitrary moments.

6.2 General Moments

In general, a moment of the form

$$\left\langle x^i p_x^j y^k p_y^l z^m p_z^n \right\rangle ,$$

that is defined in the dynamical variables with exponents $i,j,k,l,m,n \in \mathbb{N}_0$, is computed according to (4.10) by

$$\left\langle x^i p_x^j y^k p_y^l z^m p_z^n \right\rangle = \int_{\mathbb{R}^6} x^i p_x^j y^k p_y^l z^m p_z^n f(x,y,z,p_x,p_y,p_z) \,\mathrm{d}x \,\mathrm{d}p_x \,\mathrm{d}y \,\mathrm{d}p_y \,\mathrm{d}z \,\mathrm{d}p_z, \tag{6.7}$$

with f being a probability density function. The total number of moments grows with the order pursuant to (2.1). As an example, the second moment matrix defined in (6.1) already counts 21 different moments.

6.2.1 Mapping

The example in Sec. 6.1.1 showed another representation of (6.2) making it possible to generalize this formula for arbitrary orders and moments denoted by (6.3). We first conclude that the new state of the k-th order moment of a single variable is accomplished by taking the k-th power of its polynomial, followed by a summing up of all moments that occur as monomials in the new polynomial. The coefficients of the polynomial can be thought of the weights of each moment that contributes to its transport. Mixed moments, i.e. moments that consist of a product between different variables, are tracked accordingly. But this time the product has to be taken between all polynomials of the appropriate variables.

So, lets assume the six-dimensional phase space with canonical pairs (x, p_x), (y, p_y) and (z, p_z), where the variables are mapped by

$$\begin{aligned} x \mapsto \tilde{x} = g_1(\vec{q}, \vec{p}), \qquad & p_x \mapsto \tilde{p}_x = g_2(\vec{q}, \vec{p}), \\ y \mapsto \tilde{y} = g_3(\vec{q}, \vec{p}), \qquad & p_y \mapsto \tilde{p}_y = g_4(\vec{q}, \vec{p}), \\ z \mapsto \tilde{z} = g_5(\vec{q}, \vec{p}), \qquad & p_z \mapsto \tilde{p}_z = g_6(\vec{q}, \vec{p}), \end{aligned}$$

with g_i $(i = 1, \ldots, 6)$ being multivariate polynomials in $\vec{q} = (x, y, z)$ and $\vec{p} = (p_x, p_y, p_z)$. Then, the general formula to transport moments is

$$\left\langle \tilde{x}^i \tilde{p}_x^j \tilde{y}^k \tilde{p}_y^l \tilde{z}^m \tilde{p}_z^n \right\rangle = \left\langle g_1^i(\vec{q}, \vec{p}) \cdot g_2^j(\vec{q}, \vec{p}) \cdot g_3^k(\vec{q}, \vec{p}) \cdot g_4^l(\vec{q}, \vec{p}) \cdot g_5^m(\vec{q}, \vec{p}) \cdot g_6^n(\vec{q}, \vec{p}) \right\rangle \tag{6.8a}$$

$$= \lambda_0 \langle x \rangle + \ldots + \lambda_5 \langle p_z \rangle + \lambda_6 \left\langle x^2 \right\rangle + \ldots + \lambda_{26} \left\langle p_z^2 \right\rangle + \lambda_{27} \left\langle x^3 \right\rangle + \ldots \tag{6.8b}$$

$$= \sum_{\alpha} \Lambda_1^{\alpha} \sigma_1^{\alpha} + \sum_{\alpha,\beta} \Lambda_2^{\alpha\beta} \sigma_2^{\alpha\beta} + \sum_{\alpha,\beta,\gamma} \Lambda_3^{\alpha\beta\gamma} \sigma_3^{\alpha\beta\gamma} + \sum_{\alpha,\beta,\gamma,\delta} \Lambda_4^{\alpha\beta\gamma\delta} \sigma_4^{\alpha\beta\gamma\delta} + \ldots \tag{6.8c}$$

with exponents $i, j, k, l, m, n \in \mathbb{N}_0$, transport coefficients λ_r $(r \in \mathbb{N}_0)$ and tensor indices $\alpha, \beta, \gamma, \delta$. The k-th order tensor Λ_k in (6.8c) holds the coefficients of (6.8b). In case of Λ_2 this corresponds to

$$\Lambda_2 = \begin{pmatrix} \lambda_6 & \lambda_7 & \lambda_8 & \lambda_9 & \lambda_{10} & \lambda_{11} \\ & \lambda_{12} & \lambda_{13} & \lambda_{14} & \lambda_{15} & \lambda_{16} \\ & & \lambda_{17} & \lambda_{18} & \lambda_{19} & \lambda_{20} \\ & & & \lambda_{21} & \lambda_{22} & \lambda_{23} \\ & & & & \lambda_{24} & \lambda_{25} \\ & & & & & \lambda_{26} \end{pmatrix},$$

and therefore

$$\sum_{\alpha,\beta} \Lambda_2^{\alpha\beta} \sigma_2^{\alpha\beta} = \lambda_6 \left\langle x^2 \right\rangle + \lambda_7 \langle x p_x \rangle + \ldots + \lambda_{26} \left\langle p_z^2 \right\rangle.$$

Due to the fact that a multiplication of polynomials (6.8a) is again a polynomial and that an integral over a sum can be rewritten as a sum of integrals, verifies the correctness of above equation by intuition.
Thanks to the TPSA representation we're able to compute (6.8c) by simply iterating over all monomials of the polynomial and summing up all corresponding moments with respect to the monomial coefficients.

6.2.1.1 Programming Example

A small program verifies the above explained theory. We use a one-dimensional phase space (q, p) with the non-linear map

$$\mathcal{M}: \quad \begin{aligned} q &\mapsto 1 + qp + q^2, \\ p &\mapsto p^2 - \tfrac{1}{2} q. \end{aligned}$$

It generates N particles with coordinate q and momentum p being normally distributed with $\mathcal{N}_q(0, 0.25)$ and, respectively, $\mathcal{N}_p(0, 0.01)$. The moments are evaluated using the discretized variant of (6.7), i.e.

$$\left\langle q^i p^j \right\rangle = \frac{1}{N} \sum_{k=0}^{N-1} q^i p^j,$$

where $i, j \in \mathbb{N}_0$ are exponents again. In Tab. 6.1 are the results of Appendix G18 that maps either particles or moments. The fact that both methods return the same results confirms the correctness numerically.

moment	particle-based	moment-based
$\langle q^2 \rangle$	1.69089	1.69089
$\langle qp \rangle$	0.0117429	0.0117429
$\langle p^3 \rangle$	0.00178635	0.00178635
$\langle qp^2 \rangle$	0.109954	0.109954
$\langle q^2 p^3 \rangle$	0.00552552	0.00552552

Table 6.1: Results of Appendix G18 with input parameters $N = 10^6$ and seed 42. The second and third column are the results of a particle-based and, respectively, moment-based tracking.

7 Matched Moments

During one turn in a cyclotron the bunch changes continuously its shape due to focussing and defocussing forces. A distribution is called stationary if for any position s in the orbit the moments remain unchanged, i.e.

$$\left\langle x^i p_x^j y^k p_y^l z^m p_z^n \right\rangle (s) \equiv \left\langle x^i p_x^j y^k p_y^l z^m p_z^n \right\rangle (s+L) \quad \forall s \geq 0, \tag{7.1}$$

where L is the length of the orbit and $\left\langle x^i p_x^j y^k p_y^l z^m p_z^n \right\rangle$ specifies a general moment with superscripts i, j, k, l, m, $n \in \mathbb{N}_0$ denoting the occurrence of each dynamical variable. In [3] the estimates of the second order moments, i.e. any combination with $i+j+k+l+m+n=2$, are improved by using the fact that the eigenvectors of the stationary distribution are identical to the eigenvectors of the 6×6 transfer matrix. Through inserting user-defined bunch emittances as eigenvalues of the distribution the moments got constrained. The generalization of this approach to systems including non-linear effects would involve the solution of eigenvalue decompositions for tensors with degree $d > 2$. However, starting from the general definition (7.1), we obtain a more flexible method.

7.1 General Description

The definition of a stationary moment in equation (7.1) gives rise to write the task as a minimization problem where the difference of a moment between subsequent turns should be diminished, i.e.

$$\arg\min \frac{1}{2} \left|\left| \left\langle x^i p_x^j y^k p_y^l z^m p_z^n \right\rangle (s+L) - \left\langle x^i p_x^j y^k p_y^l z^m p_z^n \right\rangle (s) \right|\right|_2^2 ,$$

where $||\cdot||_2$ specifies the L_2-norm. The type of norm basically doesn't matter but the Euclidean norm is a common choice. The position s on the path where we try to minimize the difference is not relevant. This is motivated by the assumption that in case of matched moments at position s, the moments are also matched at $s + \Delta s$ for $\Delta s \ll 1$.
In the following we write the position s of the path as a subscript, i.e. $\langle \cdot \rangle_s$, for the sake of clarity. The values of the moments of the next cycle $s+L$ are available to us by transporting the current moments with the one turn transfer map $\mathcal{M}$. Though, we have a function for every moment

$$f_{s+L}\left(\langle x \rangle_s , \langle p_x \rangle_s , \ldots , \langle p_z \rangle_s , \left\langle x^2 \right\rangle_s , \langle x p_x \rangle_s , \ldots , \left\langle p_z^2 \right\rangle_s , \left\langle x^3 \right\rangle_s , \ldots \right) ,$$

that depends on all present moments. Because the phase space directions are normally coupled, the functions contain also moments of other orientations. Therefore, the minimization problem can't just be solved for every moment separately. The task can now be written in a more compact form as

$$\arg\min \frac{1}{2} ||A\vec{x}_s - \vec{x}_s||_2^2 , \tag{7.2}$$

where the rows of $A \in \mathbb{R}^{r \times r}$ store the coefficients of the polynomials that describe the transport of the r moments contained in $\vec{x}_s = \left(\langle x \rangle_s , \langle p_x \rangle_s , \ldots , \left\langle x^2 \right\rangle_s , \langle x p_x \rangle_s , \ldots , \left\langle x^3 \right\rangle_s , \ldots \right)^\top \in \mathbb{R}^{r \times 1}$. The matrix A and the vector $\vec{x}_s$ are known to us. The unknowns are the moments of the next

turn that are basically obtained through a matrix-vector multiplication, i.e. $\vec{x}_{s+L} = A\vec{x}_s$. Thus, another form of equation (7.2) is

$$\arg\min \frac{1}{2} ||\vec{x}_{s+L} - \vec{x}_s||_2^2 . \tag{7.3}$$

For a matched distribution, i.e.

$$\vec{x}_{s+L} \equiv \vec{x}_s \quad \forall s \in [0, L[,$$

equation (7.3) is minimal for any s. In that case the transfer map $\mathcal{M}$ and, respectively, the matrix A that depend on the moments, are stationary. If we assume that A represents exactly that mapping, we can rewrite (7.2) by

$$\arg\min \frac{1}{2} ||A\vec{x}_{s+L} - \vec{x}_s||_2^2 .$$

In order to ensure a physical solution we incorporate some constraints. In case of a matched distribution the emittances are constant. Therefore, we restrain the least squares method by [8, eq. 4.106]

$$\varepsilon_x = \sqrt{\langle x^2 \rangle \langle p_x^2 \rangle - \langle x p_x \rangle^2}, \qquad \varepsilon_y = \sqrt{\langle y^2 \rangle \langle p_y^2 \rangle - \langle y p_y \rangle^2}, \qquad \varepsilon_z = \sqrt{\langle z^2 \rangle \langle p_z^2 \rangle - \langle z p_z \rangle^2}, \tag{7.4}$$

where ε_x, ε_y, ε_z are the user-defined emittances. The non-linear constrained least squares problem looks then as

$$\arg\min \frac{1}{2} ||A\vec{x}_{s+L} - \vec{x}_s||_2^2 \quad \text{s.t.} \quad g_w(\vec{x}_{s+L}) = 0 \quad \forall w = x, y, z,$$

with

$$g_w(\vec{x}_{s+L}) = \sqrt{\langle w^2 \rangle_{s+L} \langle p_w^2 \rangle_{s+L} - \langle w p_w \rangle_{s+L}^2} - \varepsilon_w. \tag{7.5}$$

These conditions can be incorporated through Lagrange multipliers $\vec{\lambda}$ (see e.g. [27, p. 436]) where the Lagrangian is given by

$$\mathcal{L}(\vec{x}_{s+L}, \vec{\lambda}) = \frac{1}{2} ||A\vec{x}_{s+L} - \vec{x}_s||_2^2 + \vec{\lambda}^\top \vec{g}(\vec{x}_{s+L}) , \tag{7.6}$$

with $\vec{g} = (g_x, g_y, g_z)^\top$ as constraint vector. We solve this problem by setting the first derivative of the Lagrangian with respect to each parameter to zero. This yields following equations:

$$\frac{\partial \mathcal{L}}{\partial \vec{x}_{s+L}} = A^\top A\vec{x}_{s+L} - A^\top \vec{x}_s + J_g^\top \vec{\lambda} \stackrel{!}{=} \vec{0}, \qquad \frac{\partial \mathcal{L}}{\partial \vec{\lambda}} = \vec{g}(\vec{x}_{s+L}) \stackrel{!}{=} \vec{0}, \tag{7.7}$$

where

$$J_g = \begin{pmatrix} \nabla_{\vec{x}_{s+L}} g_x(\vec{x}_{s+L}) \\ \nabla_{\vec{x}_{s+L}} g_y(\vec{x}_{s+L}) \\ \nabla_{\vec{x}_{s+L}} g_z(\vec{x}_{s+L}) \end{pmatrix} \in \mathbb{R}^{3 \times r}. \tag{7.8}$$

The detailed calculation of those derivatives is given in Appendix F. The derivative of g_w ($w = x, y, z$) with respect to $\vec{x}_{s+L}$ is

$$\nabla_{\vec{x}_{s+L}} g_w = \begin{cases} \frac{\langle p_w^2 \rangle}{2\sqrt{\langle w^2 \rangle \langle p_w^2 \rangle - \langle w p_w \rangle^2}} & \text{if} \quad \frac{\mathrm{d}}{\mathrm{d}\langle w^2 \rangle}, \\ \frac{\langle w^2 \rangle}{2\sqrt{\langle w^2 \rangle \langle p_w^2 \rangle - \langle w p_w \rangle^2}} & \text{if} \quad \frac{\mathrm{d}}{\mathrm{d}\langle p_w^2 \rangle}, \\ \frac{-\langle w p_w \rangle}{\sqrt{\langle w^2 \rangle \langle p_w^2 \rangle - \langle w p_w \rangle^2}} & \text{if} \quad \frac{\mathrm{d}}{\mathrm{d}\langle w p_w \rangle}, \\ 0 & \text{otherwise.} \end{cases} \tag{7.9}$$

In order to obtain a numerical solution of (7.7), we make use of the Newton-Raphson method. In the following section we describe the method with focus on our problem.

7.2 Newton-Raphson Method

The Newton-Raphson method solves the problem of finding a root of a system of equations

$$\vec{F}(\vec{y}) = \vec{0},$$

by following iteration scheme:

$$\vec{y}_{k+1} = \vec{y}_k - J_F(\vec{y}_k)^{-1}\vec{F}(\vec{y}_k) \quad (k \geq 0), \tag{7.10}$$

where $J_F(\vec{y})$ is the Jacobian matrix of $\vec{F}$.
In each iteration step a linear system of equations has to be solved. Thus, the Jacobian matrix has to be non-singular such that the solution is unique. In our case the non-linear function is given by (7.7), i.e.

$$\vec{F} = \begin{pmatrix} A^\top A\vec{x}_{s+L} - A^\top\vec{x}_s + J_g^\top\vec{\lambda} \\ \vec{g}(\vec{x}_{s+L}) \end{pmatrix} \in \mathbb{R}^{(r+3)\times 1}, \tag{7.11}$$

with J_g defined in (7.8) and Lagrange multipliers $\vec{\lambda}$. Therefore, the Jacobian matrix is

$$J_F = \nabla_{\vec{x}_{s+L},\vec{\lambda}}\vec{F} = \begin{pmatrix} A^\top A + H_g(\vec{x}_{s+L},\vec{\lambda}) & J_g^\top \\ J_g & 0_{3\times 3} \end{pmatrix} \in \mathbb{R}^{(r+3)\times(r+3)}, \tag{7.12}$$

with Hessian $H_g(\vec{x}_{s+L},\vec{\lambda}) = \nabla_{\vec{x}_{s+L}}(J_g^\top\vec{\lambda}) \in \mathbb{R}^{r\times r}$ (see Appendix F). After applying the Newton-Raphson method (7.10) we obtain the new estimate of the moments in the vector $\vec{y} = (\vec{x}_{s+L},\vec{\lambda})^\top$. In case of a singular Jacobian matrix J_F there's no solution.

7.3 Linear Matching Example

On the basis of (1.5) and a linear space charge approximation, the polynomials of mapping the dynamical variables by one turn are given by

$$\begin{aligned}
x &\mapsto a_{11}x + a_{12}p_x + a_{15}z + a_{16}p_z, & p_x &\mapsto a_{21}x + a_{22}p_x + a_{25}z + a_{26}p_z,\\
y &\mapsto a_{33}y + a_{34}p_y, & p_y &\mapsto a_{43}y + a_{44}p_y,\\
z &\mapsto a_{51}x + a_{52}p_x + a_{55}z + a_{56}p_z, & p_z &\mapsto a_{61}x + a_{62}p_x + a_{65}z + a_{66}p_z,
\end{aligned}$$

where a_{nm} represents the element (n,m) of the 6×6 transfer matrix. By applying (6.8) for all second order moments, we obtain the transport equations from the initial state i to the final state f (see Appendix G5):

$$\begin{aligned}
\langle x^2\rangle_f &= a_{11}^2\langle x^2\rangle_i + 2a_{11}a_{12}\langle xp_x\rangle_i + 2a_{11}a_{15}\langle xz\rangle_i + 2a_{11}a_{16}\langle xp_z\rangle_i + a_{12}^2\langle p_x^2\rangle_i\\
&\quad + 2a_{12}a_{15}\langle p_xz\rangle_i + 2a_{12}a_{16}\langle p_xp_z\rangle_i + a_{15}^2\langle z^2\rangle_i + 2a_{15}a_{16}\langle zp_z\rangle_i + a_{16}^2\langle p_z^2\rangle_i,\\
\langle xp_x\rangle_f &= a_{11}a_{21}\langle x^2\rangle_i + (a_{11}a_{22}+a_{12}a_{21})\langle xp_x\rangle_i + (a_{15}a_{21}+a_{11}a_{25})\langle xz\rangle_i\\
&\quad + (a_{16}a_{21}+a_{11}a_{26})\langle xp_z\rangle_i + a_{12}a_{22}\langle p_x^2\rangle_i + (a_{15}a_{22}+a_{12}a_{25})\langle p_xz\rangle_i\\
&\quad + (a_{16}a_{22}+a_{12}a_{26})\langle p_xp_z\rangle_i + a_{15}a_{25}\langle z^2\rangle_i + (a_{16}a_{25}+a_{15}a_{26})\langle zp_z\rangle_i + a_{16}a_{26}\langle p_z^2\rangle_i,
\end{aligned}$$

$$
\begin{aligned}
\langle xy\rangle_f &= a_{11}a_{33}\langle xy\rangle_i + a_{11}a_{34}\langle xp_y\rangle_i + a_{12}a_{33}\langle p_x y\rangle_i + a_{12}a_{34}\langle p_x p_y\rangle_i + a_{15}a_{33}\langle yz\rangle_i \\
&\quad + a_{16}a_{33}\langle yp_z\rangle_i + a_{15}a_{34}\langle p_y z\rangle_i + a_{16}a_{34}\langle p_y p_z\rangle_i , \\
\langle xp_y\rangle_f &= a_{11}a_{43}\langle xy\rangle_i + a_{11}a_{44}\langle xp_y\rangle_i + a_{12}a_{43}\langle p_x y\rangle_i + a_{12}a_{44}\langle p_x p_y\rangle_i + a_{15}a_{43}\langle yz\rangle_i \\
&\quad + a_{16}a_{43}\langle yp_z\rangle_i + a_{15}a_{44}\langle p_y z\rangle_i + a_{16}a_{44}\langle p_y p_z\rangle_i , \\
\langle xz\rangle_f &= a_{11}a_{51}\langle x^2\rangle_i + (a_{12}a_{51}+a_{11}a_{52})\langle xp_x\rangle_i + (a_{15}a_{51}+a_{11}a_{55})\langle xz\rangle_i \\
&\quad + (a_{16}a_{51}+a_{11}a_{56})\langle xp_z\rangle_i + a_{12}a_{52}\langle p_x^2\rangle_i + (a_{15}a_{52}+a_{12}a_{55})\langle p_x z\rangle_i \\
&\quad + (a_{16}a_{52}+a_{12}a_{56})\langle p_x p_z\rangle_i + a_{15}a_{55}\langle z^2\rangle_i + (a_{16}a_{55}+a_{15}a_{56})\langle zp_z\rangle_i + a_{16}a_{56}\langle p_z^2\rangle_i , \\
\langle xp_z\rangle_f &= a_{11}a_{61}\langle x^2\rangle_i + (a_{12}a_{61}+a_{11}a_{62})\langle xp_x\rangle_i + (a_{15}a_{61}+a_{11}a_{65})\langle xz\rangle_i \\
&\quad + (a_{16}a_{61}+a_{11}a_{66})\langle xp_z\rangle_i + a_{12}a_{62}\langle p_x^2\rangle_i + (a_{15}a_{62}+a_{12}a_{65})\langle p_x z\rangle_i \\
&\quad + (a_{16}a_{62}+a_{12}a_{66})\langle p_x p_z\rangle_i + a_{15}a_{65}\langle z^2\rangle_i + (a_{16}a_{65}+a_{15}a_{66})\langle zp_z\rangle_i + a_{16}a_{66}\langle p_z^2\rangle_i , \\
\langle y^2\rangle_f &= a_{33}^2\langle y^2\rangle_i + 2a_{33}a_{34}\langle yp_y\rangle_i + a_{34}^2\langle p_y^2\rangle_i , \\
\langle yp_y\rangle_f &= a_{33}a_{43}\langle y^2\rangle_i + (a_{34}a_{43}+a_{33}a_{44})\langle yp_y\rangle_i + a_{34}a_{44}\langle p_y^2\rangle_i , \\
\langle p_y^2\rangle_f &= a_{43}^2\langle y^2\rangle_i + 2a_{43}a_{44}\langle yp_y\rangle_i + a_{44}^2\langle p_y^2\rangle_i ,
\end{aligned}
$$

where the moments $\langle p_x^2\rangle$, $\langle p_x y\rangle$, $\langle p_x p_y\rangle$, $\langle p_x z\rangle$, $\langle p_x p_z\rangle$, $\langle yz\rangle$, $\langle yp_z\rangle$, $\langle p_y z\rangle$, $\langle p_y p_z\rangle$, $\langle z^2\rangle$, $\langle zp_z\rangle$ and $\langle p_z^2\rangle$ are transferred as one of the appropriate moments in horizontal direction. The vector of unknowns $\vec{x} \in \mathbb{R}^{21\times 1}$ is therefore given by

$$
\vec{x} = \left(\langle x^2\rangle, \langle xp_x\rangle, \ldots, \langle p_x^2\rangle, \ldots, \langle y^2\rangle, \ldots, \langle z^2\rangle, \langle zp_z\rangle, \langle p_z^2\rangle\right)^\top .
$$

From the transport equations of the second order moments, we get the non-zero pattern of the matrix $A \in \mathbb{R}^{21\times 21}$ of (7.6). Due to reasons of clarity we just use the symbol $\star$ to represent the non-zero elements, i.e.

$$
A = \begin{pmatrix}
\star & \star & 0 & 0 & \star & \star & \star & 0 & 0 & \star & \star & 0 & 0 & 0 & 0 & 0 & 0 & \star & \star & \star \\
\star & \star & 0 & 0 & \star & \star & \star & 0 & 0 & \star & \star & 0 & 0 & 0 & 0 & 0 & 0 & \star & \star & \star \\
0 & 0 & \star & \star & 0 & 0 & 0 & \star & \star & 0 & 0 & 0 & 0 & \star & \star & 0 & \star & \star & 0 & 0 & 0 \\
0 & 0 & \star & \star & 0 & 0 & 0 & \star & \star & 0 & 0 & 0 & 0 & \star & \star & 0 & \star & \star & 0 & 0 & 0 \\
\star & \star & 0 & 0 & \star & \star & \star & 0 & 0 & \star & \star & 0 & 0 & 0 & 0 & 0 & 0 & 0 & \star & \star & \star \\
\star & \star & 0 & 0 & \star & \star & \star & 0 & 0 & \star & \star & 0 & 0 & 0 & 0 & 0 & 0 & 0 & \star & \star & \star \\
\star & \star & 0 & 0 & \star & \star & \star & 0 & 0 & \star & \star & 0 & 0 & 0 & 0 & 0 & 0 & 0 & \star & \star & \star \\
0 & 0 & \star & \star & 0 & 0 & 0 & \star & \star & 0 & 0 & 0 & 0 & \star & \star & 0 & \star & \star & 0 & 0 & 0 \\
0 & 0 & \star & \star & 0 & 0 & 0 & \star & \star & 0 & 0 & 0 & 0 & \star & \star & 0 & \star & \star & 0 & 0 & 0 \\
\star & \star & 0 & 0 & \star & \star & \star & 0 & 0 & \star & \star & 0 & 0 & 0 & 0 & 0 & 0 & 0 & \star & \star & \star \\
\star & \star & 0 & 0 & \star & \star & \star & 0 & 0 & \star & \star & 0 & 0 & 0 & 0 & 0 & 0 & 0 & \star & \star & \star \\
0 & 0 & 0 & 0 & 0 & 0 & 0 & 0 & 0 & 0 & 0 & \star & \star & 0 & 0 & \star & 0 & 0 & 0 & 0 & 0 \\
0 & 0 & 0 & 0 & 0 & 0 & 0 & 0 & 0 & 0 & 0 & \star & \star & 0 & 0 & \star & 0 & 0 & 0 & 0 & 0 \\
0 & 0 & \star & \star & 0 & 0 & 0 & \star & \star & 0 & 0 & 0 & 0 & \star & \star & 0 & \star & \star & 0 & 0 & 0 \\
0 & 0 & \star & \star & 0 & 0 & 0 & \star & \star & 0 & 0 & 0 & 0 & \star & \star & 0 & \star & \star & 0 & 0 & 0 \\
0 & 0 & 0 & 0 & 0 & 0 & 0 & 0 & 0 & 0 & 0 & \star & \star & 0 & 0 & \star & 0 & 0 & 0 & 0 & 0 \\
0 & 0 & \star & \star & 0 & 0 & 0 & \star & \star & 0 & 0 & 0 & 0 & \star & \star & 0 & \star & \star & 0 & 0 & 0 \\
0 & 0 & \star & \star & 0 & 0 & 0 & \star & \star & 0 & 0 & 0 & 0 & \star & \star & 0 & \star & \star & 0 & 0 & 0 \\
\star & \star & 0 & 0 & \star & \star & \star & 0 & 0 & \star & \star & 0 & 0 & 0 & 0 & 0 & 0 & 0 & \star & \star & \star \\
\star & \star & 0 & 0 & \star & \star & \star & 0 & 0 & \star & \star & 0 & 0 & 0 & 0 & 0 & 0 & 0 & \star & \star & \star \\
\star & \star & 0 & 0 & \star & \star & \star & 0 & 0 & \star & \star & 0 & 0 & 0 & 0 & 0 & 0 & 0 & \star & \star & \star
\end{pmatrix} .
$$

Its structure shows that the matrix is symmetric concerning the position of the non-zero elements. The entries, however, aren't equal. Consequently, the symmetric matrix $A^\top A$ indicates the identical pattern. The Jacobian matrix $J_g \in \mathbb{R}^{3\times 21}$ on the other hand has following non-zero pattern:

$$J_g = \begin{pmatrix} \star & \star & 0 & 0 & 0 & 0 & \star & 0 & 0 & 0 & 0 & 0 & 0 & 0 & 0 & 0 & 0 & 0 & 0 & 0 & 0 \\ 0 & 0 & 0 & 0 & 0 & 0 & 0 & 0 & 0 & 0 & 0 & \star & \star & 0 & 0 & \star & 0 & 0 & 0 & 0 & 0 \\ 0 & 0 & 0 & 0 & 0 & 0 & 0 & 0 & 0 & 0 & 0 & 0 & 0 & 0 & 0 & 0 & 0 & 0 & \star & \star & \star \end{pmatrix},$$

with values obtained through (7.9). The Hessian $H_g \in \mathbb{R}^{21\times 21}$ looks according to Appendix F like

$$H_g = \begin{pmatrix}
\star & \star & 0 & 0 & 0 & 0 & \star & 0 & 0 & 0 & 0 & 0 & 0 & 0 & 0 & 0 & 0 & 0 & 0 & 0 & 0 \\
\star & \star & 0 & 0 & 0 & 0 & \star & 0 & 0 & 0 & 0 & 0 & 0 & 0 & 0 & 0 & 0 & 0 & 0 & 0 & 0 \\
0 & 0 & 0 & 0 & 0 & 0 & 0 & 0 & 0 & 0 & 0 & 0 & 0 & 0 & 0 & 0 & 0 & 0 & 0 & 0 & 0 \\
0 & 0 & 0 & 0 & 0 & 0 & 0 & 0 & 0 & 0 & 0 & 0 & 0 & 0 & 0 & 0 & 0 & 0 & 0 & 0 & 0 \\
0 & 0 & 0 & 0 & 0 & 0 & 0 & 0 & 0 & 0 & 0 & 0 & 0 & 0 & 0 & 0 & 0 & 0 & 0 & 0 & 0 \\
0 & 0 & 0 & 0 & 0 & 0 & 0 & 0 & 0 & 0 & 0 & 0 & 0 & 0 & 0 & 0 & 0 & 0 & 0 & 0 & 0 \\
\star & \star & 0 & 0 & 0 & 0 & \star & 0 & 0 & 0 & 0 & 0 & 0 & 0 & 0 & 0 & 0 & 0 & 0 & 0 & 0 \\
0 & 0 & 0 & 0 & 0 & 0 & 0 & 0 & 0 & 0 & 0 & 0 & 0 & 0 & 0 & 0 & 0 & 0 & 0 & 0 & 0 \\
0 & 0 & 0 & 0 & 0 & 0 & 0 & 0 & 0 & 0 & 0 & 0 & 0 & 0 & 0 & 0 & 0 & 0 & 0 & 0 & 0 \\
0 & 0 & 0 & 0 & 0 & 0 & 0 & 0 & 0 & 0 & 0 & 0 & 0 & 0 & 0 & 0 & 0 & 0 & 0 & 0 & 0 \\
0 & 0 & 0 & 0 & 0 & 0 & 0 & 0 & 0 & 0 & 0 & 0 & 0 & 0 & 0 & 0 & 0 & 0 & 0 & 0 & 0 \\
0 & 0 & 0 & 0 & 0 & 0 & 0 & 0 & 0 & 0 & 0 & \star & \star & 0 & 0 & \star & 0 & 0 & 0 & 0 & 0 \\
0 & 0 & 0 & 0 & 0 & 0 & 0 & 0 & 0 & 0 & 0 & \star & \star & 0 & 0 & \star & 0 & 0 & 0 & 0 & 0 \\
0 & 0 & 0 & 0 & 0 & 0 & 0 & 0 & 0 & 0 & 0 & 0 & 0 & 0 & 0 & 0 & 0 & 0 & 0 & 0 & 0 \\
0 & 0 & 0 & 0 & 0 & 0 & 0 & 0 & 0 & 0 & 0 & 0 & 0 & 0 & 0 & 0 & 0 & 0 & 0 & 0 & 0 \\
0 & 0 & 0 & 0 & 0 & 0 & 0 & 0 & 0 & 0 & 0 & \star & \star & 0 & 0 & \star & 0 & 0 & 0 & 0 & 0 \\
0 & 0 & 0 & 0 & 0 & 0 & 0 & 0 & 0 & 0 & 0 & 0 & 0 & 0 & 0 & 0 & 0 & 0 & 0 & 0 & 0 \\
0 & 0 & 0 & 0 & 0 & 0 & 0 & 0 & 0 & 0 & 0 & 0 & 0 & 0 & 0 & 0 & 0 & 0 & 0 & 0 & 0 \\
0 & 0 & 0 & 0 & 0 & 0 & 0 & 0 & 0 & 0 & 0 & 0 & 0 & 0 & 0 & 0 & 0 & 0 & \star & \star & \star \\
0 & 0 & 0 & 0 & 0 & 0 & 0 & 0 & 0 & 0 & 0 & 0 & 0 & 0 & 0 & 0 & 0 & 0 & \star & \star & \star \\
0 & 0 & 0 & 0 & 0 & 0 & 0 & 0 & 0 & 0 & 0 & 0 & 0 & 0 & 0 & 0 & 0 & 0 & \star & \star & \star
\end{pmatrix}.$$

7.4 Non-Linear Matching Example

In this section we give a short example where we perturb the Gaussian distribution by a non-linear term in horizontal direction. In [28, eq. 12] the usage of higher order terms in the Gaussian distribution is mentioned. However, we use an artificial third order term that might have no physical meaning.

7.4.1 Assumptions

Since our program is based on the "Truncated-Power-Series-Algebra" that assumes small deviations from the reference particle, we still assume a centered beam, i.e. $\langle x\rangle = \langle y\rangle = \langle z\rangle = 0$. For our example we suppose that $\langle E_x\rangle = \langle E_y\rangle = \langle E_z\rangle = 0$ holds true as well. This example should only cover moments up to third order that's why we take all moments of fourth order and higher equal to zero.

7.4.2 Distribution Perturbation

In our example we perturb the charge distribution by a fixed non-linear term of third order, i.e.

$$f(x,y,z) = f_G\left(\frac{x^2}{a_x^2}+\frac{y^2}{a_y^2}+\frac{z^2}{a_z^2}\right)\cdot\exp\left[-k\left\langle x^3\right\rangle\frac{x^3}{a_x^3}\right], \tag{7.13}$$

where f_G represents the Gaussian distribution as in (4.6), k is some constant that specifies the percentage of influence and a_w ($w = x, y, z$) are the semi-principal axes as before. As already mentioned, we do not claim that it has some physical meaning or relevance. However, it should give us a first insight into non-linear matching.

7.4.3 Electric Field Approximation

In order to include higher order moments into the space charge maps we have to approximate the electric field by a polynomial of at least degree 2.
Due to the assumptions made in Sec. 7.4.1 the linear system of equations (4.11) is given in each direction by

$$\begin{pmatrix}\langle 1\rangle & 0 & \langle w^2\rangle\\ 0 & \langle w^2\rangle & \langle w^3\rangle\\ \langle w^2\rangle & \langle w^3\rangle & 0\end{pmatrix}\cdot\begin{pmatrix}c_{0,w}\\ c_{1,w}\\ c_{2,w}\end{pmatrix}=\begin{pmatrix}0\\ \langle E_w w\rangle\\ \langle E_w w^2\rangle\end{pmatrix},$$

with solution (see Appendix G6)

$$\begin{aligned}
c_{0,w} &= \frac{\langle w^2\rangle\cdot\left[\langle w^2\rangle\langle w^2E_w\rangle-\langle w^3\rangle\langle wE_w\rangle\right]}{\langle w^2\rangle^3+\langle w^3\rangle^2},\\
c_{1,w} &= \frac{\langle w^2\rangle^2\langle wE_w\rangle+\langle w^3\rangle\langle w^2E_w\rangle}{\langle w^2\rangle^3+\langle w^3\rangle^2},\\
c_{2,w} &= \frac{\langle w^3\rangle\langle wE_w\rangle-\langle w^2\rangle\langle w^2E_w\rangle}{\langle w^2\rangle^3+\langle w^3\rangle^2}.
\end{aligned}$$

In contrast to the Gaussian without perturbation, the coefficients of the monomials with even power, i.e. $c_{0,w}$ and $c_{2,w}$, are non-zero as well.

7.4.4 Additional Constraints in Lagrangian

The second order approximation of the electric field requires the tracking of first, second and third order moments. Hence, we have to make sure that physics and the assumptions in Sec. 7.4.1 are still satisfied after the Newton-Raphson method. We accomplish that by additional Lagrange multipliers $\vec{\psi}\in\mathbb{R}^{6\times 1}$. So, the Lagrangian of (7.6) gets slightly modified to

$$\mathcal{L}(\vec{x}_{s+L},\vec{\lambda},\vec{\psi}) = \frac{1}{2}\,||A\vec{x}_{s+L}-\vec{x}_s||_2^2+\vec{\lambda}^\top\vec{g}\,(\vec{x}_{s+L})+\vec{\psi}^\top\vec{h}(\vec{x}_{s+L}),$$

with

$$\vec{h}(\vec{x}_{s+L}) := \begin{pmatrix}\langle x\rangle_{s+L}\\ \langle p_x\rangle_{s+L}\\ \langle y\rangle_{s+L}\\ \langle p_y\rangle_{s+L}\\ \langle z\rangle_{s+L}\\ \langle p_z\rangle_{s+L}\end{pmatrix}.$$

Hence, the vector in (7.11) extends to

$$\vec{F} = \begin{pmatrix} A^\top A\vec{x}_{s+L} - A^\top \vec{x}_s + J_g^\top \vec{\lambda} + J_h^\top \vec{\psi} \\ \vec{g}(\vec{x}_{s+L}) \\ \vec{h}(\vec{x}_{s+L}) \end{pmatrix} \in \mathbb{R}^{(r+9)\times 1},$$

where the Jacobian is given by

$$J_F = \nabla_{\vec{x}_{s+L},\vec{\lambda},\vec{\psi}} \vec{F} = \begin{pmatrix} A^\top A + H_g(\vec{x}_{s+L},\vec{\lambda}) + H_h(\vec{x}_{s+L},\vec{\psi}) & J_g^\top & J_h^\top \\ J_g & 0_{3\times 3} & 0_{3\times 6} \\ J_h & 0_{6\times 3} & 0_{6\times 6} \end{pmatrix} \in \mathbb{R}^{(r+9)\times(r+9)}.$$

The Hessian $H_h(\vec{x}_{s+L},\vec{\psi})$ is a $r \times r$ zero-matrix and the Jacobian matrix of the constraint is $J_h = \begin{pmatrix} I_{6\times 6} & 0_{6\times(r-6)} \end{pmatrix}$. It has to be mentioned that the vector $\vec{x}_s$ now also contains the moment $\langle 1 \rangle$. The non-zero pattern of the coefficient matrix A is indicated in Fig. 7.1.

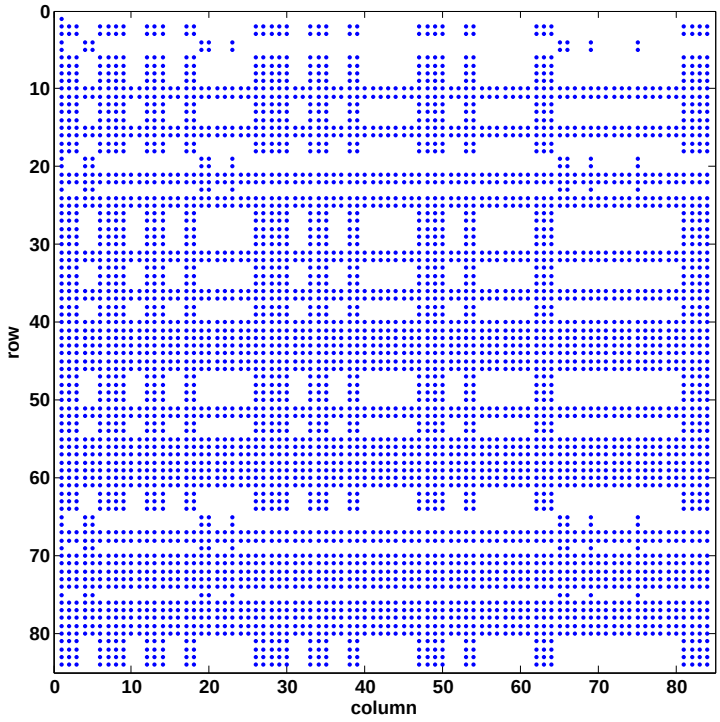

Figure 7.1: Non-zero pattern (#non-zeros: 4641) of coefficient matrix $A \in \mathbb{R}^{84\times 84}$. It stores the coefficients of the polynomials to transport first, second and third order moments.

It basically shows that moments of higher order are also influenced by moments of lower order, and vice versa. Since the vertical direction is decoupled from the horizontal and longitudinal direction, the coefficient matrix contains some bigger "gaps". It's clear that the matrix is more dense the more couplings between the directions exist.
In Sec. 9.6 we show results where we tried to match moments based on this example.

8 Implementation

8.1 C/C++ Libraries

The implementation is based on following libraries:

- DA library (AMAS group at PSI),
- Boost library [20],
- Cubature (version: 1.0.2) [24].

In some programming examples we make also use of the usual GSL library [21].

8.2 Initial Source Code Generalizations

The program of [7] consists of five classes: ClosedOrbitFinder, SigmaGenerator, RDM, MapGenerator and MagneticField. It has also a namespace physics that defines constants.
This section discusses all source code changes that are initially done in order to generalize the program.
In a first step we removed the RDM-class. It was used to decouple the 4×4 transfer matrix, i.e. without vertical direction, in order to obtain better estimates of the searched stationary moments. Although this technique could probably be extended to higher orders, we replaced it by a standard eigenvalue decomposition solver that diagonalized the whole 6×6 transfer matrix.
Further, we generalized the implementation of the map construction. Before, the transport matrices of the space charge and magnets of the cyclotron were hard-coded. Now, the MapGenerator-class is able to handle any Hamiltonian as a function and generates a map to arbitrary order according to formula (3.1) and based on the provided DA library (see Sec. 8.5.4).
These changes are the fundament in order to incorporate the generalizations for the non-linear theory.

8.3 Data Structures

In [7] the moments are stored in a 6×6 matrix representing the second order moment matrix σ_2. In order to keep track of other moments too, we changed the underlying data structure completely. Since the complexity of the task grows as illustrated in Fig. 2.1, a fast insert is reasonable. Additionally, we would like to have random access in order to get the second order moments. These are needed in the computation of the space charge maps and in the constraints of the Newton-Raphson method. That's why we decided to store all moments in a STL deque where they are kept in increasing order, i.e.

$$\langle x \rangle, \langle p_x \rangle, \ldots, \langle p_z \rangle, \langle x^2 \rangle, \langle x p_x \rangle, \ldots, \langle p_z^2 \rangle, \langle x^3 \rangle, \langle x^2 p_x \rangle, \ldots, \langle x^2 p_z \rangle, \ldots$$

Due to the trajectory discretization we store all moments for every step. For this purpose we chose a STL vector. Hence, the memory to store for example every moment up to fourth order (209 moments, see Fig. 2.1) as a double, i.e. 8 B, with 10^3 trajectory steps is

$$8 \cdot 209 \cdot 10^3 \text{ B} = 1\,672\,000 \text{ B} \approx 1.6 \text{ MB}.$$

On the other hand, a particle-based simulation in the six-dimensional phase space that needs approximately the same amount of memory could track

$$\frac{1\,672\,000\ \mathrm{B}}{6 \cdot 8\ \mathrm{B}} = 34\,833.\overline{3} \approx 34\,833$$

particles. Such a simulation would give not reliable statistics.
All map manipulations are performed using the DA library where a map is hold in a FVps (fixed vector power series) object. This class contains all necessary operations, e.g. the Lie transformation (3.1), that are essential in our computations.
Our Newton-Raphson method implementation is based on the provided containers and functions of uBLAS that is part of the Boost library.

8.4 Class Diagram

The project got complemented with additional classes: Moment, MomentTracker, SpaceCharge and LSE. The complete class structure is shown in Fig. 8.1. The class LSE provides a function to solve a linear system of equations. It simply combines several functions of the uBLAS package that is part of the Boost library. This functionality is applied in the class SpaceCharge to get the coefficients of the electric field approximation according to (4.11). The class SpaceCharge itself is used to compute transfer maps to arbitrary order.
As the name implies, the class MomentTracker provides methods for tracking moments. It inherits all public members of the class Moment that includes functions to compute general moments of the form (6.7). Moments are either tracked by evaluating all required moments through integration or by passing all moments to the function as argument. We apply the latter approach in the class SigmaGenerator to update the moments of each trajectory.
Some physical constants that are used during the computation are all defined in the namespace physics, where we differ between SI units and natural units, i.e. $c = 1$, $q = 1$ e.

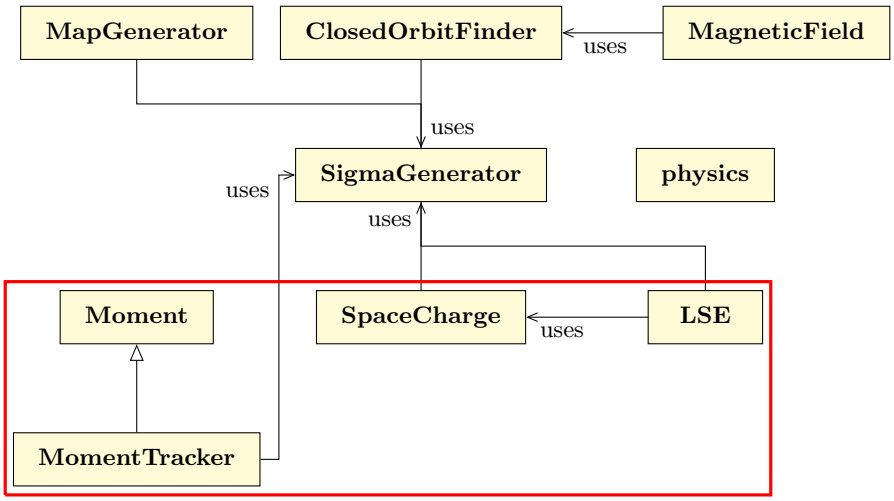

Figure 8.1: UML diagram. All classes in the box (red) are added to the implementation of [7]. A more detailed diagram of the already existed classes can be found in [7, ch. 4.1]. The library dependence on GSL (Cubature), DA and Boost isn't indicated. A better overview of the functionalities of all classes is provided by our Doxygen.

8.5 Source Code Details

In this section we discuss some program details with small code fragments. We focus on essential steps in the process of finding a matched distribution, e.g. initialization and update of moments.

8.5.1 Choice of Semi-Principal Axes

The choice of the semi-principal axes depends on the particle distribution. As written in [8, eq. 11.34], the semi-principal axes relate to the bunch size in case of a uniform distribution by

$$a_x = \sqrt{5\,\langle x^2\rangle}, \qquad a_y = \sqrt{5\,\langle y^2\rangle}, \qquad a_z = \sqrt{5\,\langle z^2\rangle}. \tag{8.1}$$

On the assumption of a Gaussian distribution we apply [8, eq. 4.107], i.e.

$$a_x = \sqrt{\langle x^2\rangle}, \qquad a_y = \sqrt{\langle y^2\rangle}, \qquad a_z = \sqrt{\langle z^2\rangle}.$$

8.5.2 Number of Particles

The relation given in [8, p. 372] states that the number of particles of a bunch is proportional to the average current:

$$N = \frac{I\lambda}{cq},$$

with wavelength λ. The wavelength, on the other hand, can be computed by [3, p. 7]

$$\lambda = \frac{2\pi c}{\omega_o N_h},$$

where ω_o is the nominal orbital frequency and N_h the harmonic number of the cyclotron. Therefore, the number of particles is given by

$$N = \left\lceil \frac{2\pi I}{q\omega_o N_h} \right\rceil.$$

In order to obtain no floating point values we round the fraction to the next higher integer.

8.5.3 Initialization of the Higher Order Moments

In chapter VIII of [3, p. 6 - 7] are formulas derived that compute the second order moments of a spherical beam. Based on this approach we could derive formulas that describe physical meaningful starting values for other moments. Since our goal is to track moments of arbitrary order this is not general enough. Instead, one could initialize the second order moments as before and then apply the moments $\langle x^2\rangle$, $\langle p_x^2\rangle$, $\langle y^2\rangle$, $\langle p_y^2\rangle$, $\langle z^2\rangle$, $\langle p_z^2\rangle$ to evaluate arbitrary moments (6.7) by integration.
We decided to keep the implementation of [7] where the second order moments are initialized using the assumption of a spherical beam that is described in [3, p. 6 - 7]. We initialize, however, all higher order moments with "random" numbers. Depending on the pseudo random number generator, seed and range, this might then yield different stationary distributions.

8.5.4 Map Generation from a Hamiltonian

Originally, the class MapGenerator contained the linear focussing and defocussing matrices hard-coded. Thanks to the DA library that includes functions to compute (3.1), we're able to evaluate maps to arbitrary order for any Hamiltonian. We obtain that by defining a Hamiltonian as a λ-expressions (see e.g. [30]). The only requirement on this expression is that the return-type is a DA object.
In Lst. 8.1 is a code snippet that shows the main part of the computation of a drift map (full example in Appendix G19). It is based on the Hamiltonian given by [31, eq. 39], i.e.

$$H = \frac{\delta}{\beta_0} - \sqrt{\left(\frac{1}{\beta_0} + \delta\right)^2 - p_x^2 - p_y^2 - \frac{1}{\beta_0^2\gamma_0^2}},$$

with transfer matrix [31, eq. 45]

$$M_{drift}(s = L) = \begin{pmatrix} 1 & L & 0 & 0 & 0 & 0 \\ 0 & 1 & 0 & 0 & 0 & 0 \\ 0 & 0 & 1 & L & 0 & 0 \\ 0 & 0 & 0 & 1 & 0 & 0 \\ 0 & 0 & 0 & 0 & 1 & \frac{L}{\beta_0^2\gamma_0^2} \\ 0 & 0 & 0 & 0 & 0 & 1 \end{pmatrix}. \tag{8.2}$$

In case of protons, $L = 1$ m and $E = 0.590$ GeV ($\beta_0\gamma_0 \approx 1.28571$) the test program yields a linear map stored in a DA vector as shown in Output 8.1. It is identical to the result obtained with (8.2).

```
1  // define Hamiltonian for the drift
2  Hamiltonian H = [&](double bet0, double gam0) {
3    return (delta/bet0) - sqrt((1./bet0 + delta)*(1./bet0 + delta) - (px*px) - (py*py) -
         1./(bet0*bet0*gam0*gam0), order);
4  };
5
6  std::cout << H(bet0,gam0) << std::endl;
7
8  // generate linear drift map
9  Map_type mapgen;
10 std::cout << mapgen.generateMap(H(bet0,gam0), L, 1) << std::endl;
```

Listing 8.1: Computation of the drift map in the linear approximation.

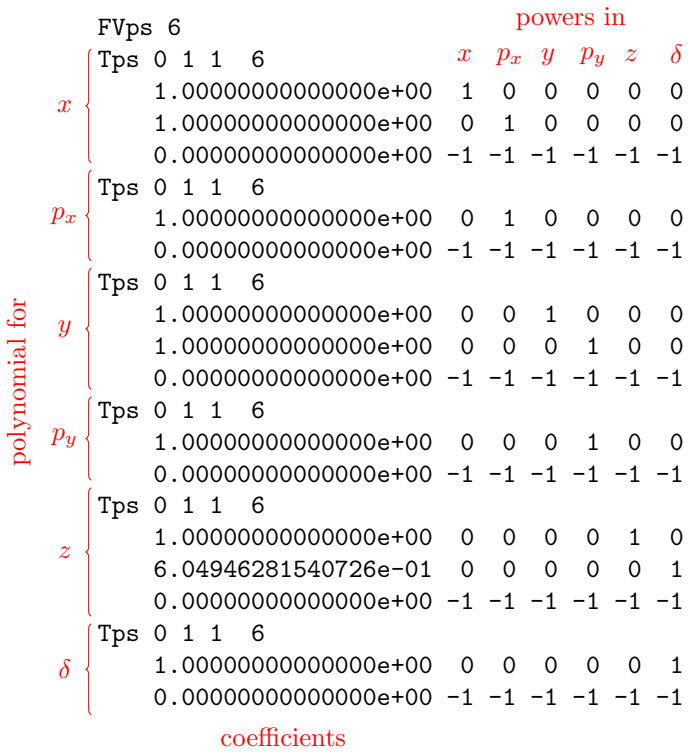

Output 8.1: Linear drift map obtained by Appendix G19 with a drift length of $L = 1$ m, energy 0.590 GeV and particle rest mass of 0.938272 GeV (i.e. protons).

8.5.5 Updating Moments

Because the one turn transfer map isn't decoupled, we apply the projected emittances in the Newton-Raphson method in order to compute the moments of the initial trajectory element. We get them by computing (7.4) using the initial guesses of the second order moments. In the model of [7], however, the user-defined emittances are basically used as eigenvalues directly.
It might happen that the initial guess is far away from the solution. In this case the Newton-Raphson method doesn't find a solution. That's why we restart the procedure after 50 Newton steps with Lagrange multipliers that are ten times bigger than the initial value of the previous attempt. At the beginning of the method they are all set equal to one.
The one turn transfer map allows us to update the values of the initial moments by a root finding problem. In order to compute the moments of each discretization step s, we track the initial moments iteratively, as also described in [7, ch. 4.5.2] for the second order moments, i.e.

$$\sigma_k(s + \Delta s) = \mathcal{M}(s, s + \Delta s) \circ \sigma_k(s) \circ \mathcal{M}(s, s + \Delta s), \tag{8.3}$$

where $\mathcal{M}(s, s + \Delta s)$ represents the map from s to $s + \Delta s$. This is based on the assumption that the moments change slowly for a step size $\Delta s \ll 1$.
The code fragment Lst. 8.2 shows the computation of the moments for each trajectory step as it is indicated by (8.3). In the first step the transfer map from s to $s + \Delta s$ is calculated (line 6). Then, we iterate over all moments that we consider during our computation and track them with a function of the class MomentTracker. The corresponding values of the moments are hold in

the container sigmas_m. In order to obtain correct results we need to store the tracked moments temporarily in an other container (specified by sigma on line 16).
Thanks to the DA library the function is very general, i.e. it is able to track any moment of any order.

```
1  Map M;
2  MomentTracker<value_type, 6> mtracker;
3
4  for(size_type i=1; i<nStepsPerSector_m; ++i) {
5   // transfer map for one trajectory step
6   M = Mscs[i - 1] * Mcycs[i - 1];
7
8   // iterate over all moments of a specific order (in increasing order)
9   for(typename list_type::const_iterator it=moments.cbegin(); it!=moments.cend(); ++it)
10  {
11    for(int idx=Series::orderStart(*it); idx!=Series::orderEnd(*it); ++idx)
12    {
13      // get the exponent of the idx-th monomial
14      FMonomial<6> mo = Series::getExponents(idx);
15      // track moment and store it temporarily in an other container
16      sigma.push_back(mtracker.track({mo[0],mo[1],mo[2],mo[3],mo[4],mo[5]}, sigmas_m[i-1],
              M, truncOrder_m, firstMoments));
17    }
18  }
19
20  // copy updated moments back to real container
21  std::copy(sigma.begin(), sigma.end(), sigmas_m[i].begin());
22
23  sigma.clear();
24 }
```

Listing 8.2: Update of moments for each trajectory step. The whole function is in Appendix G20.

8.5.6 Convergence Criterion

In the program of [7] the distribution is considered stationary if the L_2-error between successive turns is smaller than a user-defined tolerance ϵ, i.e.

$$||\tilde{\sigma}_2(s+L) - \tilde{\sigma}_2(s)||_2 < \epsilon,$$

where L is the path length and $\tilde{\sigma}_2$ represents the vectorized form of the matrix σ_2 in order to apply the vector norm. Since our model might also track higher order moments, we generalized this stopping criterion to

$$\sqrt{\sum_k ||\tilde{\sigma}_k(s+L) - \tilde{\sigma}_k(s)||_2^2},$$

where the sum goes over all orders k and $\tilde{\sigma}_k$ is again the vectorized form of the tensor σ_k.

9 Results

9.1 Hardware

All runtime and stability measurements were performed on the PSI cluster called *Merlin4* where following modules were used for compiling:

- gcc/4.8.4,
- gsl/1.15,
- boost/1.57.0.

Further, the C++ flags `-O3 -std=c++11 -fopenmp -Wall -Werror` were applied. The simulation were run on nodes with two Intel Sandy Bridge CPUs E5-2670 with 2.60 GHz [25], therefore, we could run the simulations using 16 cores.

9.2 Measurement Setup

In the following table we show the configuration settings for the simulations with the PSI Ring Cyclotron and PSI Injector 2.

	PSI Injector 2	PSI Ring Cyclotron
energy range [MeV]	0.87 - 72	72 - 590
harmonic number N_h	10	6
RF frequency ν_{rf} [MHz]	50.650	50.650
proton rest mass m_0 [MeV]	938.272	938.272
angle start [deg]	45	0
#maps per turn	1440	1440
#sectors	4	8
#maps per sector	360	180
max. #function evaluations in integration	100 000	100 000
truncation order (linear theory)	2	2
max. #closed orbit iterations	100	100
magnetic field file	inj72_all_sectors_bfld.dat	ring590_bfld.dat

Table 9.1: Fixed input parameters of the simulations.

In the computation of a non-linear matching (see Sec. 9.6) the truncation order was changed to three. All matching simulations are performed over one sector of the machines — instead over one turn — due to their symmetry.

9.3 Linear Matching

This section compares results with the program of [7], where a slightly modified version was used. Instead of the hard-coded maps it uses the approach described in Sec. 8.5.4 where the maps are computed starting from the Hamiltonian. The space charge strengths, however, are still computed according to [3] or, respectively, [8, ch. 11.4] such that the result is identical to the unmodified version.
All simulations in this section, except those with a Gaussian charge distribution, considered a distribution to be stationary if the L_2-error, as defined in Sec. 8.5.6, was lower than 10^{-4}. Because the computations of the moment integrals take longer with the Gaussian charge distribution, we required a L_2-error smaller than 10^{-3} for the stationary distribution.

9.3.1 PSI Ring Cyclotron

Instead of (4.17), the program of [7] uses the uniform charge distribution given by [8, p. 372]

$$\rho = \frac{3I\lambda}{4\pi c a_x a_y a_z} = \frac{3Q}{4\pi a_x a_y a_z},$$

with the total charge defined by [8, p. 372]

$$Q = \frac{I\lambda}{c}.$$

Since the moment integrals are evaluated on the interval $[-1, 1]$, we need to normalize the charge distribution in order to obtain an equivalent uniform charge distribution, i.e.

$$f = \frac{1}{8}\frac{3}{4\pi a_x a_y a_z}. \tag{9.1}$$

Further, we apply the relation (8.1) between the semi-principal axes and the rms values. The matched second order moment matrix for $E = 72$ MeV, $I = 2.2$ mA and $\varepsilon_x = \varepsilon_y = \varepsilon_z = 1\ \pi$ mm mrad is

$$\sigma_2 = \begin{pmatrix} 13.3619 & 0.1482 & 0 & 0 & -0.0507 & 3.5617 \\ 0.1482 & 1.4944 & 0 & 0 & 2.7565 & 0.0294 \\ 0 & 0 & 6.9437 & -0.0276 & 0 & 0 \\ 0 & 0 & -0.0276 & 1.4215 & 0 & 0 \\ -0.0507 & 2.7565 & 0 & 0 & 10.3282 & -0.0598 \\ 3.5617 & 0.0294 & 0 & 0 & -0.0598 & 1.9315 \end{pmatrix}$$

at a L_2-error of $9.9486 \cdot 10^{-5}$ and

$$\sigma_2 = \begin{pmatrix} 13.3556 & 0.1497 & 0 & 0 & 0.1155 & 3.4643 \\ 0.1497 & 1.4759 & 0 & 0 & 2.8356 & 0.0307 \\ 0 & 0 & 7.0713 & -0.0278 & 0 & 0 \\ 0 & 0 & -0.0278 & 1.3958 & 0 & 0 \\ 0.1155 & 2.8356 & 0 & 0 & 10.9279 & 0.0287 \\ 3.4643 & 0.0307 & 0 & 0 & 0.0287 & 1.8019 \end{pmatrix}, \tag{9.2}$$

with the model of [7] at a L_2-error of $9.8169 \cdot 10^{-5}$. The L_2-error between the two results is 0.7044. By using the uniform distribution defined in (4.17) we obtain with the identical setting subsequent solution:

$$\sigma_2 = \begin{pmatrix} 13.8674 & 0.1516 & 0 & 0 & -0.0992 & 3.8996 \\ 0.1516 & 1.4400 & 0 & 0 & 2.7100 & 0.0338 \\ 0 & 0 & 7.0132 & -0.0277 & 0 & 0 \\ 0 & 0 & -0.0277 & 1.4074 & 0 & 0 \\ -0.0992 & 2.7100 & 0 & 0 & 9.6444 & -0.0851 \\ 3.8996 & 0.0338 & 0 & 0 & -0.0851 & 2.0688 \end{pmatrix}, \tag{9.3}$$

where the L_2-error is $9.9943 \cdot 10^{-5}$. The simulation with the Gaussian distribution yields

$$\sigma_2 = \begin{pmatrix} 13.6190 & 0.1477 & 0 & 0 & 0.0049 & 3.6101 \\ 0.1477 & 1.4661 & 0 & 0 & 2.8488 & 0.0276 \\ 0 & 0 & 7.1022 & -0.0278 & 0 & 0 \\ 0 & 0 & -0.0278 & 1.3898 & 0 & 0 \\ 0.0049 & 2.8488 & 0 & 0 & 10.7105 & -0.0305 \\ 3.6101 & 0.0276 & 0 & 0 & -0.0305 & 1.8623 \end{pmatrix}, \tag{9.4}$$

at a L_2-error of $9.9639 \cdot 10^{-4}$.
The results seem to agree approximately, especially the vertical direction. On closer examination, however, one recognizes that the signs in longitudinal direction, i.e. $\langle xz \rangle$ and $\langle zp_z \rangle$, differ (marked in red) with respect to the reference solution in (9.2). The difference between the projected emittances is

$$\begin{aligned} \tilde{\varepsilon}_x^{(9.2)} - \tilde{\varepsilon}_x^{(9.3)} &\approx 4.437\,299\,153 - 4.466\,039\,695 = -0.028\,740\,542, \\ \tilde{\varepsilon}_y^{(9.2)} - \tilde{\varepsilon}_y^{(9.3)} &\approx 3.141\,592\,654 - 3.141\,591\,602 = 0.000\,001\,052, \\ \tilde{\varepsilon}_z^{(9.2)} - \tilde{\varepsilon}_z^{(9.3)} &\approx 4.437\,299\,154 - 4.466\,039\,272 = -0.028\,740\,118. \end{aligned}$$

When we compare the convergence behavior (see Fig. 9.1a) we recognize that the program with the generalized space charge model requires more iteration steps to obtain the specified L_2-error. While the total number of iterations of the reference [7] is 223, the run with the uniform distribution as defined in (4.17) needs 1980 (+787.89 %) steps and 312 (+39.91 %) iterations with (9.1). The simulation that used the Gaussian distribution isn't comparable with the others since only an error smaller than 10^{-3} was required. The algorithm stopped at 151 iterations.
In Fig. 9.1b we added lines that indicate the change of the relative tolerance in the moment integration of the space charge map computations. Although we change the precision, the L_2-error isn't influenced in the sense that it shows a small peak.

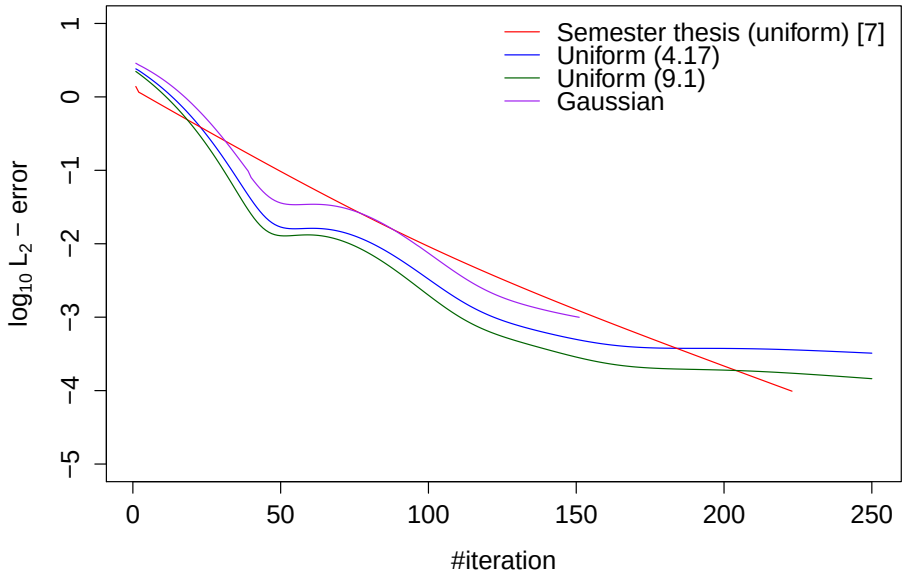

(a) The curves in blue and green are truncated at 250 steps.

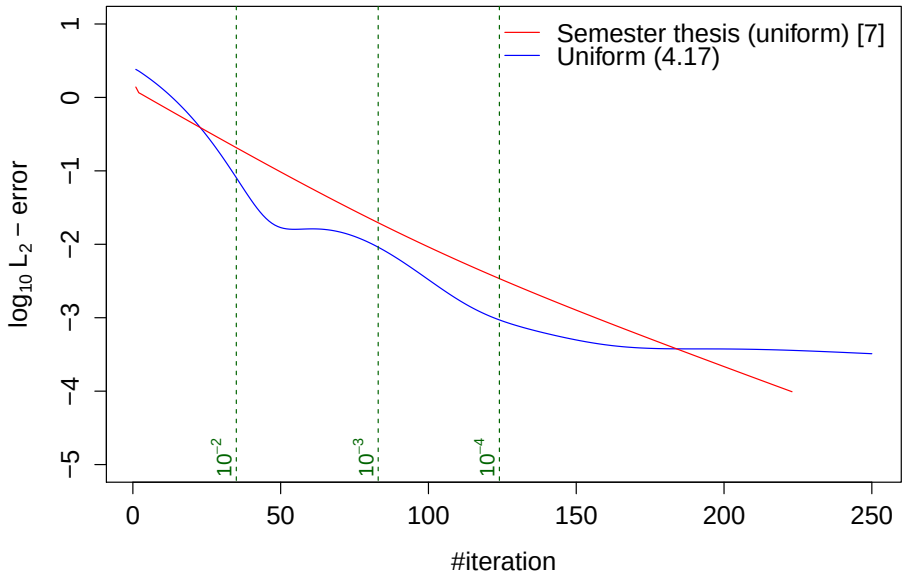

(b) The curve in blue is truncated at 250 steps. The dashed green lines in vertical direction represent the relative tolerance adaptions of the moment integration during the space charge map computation.

Figure 9.1: PSI Ring Cyclotron. Convergence with $E = 72$ MeV, $I = 2.2$ mA and $\varepsilon_x = \varepsilon_y = \varepsilon_z = 1$ πmm mrad.

9.3.2 PSI Injector 2

When running the model of [7] with $E = 2$ MeV, $\varepsilon_x = \varepsilon_y = \varepsilon_z = 5$ πmm mrad and $I = 4$ mA, we get

$$\sigma_2 = \begin{pmatrix} 10.7995 & -0.1329 & 0 & 0 & -0.1096 & 12.8163 \\ -0.1329 & 33.4476 & 0 & 0 & 19.8137 & -0.0401 \\ 0 & 0 & 2.8000 & -0.1438 & 0 & 0 \\ 0 & 0 & -0.1438 & 38.3166 & 0 & 0 \\ -0.1096 & 19.8137 & 0 & 0 & 16.6954 & -0.0859 \\ 12.8163 & -0.0401 & 0 & 0 & -0.0859 & 21.6351 \end{pmatrix}, \tag{9.5}$$

at a L_2-error of $9.7711 \cdot 10^{-5}$. The generalized model with (4.17) yields a second order moment matrix of

$$\sigma_2 = \begin{pmatrix} 8.5436 & -0.0976 & 0 & 0 & -0.0887 & 11.0266 \\ -0.0976 & 25.2187 & 0 & 0 & 14.1538 & -0.0268 \\ 0 & 0 & 2.7185 & -0.1437 & 0 & 0 \\ 0 & 0 & -0.1437 & 39.4659 & 0 & 0 \\ -0.0887 & 14.1538 & 0 & 0 & 10.9686 & -0.0839 \\ 11.0266 & -0.0268 & 0 & 0 & -0.0839 & 19.6430 \end{pmatrix}, \tag{9.6}$$

with a L_2-error of $9.8892 \cdot 10^{-5}$. The second order moments in case of a Gaussian distribution look like

$$\sigma_2 = \begin{pmatrix} 8.7932 & -0.1058 & 0 & 0 & -0.0912 & 10.0431 \\ -0.1058 & 24.5032 & 0 & 0 & 15.6742 & -0.0472 \\ 0 & 0 & 2.8673 & -0.1444 & 0 & 0 \\ 0 & 0 & -0.1444 & 37.4182 & 0 & 0 \\ -0.0912 & 15.6742 & 0 & 0 & 13.7296 & -0.0855 \\ 10.0431 & -0.0472 & 0 & 0 & -0.0855 & 15.6928 \end{pmatrix}$$

where the L_2-error is $9.51764 \cdot 10^{-4}$. Although the vertical direction and the coupling terms (except to $\langle p_x z \rangle$) are close to the reference solution, the horizontal and longitudinal direction vary of the order of 2 - 9 on the diagonal. The computation of the projected emittances of (9.5) and (9.6) shows a significant discrepancy in the horizontal and longitudinal direction:

$$\begin{aligned} \tilde{\varepsilon}_x^{(9.5)} - \tilde{\varepsilon}_x^{(9.6)} &\approx 19.005\,254\,373 - 14.678\,179\,709 = 4.327\,074\,664 \quad (\approx -22.77\ \%), \\ \tilde{\varepsilon}_y^{(9.5)} - \tilde{\varepsilon}_y^{(9.6)} &\approx 10.356\,920\,467 - 10.356\,997\,608 = -7.7141 \cdot 10^{-5}, \\ \tilde{\varepsilon}_z^{(9.5)} - \tilde{\varepsilon}_z^{(9.6)} &\approx 19.005\,243\,217 - 14.678\,186\,897 = 4.327\,056\,32 \quad (\approx -22.77\ \%). \end{aligned}$$

In contrast to the PSI Ring Cyclotron, the change in the relative tolerance of the moment integration causes an increase of the L_2-error, but, only in case of the Gaussian charge distribution. The curve is also more wiggly than the simulation with the uniform distribution (4.17) that is shown in Fig. 9.2b. There, the tolerance change indicates no impact. But the curve has bumps that seem to appear regularly.
As we have already observed for the PSI Ring Cyclotron, the number of iterations increases significantly. Instead of the original 335 steps for the computation of (9.5), it requires now 1409 iterations for the computation of (9.6). That's a percentage rise of approximately 320.60 %.

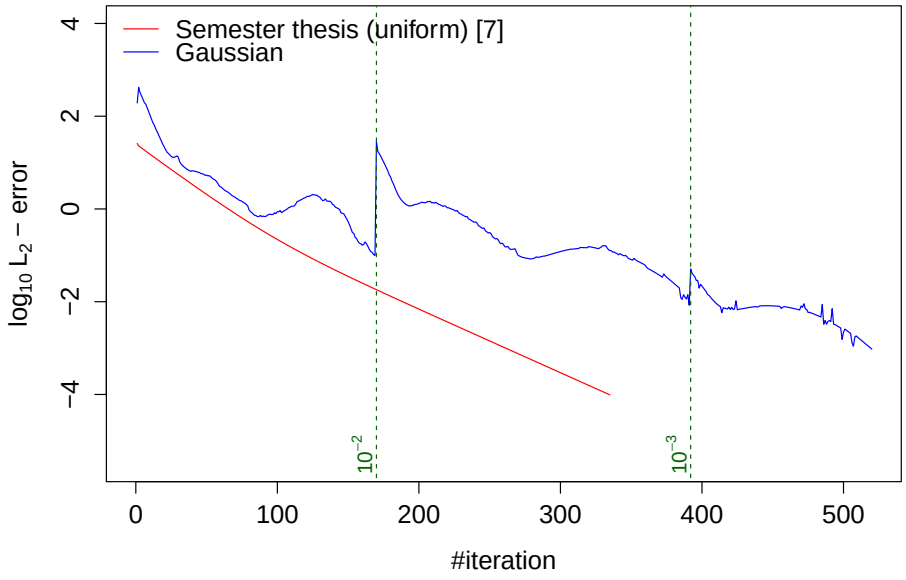

(a) Convergence with the Gaussian distribution.

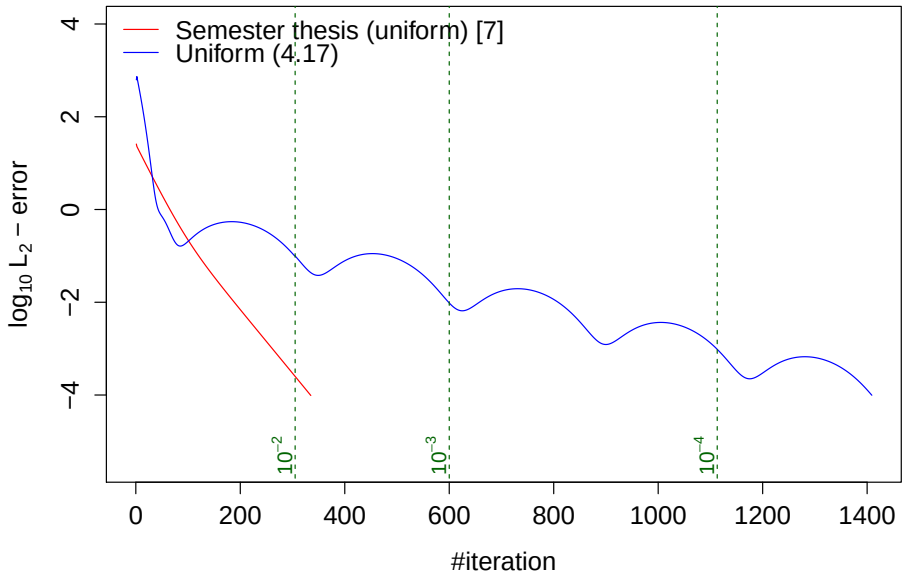

(b) Convergence with the uniform distribution (4.17).

Figure 9.2: PSI Injector 2. Convergence with $E = 2$ MeV, $I = 4$ mA and $\varepsilon_x = \varepsilon_y = \varepsilon_z = 5\ \pi$mm mrad. The dashed green lines in vertical direction represent the relative tolerance adaptions of the moment integration during the space charge map computation.

9.4 Linear Stability Analysis

The success of finding a matched distribution depends on the intensity, emittances and energy. Since there are basically infinite many settings, we restrict our simulations to a specific energy with varying intensity and emittances. The intensity ranges from 0.5 mA to 10 mA in steps of 0.5 mA. The emittances are increased by 1 πmm mrad starting from 1 πmm mrad to 10 πmm mrad and are kept equal in all dimensions. The simulations are performed using the uniform distribution that is given by (4.17).
Because the program normalizes the emittances by $\beta\gamma$, their value differs from 1 - 10 πmm mrad for higher energies as e.g. in Fig. 9.4.
Based on the assumption that no convergence appears at all if no matched distribution exists, we stopped the program after reaching a L_2-error of 0.1.
The striped regions in blue of Fig. 9.3 and Fig. 9.4 are configurations that didn't converge within 2 hours of execution time whereas all configurations that have a white color diverged.
At first sight the diagrams basically indicate that the higher the emittances, while keeping the intensity fixed, the more iterations are required. On the other hand, when keeping the emittances fixed, the number of iterations decreases the higher the intensity.
The stability plot of the PSI Ring Cyclotron shows also a drastic increase of the number of iterations for emittances higher than 3 πmm mrad.

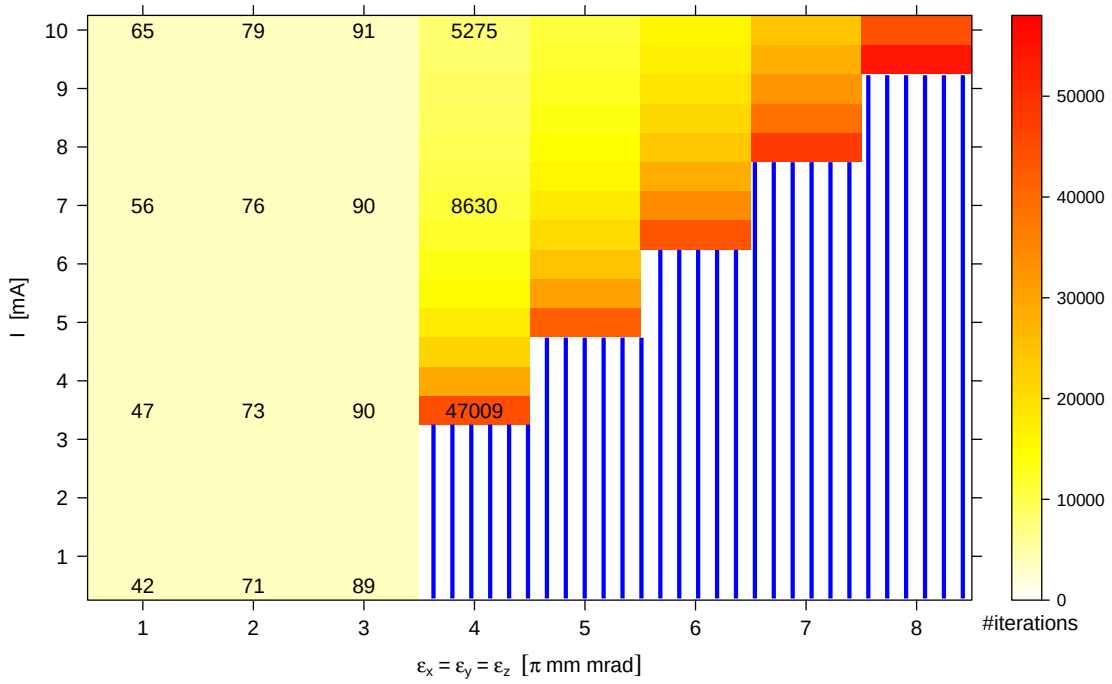

Figure 9.3: PSI Ring Cyclotron at 72 MeV and uniform distribution defined in (4.17). Normalization factor (4 digits): $\beta\gamma = 0.3992$ for 72 MeV. Blue region: Computation exceeded time limit (2 hours).

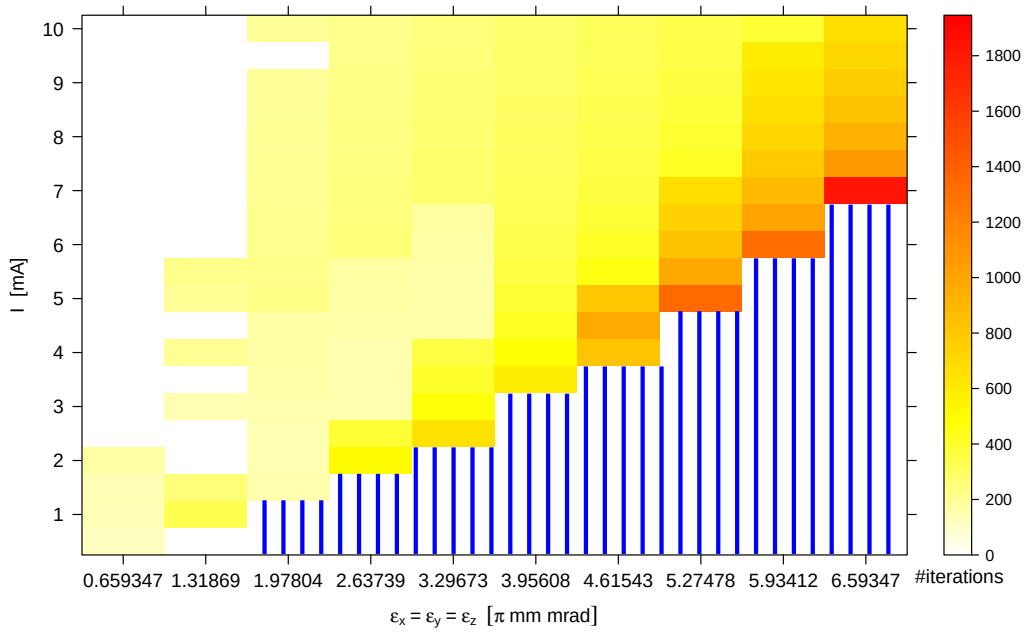

Figure 9.4: PSI Injector 2 at 2 MeV and uniform distribution defined in (4.17). Normalization factors (4 digits): $\beta\gamma = 0.0431$ for 870 keV and $\beta\gamma = 0.0653$ for 2 MeV. Blue region: Computation exceeded time limit (2 hours).

For some emittances, e.g. $\varepsilon_x = \varepsilon_y = \varepsilon_z = 1.3187\ \pi$ mm mrad, the PSI Injector 2 shows gaps where no convergence appears.

9.5 Timing of the Space charge Map Construction

The construction of the space charge maps is more expensive than in [7] due to the evaluation of the multidimensional moment integrals. The required time depends on various numerical parameters like the allowed relative tolerance, the maximum number of function evaluations (during the integration process) and the total number of trajectory steps. It's clear that the accuracy gets increased the higher the number of trajectory steps N and the smaller the relative tolerance are chosen. Unfortunately, the computation time grows as well. That's why we decided to change the relative error adaptively during the process of finding a matched distribution, i.e. it's decreased by a factor of 10 if the L_2-error is smaller than the current tolerance, since it makes no sense to require high precision in case of bad guesses of the stationary distribution.
In Fig. 9.5 are results that show the time needed to build up all space charge maps for one sector of the machines with increasing order. The plots illustrate the expected behavior dependent on the relative tolerance and truncation order.

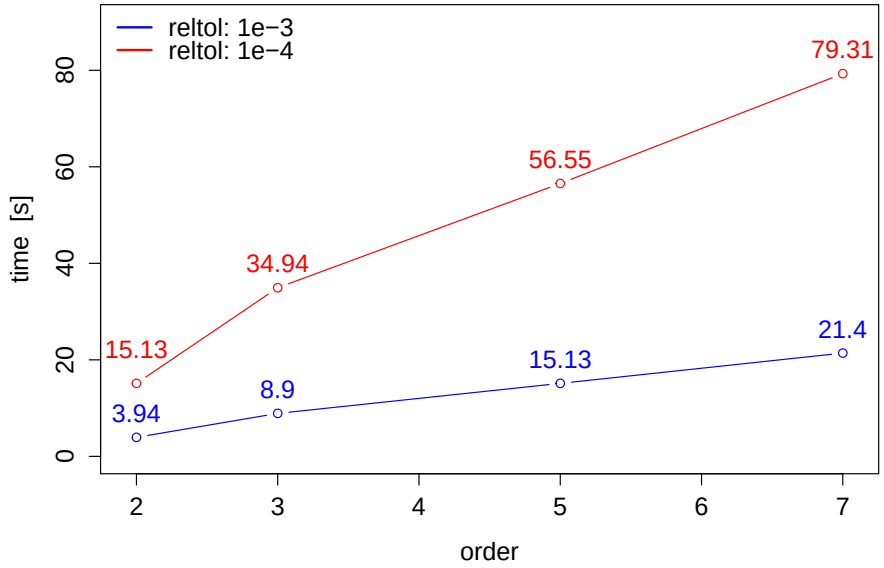

(a) PSI Ring Cyclotron with $E = 72$ MeV, $I = 2.2$ mA and $\varepsilon_x = \varepsilon_y = \varepsilon_z = 1$ πmm mrad.

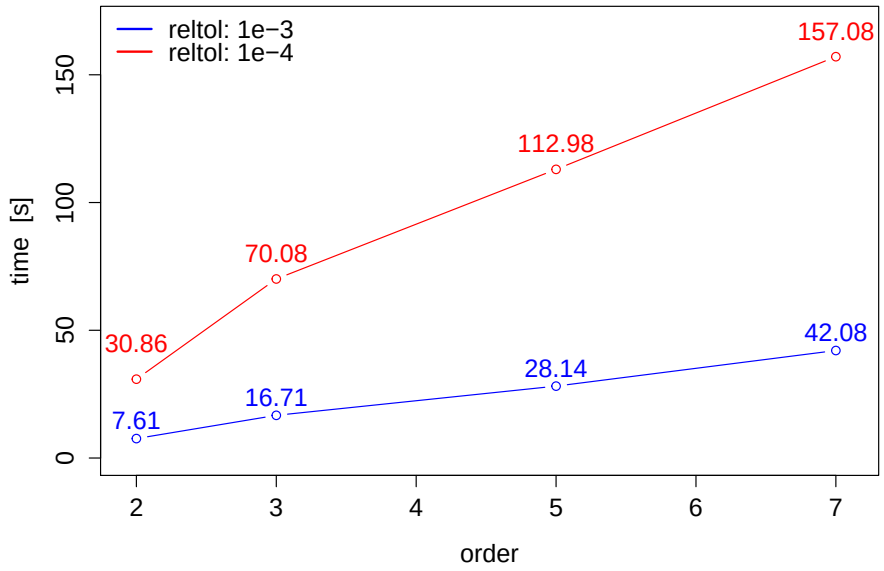

(b) PSI Injector 2 with $E = 2$ MeV, $I = 4$ mA and $\varepsilon_x = \varepsilon_y = \varepsilon_z = 5$ πmm mrad.

Figure 9.5: Time required to compute all space charge maps for one sector, i.e. 180 maps for PSI Ring Cyclotron and 360 maps for PSI Injector 2, with Gaussian distribution. The simulation was performed with a relative tolerance for the integrals of 10^{-3} and 10^{-4}. The maximum number of function evaluations was limited to 10^5. The program was run with 16 threads.

9.6 Non-Linear Matching

We present here the result of matching moments based on the example of Sec. 7.4. The third order moments are initialized uniformly in the range of $[-0.01, 0.01]$ with the pseudo random number generator Mersenne-Twister (standard C++11) with seed 42. Further, the prefactor in (7.13) was set to $k = 0.1$.
Since the identical simulation didn't converge for the PSI Injector 2, we only show the result of the Ring Cyclotron.

9.6.1 PSI Ring Cyclotron

The configuration with $E = 72$ MeV, $I = 2.2$ mA and $\varepsilon_x = \varepsilon_y = \varepsilon_z = 1\ \pi$mm mrad converged to a stationary distribution with a L_2-error of $9.8451 \cdot 10^{-4}$. The convergence plot in Fig. 9.6 indicates a peak that might mainly appear due to the moment $\langle y^2 \rangle$ that decreases by 0.4. The value then increases again but the effect is softened by other moment changes.

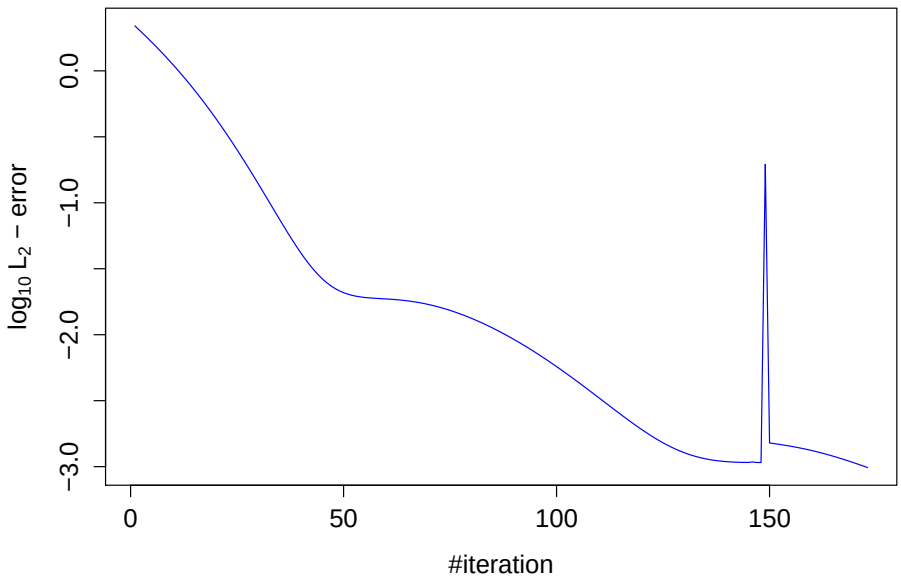

Figure 9.6: Convergence of the non-linear matching. At iteration step 149 occurs a peak.

The numerical result shows that the requirement of a centered beam is fulfilled. All first order moments are zero:

$$\sigma_1 = \begin{pmatrix} \langle x \rangle \\ \langle p_x \rangle \\ \langle y \rangle \\ \langle p_y \rangle \\ \langle z \rangle \\ \langle p_z \rangle \end{pmatrix} = \begin{pmatrix} 3.7876 \cdot 10^{-28} \\ 1.9311 \cdot 10^{-27} \\ 0 \\ -9.1335 \cdot 10^{-27} \\ 2.3774 \cdot 10^{-27} \\ 7.9089 \cdot 10^{-28} \end{pmatrix}.$$

The second order moments are given by

$$\sigma_2 = \begin{pmatrix} 13.3079 & 0.1475 & -2.8702 \cdot 10^{-5} & 1.0716 \cdot 10^{-6} & 0.0133 & 3.5389 \\ & 1.5004 & -1.0137 \cdot 10^{-5} & 1.5389 \cdot 10^{-6} & 2.7517 & 0.0282 \\ & & 6.9284 & -0.0289 & 0.0002 & -2.1458 \cdot 10^{-5} \\ & & & 1.4246 & 1.5948 \cdot 10^{-5} & -1.6469 \cdot 10^{-6} \\ & & & & 10.3186 & -0.0247 \\ & & & & & 1.9330 \end{pmatrix} \tag{9.7}$$

In contrast to the non-perturbed distribution the moments in horizontal and longitudinal direction are now coupled with the vertical direction although these values are of the order 10^{-6} to 10^{-5}. The comparison with (9.4), i.e.

$$\sigma_2 = \begin{pmatrix} 13.6190 & 0.1477 & 0 & 0 & 0.0049 & 3.6101 \\ 0.1477 & 1.4661 & 0 & 0 & 2.8488 & 0.0276 \\ 0 & 0 & 7.1022 & -0.0278 & 0 & 0 \\ 0 & 0 & -0.0278 & 1.3898 & 0 & 0 \\ 0.0049 & 2.8488 & 0 & 0 & 10.7105 & -0.0305 \\ 3.6101 & 0.0276 & 0 & 0 & -0.0305 & 1.8623 \end{pmatrix},$$

shows that the moments $\langle x^2 \rangle$, $\langle y^2 \rangle$ and $\langle z^2 \rangle$ decreased whereas the values of $\langle p_x^2 \rangle$, $\langle p_y^2 \rangle$ and $\langle p_z^2 \rangle$ increased:

$$\left(\frac{\sigma_2^{(9.7)}}{\sigma_2^{(9.4)}} - 1 \right) \cdot 100\ \% = \begin{pmatrix} -2.2843 & -0.1110 & & & 174.3475 & -1.9714 \\ & 2.3367 & & & -3.4085 & 2.2415 \\ & & -2.4471 & 3.9700 & & \\ & & & 2.5091 & & \\ & & & & -3.6590 & -18.8437 \\ & & & & & 3.7963 \end{pmatrix} \%$$

Despite those changes the projected emittances differ just slightly:

$$\begin{aligned} \tilde{\varepsilon}_x^{(9.7)} - \tilde{\varepsilon}_x^{(9.4)} &\approx 4.466\,029\,211 - 4.465\,982\,603 = 4.6608 \cdot 10^{-5} \quad (\approx 0.0104\ ‰), \\ \tilde{\varepsilon}_y^{(9.7)} - \tilde{\varepsilon}_y^{(9.4)} &\approx 3.141\,554\,302 - 3.141\,634\,084 = -7.9782 \cdot 10^{-5} \quad (\approx -0.0254\ ‰), \\ \tilde{\varepsilon}_z^{(9.7)} - \tilde{\varepsilon}_z^{(9.4)} &\approx 4.466\,009\,82 - 4.466\,008\,721 = 1.099 \cdot 10^{-6} \quad (\approx 0.0002\ ‰). \end{aligned}$$

The third order moments are all listed in Output 9.1.

$\langle x^3 \rangle$:	0.0051	$\rightarrow$	-0.1946,	$\langle x^2 p_x \rangle$:	0.0028	$\rightarrow$	$-7.5797 \cdot 10^{-5}$
$\langle x^2 y \rangle$:	0.0050	$\rightarrow$	0.0954,	$\langle x^2 p_y \rangle$:	-0.0073	$\rightarrow$	-0.0136
$\langle x^2 z \rangle$:	0.0081	$\rightarrow$	-0.0786,	$\langle x^2 p_z \rangle$:	-0.0081	$\rightarrow$	-0.0393
$\langle x p_x^2 \rangle$:	0.0015	$\rightarrow$	-0.0131,	$\langle x p_x y \rangle$:	-0.0025	$\rightarrow$	0.0042
$\langle x p_x p_y \rangle$:	-0.0045	$\rightarrow$	0.0095,	$\langle x p_x z \rangle$:	-0.0022	$\rightarrow$	-0.0231
$\langle x p_x p_z \rangle$:	-0.0098	$\rightarrow$	$5.1948 \cdot 10^{-5}$,	$\langle x y^2 \rangle$:	0.0005	$\rightarrow$	0.0070
$\langle x y p_y \rangle$:	0.0037	$\rightarrow$	0.0012,	$\langle x y z \rangle$:	0.0027	$\rightarrow$	0.0399,
$\langle x y p_z \rangle$:	0.0065	$\rightarrow$	0.0263,	$\langle x p_y^2 \rangle$:	0.0089	$\rightarrow$	0.0006
$\langle x p_y z \rangle$:	0.0051	$\rightarrow$	0.0108,	$\langle x p_y p_z \rangle$:	-0.0010	$\rightarrow$	-0.0035
$\langle x z^2 \rangle$:	-0.0091	$\rightarrow$	-0.0152,	$\langle x z p_z \rangle$:	-0.0087	$\rightarrow$	-0.0285
$\langle x p_z^2 \rangle$:	0.0050	$\rightarrow$	-0.0029,	$\langle p_x^3 \rangle$:	-0.0070	$\rightarrow$	0.0004
$\langle p_x^2 y \rangle$:	-0.0015	$\rightarrow$	0.0004,	$\langle p_x^2 p_y \rangle$:	-0.0080	$\rightarrow$	-0.0007
$\langle p_x^2 z \rangle$:	-0.0071	$\rightarrow$	-0.0051,	$\langle p_x^2 p_z \rangle$:	-0.0081	$\rightarrow$	-0.0072
$\langle p_x y^2 \rangle$:	0.0006	$\rightarrow$	-0.0007,	$\langle p_x y p_y \rangle$:	-0.0011	$\rightarrow$	0.0004
$\langle p_x y z \rangle$:	0.0055	$\rightarrow$	0.0061,	$\langle p_x y p_z \rangle$:	-0.0075	$\rightarrow$	0.0023
$\langle p_x p_y^2 \rangle$:	0.0049	$\rightarrow$	0.0004,	$\langle p_x p_y z \rangle$:	-0.0035	$\rightarrow$	0.0049
$\langle p_x p_y p_z \rangle$:	0.0050	$\rightarrow$	0.0052,	$\langle p_x z^2 \rangle$:	0.0061	$\rightarrow$	-0.0205
$\langle p_x z p_z \rangle$:	-0.0091	$\rightarrow$	-0.0124,	$\langle p_x p_z^2 \rangle$:	0.0085	$\rightarrow$	0.0003
$\langle y^3 \rangle$:	0.0049	$\rightarrow$	-0.0017,	$\langle y^2 p_y \rangle$:	-0.0017	$\rightarrow$	-0.0015
$\langle y^2 z \rangle$:	-0.0040	$\rightarrow$	-0.0310,	$\langle y^2 p_z \rangle$:	-0.0096	$\rightarrow$	0.0033
$\langle y p_y^2 \rangle$:	0.0040	$\rightarrow$	-0.0001,	$\langle y p_y z \rangle$:	-0.0008	$\rightarrow$	0.0009
$\langle y p_y p_z \rangle$:	0.0007	$\rightarrow$	$-1.1216 \cdot 10^{-5}$,	$\langle y z^2 \rangle$:	-0.0002	$\rightarrow$	0.0185
$\langle y z p_z \rangle$:	-0.0058	$\rightarrow$	0.0055,	$\langle y p_z^2 \rangle$:	0.0021	$\rightarrow$	0.0009
$\langle p_y^3 \rangle$:	-0.0001	$\rightarrow$	-0.0006,	$\langle p_y^2 z \rangle$:	-0.0023	$\rightarrow$	-0.0054
$\langle p_y^2 p_z \rangle$:	0.0033	$\rightarrow$	0.0007,	$\langle p_y z^2 \rangle$:	-0.0017	$\rightarrow$	0.0185
$\langle p_y z p_z \rangle$:	-0.0013	$\rightarrow$	0.0086,	$\langle p_y p_z^2 \rangle$:	-0.0082	$\rightarrow$	-0.0009
$\langle z^3 \rangle$:	-0.0085	$\rightarrow$	-0.1298,	$\langle z^2 p_z \rangle$:	0.0064	$\rightarrow$	-0.0073
$\langle z p_z^2 \rangle$:	-0.0004	$\rightarrow$	-0.0154,	$\langle p_z^3 \rangle$:	-0.0011	$\rightarrow$	-0.0011

Output 9.1: Initial and converged values of all third order moments. Syntax: initial $\rightarrow$ final.

10 Conclusion and Outlook

On the basis of Lie algebra and "Truncated-Power-Series-Algebra" (TPSA) the implementation of [7] got generalized. The hard-coded space charge model was replaced by a more general description where the underlying particle distribution can be freely chosen. It performs a series expansion of each component of the electric field vector that is obtained by the scalar potential of an ellipsoidally symmetric bunch where the expansion coefficients incorporate the couplings among the different dimensions.
The separately treated focussing forces are embedded into the system by a second order Hamiltonian. Its data structure is generalized such that we're able to apply the Lie transformation in order to get the linear map.
The update scheme that was based on real Dirac matrices got replaced by a Newton-Raphson method with Lagrange multipliers. This approach doesn't depend on the order and dimension of the problem. Further, it allows an easy extension with additional constraints and invariants that might be needed when matching higher order moments.
Using the linear approximation, simulations with the PSI Ring Cyclotron returned similar results for the lowest energy compared with [7]. The PSI Injector 2 is more critical. Some values, especially in the horizontal and longitudinal direction, deviate significantly from the reference solution.
As the comparison with the spherically symmetric bunch illustrated, the presented model indicates problems with the correct representation of the Gaussian charge distribution. Although the shape of the electric field improves the higher the truncation order, it's still a poor approximation. The matched distribution algorithm has also the problem to converge for configurations with higher energy (e.g. starting from ~ 114 MeV in case of the PSI Ring Cyclotron). It mainly arises due to the initialization using spherical symmetry where some coupling terms are equal to zero. Applying the solution of the preceding energy as initial guess of the higher energy configuration could resolve that issue.
Nevertheless, a first simulation with an additional third order term in the charge distribution converged to a stationary distribution. The solution indicated mainly a significant change in the horizontal and longitudinal extent of the bunch. But before interpreting the data too much, more simulations have to be done to verify its physical correctness. There, the question of additional constraints concerning the higher order moment arises. A comparison with Particle-in-Cell simulations could therefore be a next step. Secondly, it should be focussed on the convergence rate since the number of iterations and, thus, the computational time increased. The execution time, however, might be reduced considerably by parallelizing computationally intensive parts. A first effort was already made concerning the evaluation of the multidimensional integrals. There, a simple OpenMP parallelization results in a speedup of approximately 8 - 10 for 16 threads.

11 Acknowledgment

Firstly, I thank Dr. Andreas Adelmann. His support during the whole period of time was great as always. I also appreciate the help of Dr. Christian Baumgarten who gave useful suggestions. Although the AMAS group at PSI changes consistently, it's every time a familiar atmosphere. In that context I would like to mention Dr. Nathaniel J. Pogue. Thanks to his stories and anecdotes the daily lunch was always a highlight. Additionally, I thank Prof. Dr. Arbenz who was well-disposed to help regarding numerical issues.
The opportunity to present my thesis at the 12th International Computational Accelerator Physics Conference (ICAP'15) in Shanghai was a great pleasure which wouldn't have been possible without the travel support by Prof. Dr. Hiptmair.

A Units

quantity	symbol	SI unit	C, N unit	e, V unit
charge	q	$\mathrm{A\,s}$	C	e
charge density	ρ	$\mathrm{A\,s\,m^{-3}}$	$\mathrm{C\,m^{-3}}$	$\mathrm{e\,m^{-3}}$
current	I	A	$\mathrm{C\,s^{-1}}$	$\mathrm{e\,s^{-1}}$
electric field	$\vec{E}$	$\mathrm{kg\,m\,A^{-1}\,s^{-3}}$	$\mathrm{N\,C^{-1}}$	$\mathrm{V\,m^{-1}}$
mass	m	kg	kg	$\mathrm{MeV\,c^{-2}}$
potential	ϕ	$\mathrm{kg\,m^2\,A^{-1}\,s^{-3}}$	$\mathrm{N\,m\,C^{-1}}$	V
speed of light	c	$\mathrm{m\,s^{-1}}$	$\mathrm{m\,s^{-1}}$	1
vacuum permittivity	ε_0	$\mathrm{A^2\,s^4\,kg^{-1}\,m^{-3}}$	$\mathrm{C^2\,N^{-1}\,m^{-2}}$	$\mathrm{e\,V^{-1}\,m^{-1}}$

Table A.1: Symbols and their corresponding units. The conversions to SI units are given in Appendix G7.

B Terms as Carlson's Elliptic Integrals

Carlson [19] defined the elliptic integrals of second kind as

$$R_F(x,y,z) = \frac{1}{2}\int_0^\infty \frac{1}{\sqrt{(t+x)(t+y)(t+z)}}\,\mathrm{d}t,$$
$$R_D(x,y,z) = \frac{3}{2}\int_0^\infty \frac{1}{(t+z)^{3/2}\sqrt{(t+x)(t+y)}}\,\mathrm{d}t.$$

In order to shorten our notation we apply for all integrals that can't be expressed by above forms Carlson's bracket notation, i.e. [19, eq. 1.1]

$$[p_1,p_2,\ldots,p_n] = \int_y^x (a_1+b_1t)^{p_1/2}\cdot\ \ldots\ \cdot(a_n+b_n)^{p_n/2}\,\mathrm{d}t,$$

where in our case $n=3$ with $(a_1,a_2,a_3)=(a_x,a_y,a_z)$ and $b_1=b_2=b_3=1$. Additionally, the bounds of integration are $y=0$ and $x=\infty$.
When using the definition of $\Omega(u)$ in (4.5) and $g(u)$ in (4.7), following relations hold:

$$\int_0^\infty g(u)\,\mathrm{d}u = 2R_F(a_x^2,a_y^2,a_z^2)$$
$$\int_0^\infty \Omega(u)g(u)\,\mathrm{d}u = \frac{2}{3}\left[x^2R_D(a_y^2,a_z^2,a_x^2)+y^2R_D(a_x^2,a_z^2,a_y^2)+z^2R_D(a_x^2,a_y^2,a_z^2)\right]$$
$$\begin{aligned}\int_0^\infty \Omega^2(u)g(u)\,\mathrm{d}u &= x^4[-5,-1,-1]+2x^2y^2[-3,-3,-1]+y^4[-1,-5,-1]\\ &\quad+2x^2z^2[-3,-1,-3]+2y^2z^2[-1,-3,-3]+z^4[-1,-1,-5]\end{aligned}$$
$$\begin{aligned}\int_0^\infty \Omega^3(u)g(u)\,\mathrm{d}u &= x^6[-7,-1,-1]+3x^4y^2[-5,-3,-1]+3x^2y^4[-3,-5,-1]\\ &\quad+y^6[-1,-7,-1]+3x^4z^2[-5,-1,-3]+6x^2y^2z^2[-3,-3,-3]\\ &\quad+3y^4z^2[-1,-5,-3]+3x^2z^4[-3,-1,-5]+3y^2z^4[-1,-3,-5]\\ &\quad+z^6[-1,-1,-7]\end{aligned}$$
$$\begin{aligned}\int_0^\infty \Omega^4(u)g(u)\,\mathrm{d}u &= x^8[-9,-1,-1]+4x^6y^2[-7,-3,-1]+6x^4y^4[-5,-5,-1]\\ &\quad+4x^2y^6[-3,-7,-1]+y^8[-1,-9,-1]+4x^6z^2[-7,-1,-3]\\ &\quad+12x^4y^2z^2[-5,-3,-3]+12x^2y^4z^2[-3,-5,-3]+4y^6z^2[-1,-7,-3]\\ &\quad+6x^4z^4[-5,-1,-5]+12x^2y^2z^4[-3,-3,-5]+6y^4z^4[-1,-5,-5]\\ &\quad+4x^2z^6[-3,-1,-7]+4y^2z^6[-1,-3,-7]+z^8[-1,-1,-9]\end{aligned}$$

$$\begin{aligned}\int_0^\infty \Omega^5(u)g(u)\,\mathrm{d}u = {} & x^{10}\,[-11,-1,-1] + 5x^8y^2\,[-9,-3,-1] + 10x^6y^4\,[-7,-5,-1] \\ & + 10x^4y^6\,[-5,-7,-1] + 5x^2y^8\,[-3,-9,-1] + y^{10}\,[-1,-11,-1] \\ & + 5x^8z^2\,[-9,-1,-3] + 20x^6y^2z^2\,[-7,-3,-3] + 30x^4y^4z^2\,[-5,-5,-3] \\ & + 20x^2y^6z^2\,[-3,-7,-3] + 5y^8z^2\,[-1,-9,-3] + 10x^6z^4\,[-7,-1,-5] \\ & + 30x^4y^2z^4\,[-5,-3,-5] + 30x^2y^4z^4\,[-3,-5,-5] + 10y^6z^4\,[-1,-7,-5] \\ & + 10x^4z^6\,[-5,-1,-7] + 20x^2y^2z^6\,[-3,-3,-7] + 10y^4z^6\,[-1,-5,-7] \\ & + 5x^2z^8\,[-3,-1,-9] + 5y^2z^8\,[-1,-3,-9] + z^{10}\,[-1,-1,-11]\end{aligned}$$

All terms described by integrals are given in Appendix G8.

C Derivation of the Electric Field

Starting from the scalar potential defined in (4.4) of Sec. 4.2, the electric field is computed by using (4.8).
We only show the derivation in horizontal direction since the vertical and longitudinal direction are transformed appropriately.

$$
\begin{aligned}
E_x &= -\frac{\mathrm{d}\phi}{\mathrm{d}x} = -\frac{Qa_xa_ya_z}{4\varepsilon_0}\frac{\mathrm{d}}{\mathrm{d}x}\left[\int_0^\infty \frac{1}{\sqrt{(a_x^2+u)(a_y^2+u)(a_z^2+u)}}\int_{\Omega(u)}^\infty f(\omega)\,\mathrm{d}\omega\,\mathrm{d}u\right] \\
&= -\frac{Qa_xa_ya_z}{4\varepsilon_0}\int_0^\infty \frac{1}{\sqrt{(a_x^2+u)(a_y^2+u)(a_z^2+u)}}\frac{\mathrm{d}}{\mathrm{d}x}\left[\int_{\Omega(u)}^\infty f(\omega)\,\mathrm{d}\omega\right]\mathrm{d}u \\
&= -\frac{Qa_xa_ya_z}{4\varepsilon_0}\int_0^\infty \frac{1}{\sqrt{(a_x^2+u)(a_y^2+u)(a_z^2+u)}}\left[f(\infty)\cdot 0 - f\left(\Omega(u)\right)\frac{\mathrm{d}\Omega(u)}{\mathrm{d}x} + \int_{\Omega(u)}^\infty \underbrace{\frac{\mathrm{d}f(\omega)}{\mathrm{d}x}}_{=0}\mathrm{d}\omega\right]\mathrm{d}u \\
&= -\frac{Qa_xa_ya_z}{4\varepsilon_0}\int_0^\infty \frac{1}{\sqrt{(a_x^2+u)(a_y^2+u)(a_z^2+u)}}\left[-f\left(\Omega(u)\right)\frac{\mathrm{d}\Omega(u)}{\mathrm{d}x}\right]\mathrm{d}u \\
&= \frac{Qa_xa_ya_z}{4\varepsilon_0}\int_0^\infty \frac{1}{\sqrt{(a_x^2+u)(a_y^2+u)(a_z^2+u)}}\left[f\left(\frac{x^2}{a_x^2+u}+\frac{y^2}{a_y^2+u}+\frac{z^2}{a_z^2+u}\right)\frac{2x}{a_x^2+u}\right]\mathrm{d}u \\
&= \frac{Qa_xa_ya_z}{2\varepsilon_0}\int_0^\infty \frac{x}{(a_x^2+u)^{3/2}\sqrt{(a_y^2+u)(a_z^2+u)}}f\left(\frac{x^2}{a_x^2+u}+\frac{y^2}{a_y^2+u}+\frac{z^2}{a_z^2+u}\right)\mathrm{d}u,
\end{aligned}
$$

where it was made use of Leibniz's rule [32, p. 153]

$$
\frac{\mathrm{d}}{\mathrm{d}t}\int_{a(t)}^{b(t)} g(x,t)\,\mathrm{d}x = g(b(t),t)\frac{\mathrm{d}b(t)}{\mathrm{d}t} - g(a(t),t)\frac{\mathrm{d}a(t)}{\mathrm{d}t} + \int_{a(t)}^{b(t)}\frac{\mathrm{d}g(x,t)}{\mathrm{d}t}\,\mathrm{d}x.
$$

We can verify the expression by comparing with [6, eq. 2.3.3]

$$
E_x(x,y) = \frac{Qa_xa_y}{2\varepsilon_0}\int_0^\infty \frac{x}{(a_x^2+u)^{3/2}(a_y^2+u)^{1/2}}f\left(\frac{x^2}{a_x^2+u}+\frac{y^2}{a_y^2+u}\right)\mathrm{d}u,
$$

which is the horizontal electric field component of the potential for a continuous beam, i.e. [6, eq. 2.3.1]

$$
\phi(x,y) = \frac{Qa_xa_y}{4\varepsilon_0}\int_0^\infty\int_{S(u)}^\infty \frac{f(\omega)}{\sqrt{(a_x^2+u)(a_y^2+u)}}\,\mathrm{d}\omega\,\mathrm{d}u,
$$

where $S(u)$ is given by [6, eq. 2.3.2]

$$
S(u) = \frac{x^2}{a_x^2+u}+\frac{y^2}{a_y^2+u}.
$$

D Transformation of Moment Integrals

The following sections show the transformation of the integrals in (4.12) to finite domains in case of different charge distributions. The single moments are given by

$$\begin{aligned}
\langle x^n \rangle &= \int_{\mathbb{R}^3} x^n f\left(\frac{x^2}{a_x^2} + \frac{y^2}{a_y^2} + \frac{z^2}{a_z^2}\right) \mathrm{d}x\,\mathrm{d}y\,\mathrm{d}z, \\
\langle y^n \rangle &= \int_{\mathbb{R}^3} y^n f\left(\frac{x^2}{a_x^2} + \frac{y^2}{a_y^2} + \frac{z^2}{a_z^2}\right) \mathrm{d}x\,\mathrm{d}y\,\mathrm{d}z, \\
\langle z^n \rangle &= \int_{\mathbb{R}^3} z^n f\left(\frac{x^2}{a_x^2} + \frac{y^2}{a_y^2} + \frac{z^2}{a_z^2}\right) \mathrm{d}x\,\mathrm{d}y\,\mathrm{d}z,
\end{aligned}$$

with probability density function f. In each case we only transform the moments in horizontal direction because the other directions are modified appropriately.

D.1 Gaussian Charge Distribution

The three-dimensional elliptic Gaussian is given by (4.6), hence,

$$\begin{aligned}
\langle x^n E_x \rangle = \frac{Q}{16\pi^3 \varepsilon_0 a_x a_y a_z} \int_{-\infty}^{\infty}\int_{-\infty}^{\infty}\int_{-\infty}^{\infty}\int_{0}^{\infty} & \frac{x^{n+1}}{(a_x^2+u)^{3/2}\sqrt{(a_y^2+u)(a_z^2+u)}} \\
& \exp\left[-\frac{1}{2}\left(\frac{x^2}{a_x^2+u} + \frac{y^2}{a_y^2+u} + \frac{z^2}{a_z^2+u}\right)\right] \exp\left[-\frac{1}{2}\left(\frac{x^2}{a_x^2} + \frac{y^2}{a_y^2} + \frac{z^2}{a_z^2}\right)\right] \mathrm{d}u\,\mathrm{d}x\,\mathrm{d}y\,\mathrm{d}z.
\end{aligned}$$

By truncating at 6σ and using the proposed change of variables of [24], i.e.

$$\int_0^{\infty} f(u)\,\mathrm{d}u = \int_0^1 f\left(\frac{\mu}{1-\mu}\right) \frac{1}{(1-\mu)^2}\,\mathrm{d}\mu,$$

the integral transforms to

$$\begin{aligned}
\langle x^n E_x \rangle = K \int_{-6a_z}^{6a_z}\int_{-6a_y}^{6a_y}\int_{-6a_x}^{6a_x}\int_{0}^{1} & \frac{x^{n+1}}{(a_x^2+\frac{\mu}{1-\mu})^{3/2}\sqrt{(a_y^2+\frac{\mu}{1-\mu})(a_z^2+\frac{\mu}{1-\mu})}} \\
& \exp\left[-\frac{1}{2}\left(\frac{x^2}{\left(a_x^2+\frac{\mu}{1-\mu}\right)} + \frac{y^2}{\left(a_y^2+\frac{\mu}{1-\mu}\right)} + \frac{z^2}{\left(a_z^2+\frac{\mu}{1-\mu}\right)}\right)\right] \\
& \exp\left[-\frac{1}{2}\left(\frac{x^2}{a_x^2} + \frac{y^2}{a_y^2} + \frac{z^2}{a_z^2}\right)\right] \frac{1}{(1-\mu)^2}\,\mathrm{d}\mu\,\mathrm{d}x\,\mathrm{d}y\,\mathrm{d}z,
\end{aligned}$$

where

$$K = \frac{Q}{16\pi^3 \varepsilon_0 \operatorname{erf}\left[3\sqrt{2}\right]^3 a_x a_y a_z},$$

with error function (4.15). The single moments, i.e. $\langle x^n \rangle$, are given by

$$\langle x^n \rangle = \frac{1}{(2\pi)^{3/2} \operatorname{erf}\left[3\sqrt{2}\right]^3 a_x a_y a_z} \int_{-6a_z}^{6a_z} \int_{-6a_y}^{6a_y} \int_{-6a_x}^{6a_x} x^n \exp\left[-\frac{1}{2}\left(\frac{x^2}{a_x^2} + \frac{y^2}{a_y^2} + \frac{z^2}{a_z^2}\right)\right] \mathrm{d}x\,\mathrm{d}y\,\mathrm{d}z.$$

By reason of truncating at 6σ the normalization factor of the Gaussian distribution slightly changed, i.e. instead of

$$\int_{-\infty}^{\infty} \int_{-\infty}^{\infty} \int_{-\infty}^{\infty} \exp\left[-\frac{1}{2}\left(\frac{x^2}{a_x^2} + \frac{y^2}{a_y^2} + \frac{z^2}{a_z^2}\right)\right] \mathrm{d}x\,\mathrm{d}y\,\mathrm{d}z = (2\pi)^{3/2} a_x a_y a_z,$$

it is given by

$$\int_{-6a_z}^{6a_z} \int_{-6a_y}^{6a_y} \int_{-6a_x}^{6a_x} \exp\left[-\frac{1}{2}\left(\frac{x^2}{a_x^2} + \frac{y^2}{a_y^2} + \frac{z^2}{a_z^2}\right)\right] \mathrm{d}x\,\mathrm{d}y\,\mathrm{d}z = (2\pi)^{3/2} a_x a_y a_z \operatorname{erf}\left[3\sqrt{2}\right]^3,$$

where

$$\operatorname{erf}\left[3\sqrt{2}\right]^3 \approx 0.99999999408047414145 \approx 1.0000.$$

The corresponding computations are in Appendix G1.

D.2 Uniform Charge Distribution

The assumption of a uniform charge distribution, i.e. (4.17) with $\omega < 1$ only, leads to subsequent moment formulas:

$$\langle x^n E_x \rangle = \frac{Q}{128\varepsilon_0 a_x a_y a_z} \int_{-a_z}^{a_z} \int_{-a_y}^{a_y} \int_{-a_x}^{a_x} \int_0^{\infty} \frac{x^{n+1}}{(a_x^2+u)^{3/2}\sqrt{(a_y^2+u)(a_z^2+u)}} \mathrm{d}u\,\mathrm{d}x\,\mathrm{d}y\,\mathrm{d}z$$

$$\langle x^n \rangle = \frac{1}{8a_x a_y a_z} \int_{-a_z}^{a_z} \int_{-a_y}^{a_y} \int_{-a_x}^{a_x} x^n \,\mathrm{d}x\,\mathrm{d}y\,\mathrm{d}z.$$

Both equations are independent of the vertical and longitudinal direction, thus, each of these multidimensional integrals simplifies to a one-dimensional integration:

$$\begin{aligned}
\langle x^n E_x \rangle &= \frac{Q}{128\varepsilon_0 a_x a_y a_z} \int_0^{\infty} \frac{\mathrm{d}u}{(a_x^2+u)^{3/2}\sqrt{(a_y^2+u)(a_z^2+u)}} \int_{-a_x}^{a_x} x^{n+1}\,\mathrm{d}x \underbrace{\int_{-a_y}^{a_y} \mathrm{d}y}_{2a_y} \underbrace{\int_{-a_z}^{a_z} \mathrm{d}z}_{2a_z} \\
&= \frac{4Qa_y a_z}{128\varepsilon_0 a_x a_y a_z} \int_0^{\infty} \frac{\mathrm{d}u}{(a_x^2+u)^{3/2}\sqrt{(a_y^2+u)(a_z^2+u)}} \left[\frac{x^{n+2}}{n+2}\right]_{x=-a_x}^{x=a_x} \\
&= \frac{Q}{32\varepsilon_0 a_x} \frac{a_x^{n+2}(1-(-1)^{n+2})}{n+2} \int_0^{\infty} \frac{\mathrm{d}u}{(a_x^2+u)^{3/2}\sqrt{(a_y^2+u)(a_z^2+u)}} \\
&= \frac{Qa_x^{n+1}}{32\varepsilon_0(n+2)}(1-(-1)^{n+2}) \int_0^{\infty} \frac{\mathrm{d}u}{(a_x^2+u)^{3/2}\sqrt{(a_y^2+u)(a_z^2+u)}},
\end{aligned}$$

$$\langle x^n \rangle = \frac{1}{8a_x a_y a_z} \int_{-a_x}^{a_x} x^n \,\mathrm{d}x \underbrace{\int_{-a_y}^{a_y} \mathrm{d}y}_{2a_y} \underbrace{\int_{-a_z}^{a_z} \mathrm{d}z}_{2a_z} = \frac{1}{2a_x} \int_{-a_x}^{a_x} x^n \,\mathrm{d}x = \frac{1}{2a_x} \frac{x^{n+1}}{n+1} \Bigg|_{x=-a_x}^{x=a_x}$$

$$= \frac{a_x^n \left(1 - (-1)^{n+1}\right)}{2\,(n+1)}.$$

The former integral is up to the factor identical to Carlson's elliptic integral R_D [19]. By applying $[0, \infty[\mapsto [0, 1[$ as in Appendix D.1, we end up with

$$\langle x^n E_x \rangle = \frac{Q a_x^{n+1}}{32\varepsilon_0 (n+2)} (1 - (-1)^{n+2}) \int_0^1 \frac{\mathrm{d}\mu}{(a_x^2 + \frac{\mu}{1-\mu})^{3/2} \sqrt{(a_y^2 + \frac{\mu}{1-\mu})(a_z^2 + \frac{\mu}{1-\mu})}(1-\mu)^2},$$

$$\langle x^n \rangle = \frac{a_x^n}{2\,(n+1)} \left(1 - (-1)^{n+1}\right).$$

E Spherical Coordinates

The transformation from spherical to Cartesian coordinates defined in [27, p. 311] is given by

$$x = r\sin(\vartheta)\cos(\varphi), \qquad y = r\sin(\vartheta)\sin(\varphi), \qquad z = r\cos(\vartheta), \tag{E.1}$$

where $r \in [0, \infty[$, $\vartheta \in [0, \pi]$ and $\varphi \in [0, 2\pi[$. The Jacobian matrix is given by

$$J = \begin{pmatrix} \frac{\partial x}{\partial r} & \frac{\partial x}{\partial \vartheta} & \frac{\partial x}{\partial \varphi} \\ \frac{\partial y}{\partial r} & \frac{\partial y}{\partial \vartheta} & \frac{\partial y}{\partial \varphi} \\ \frac{\partial z}{\partial r} & \frac{\partial z}{\partial \vartheta} & \frac{\partial z}{\partial \varphi} \end{pmatrix} = \begin{pmatrix} \sin(\vartheta)\cos(\varphi) & r\cos(\vartheta)\cos(\varphi) & -r\sin(\vartheta)\sin(\varphi) \\ \sin(\vartheta)\sin(\varphi) & r\cos(\vartheta)\sin(\varphi) & r\sin(\vartheta)\cos(\varphi) \\ \cos(\vartheta) & -r\sin(\vartheta) & 0 \end{pmatrix}.$$

The determinant is then easily obtained to be

$$\begin{aligned} \det(J) = {} & \sin(\vartheta)\cos(\varphi) \cdot \begin{vmatrix} r\cos(\vartheta)\sin(\varphi) & r\sin(\vartheta)\cos(\varphi) \\ -r\sin(\vartheta) & 0 \end{vmatrix} \\ & - \sin(\vartheta)\sin(\varphi) \cdot \begin{vmatrix} r\cos(\vartheta)\cos(\varphi) & -r\sin(\vartheta)\sin(\varphi) \\ -r\sin(\vartheta) & 0 \end{vmatrix} \\ & + \cos(\vartheta) \cdot \begin{vmatrix} r\cos(\vartheta)\cos(\varphi) & -r\sin(\vartheta)\sin(\varphi) \\ r\cos(\vartheta)\sin(\varphi) & r\sin(\vartheta)\cos(\varphi) \end{vmatrix} \\ = {} & r^2\sin^3(\vartheta)\cos^2(\varphi) + r^2\sin^3(\vartheta)\sin^2(\varphi) + r^2\sin(\vartheta)\cos^2(\vartheta)\underbrace{\left(\cos^2(\varphi) + \sin^2(\varphi)\right)}_{=1} \\ = {} & r^2\sin(\vartheta)\left[\sin^2(\vartheta)\cos^2(\varphi) + \sin^2(\vartheta)\sin^2(\varphi) + \cos^2(\vartheta)\right] \\ = {} & r^2\sin(\vartheta)\underbrace{\left[\sin^2(\vartheta)\underbrace{\left(\cos^2(\varphi) + \sin^2(\varphi)\right)}_{=1} + \cos^2(\vartheta)\right]}_{=1} = r^2\sin(\vartheta). \end{aligned}$$

E.1 Spherical Gaussian

Assuming a spherical bunch, i.e. $a = a_x = a_y = a_z$, the Gaussian defined by (4.6) with (4.3) transforms to

$$\begin{aligned} f(r,\vartheta,\varphi) &= \frac{1}{(2\pi)^{3/2}a^3}\exp\left[-\frac{1}{2a^2}\left(r^2\sin^2(\vartheta)\cos^2(\varphi) + r^2\sin^2(\vartheta)\sin^2(\varphi) + r^2\cos^2(\vartheta)\right)\right] \\ &= \frac{1}{(2\pi)^{3/2}a^3}\exp\left[-\frac{1}{2a^2}\left(r^2\sin^2(\vartheta)\underbrace{\left[\cos^2(\varphi) + \sin^2(\varphi)\right]}_{1} + r^2\cos^2(\vartheta)\right)\right] \\ f(r,\vartheta) &= \frac{1}{(2\pi)^{3/2}a^3}\exp\left[-\frac{1}{2a^2}\left(r^2\underbrace{\left[\sin^2(\vartheta) + \cos^2(\vartheta)\right]}_{1}\right)\right] \\ f(r) &= \frac{1}{(2\pi)^{3/2}a^3}\exp\left[-\frac{r^2}{2a^2}\right], \end{aligned}$$

where (E.1) was applied.

F Lagrangian Derivatives

In this section we compute the derivatives (7.7) of the Lagrangian stated in (7.6) of Sec. 7.1. In a first step we calculate it with respect to the moment vector $\vec{x}_{s+L}$:

$$\begin{aligned}\frac{\partial \mathcal{L}}{\partial \vec{x}_{s+L}} &= \frac{\partial}{\partial \vec{x}_{s+L}} \left(\frac{1}{2} ||A\vec{x}_{s+L} - \vec{x}_s||_2^2 + \vec{\lambda}^\top \vec{g}\left(\vec{x}_{s+L}\right) \right) \\ &= \underbrace{\frac{1}{2} \frac{\partial}{\partial \vec{x}_{s+L}} ||A\vec{x}_{s+L} - \vec{x}_s||_2^2}_{①} + \underbrace{\frac{\partial}{\partial \vec{x}_{s+L}} \left(\vec{\lambda}^\top \vec{g}\left(\vec{x}_{s+L}\right) \right)}_{②}\end{aligned}$$

For the sake of clarity we treat those derivatives separately. The result of ① is

$$\begin{aligned}\frac{1}{2} \frac{\partial}{\partial \vec{x}_{s+L}} ||A\vec{x}_{s+L} - \vec{x}_s||_2^2 &= \frac{1}{2} \frac{\partial}{\partial \vec{x}_{s+L}} \left[\left(A\vec{x}_{s+L} - \vec{x}_s\right)^\top \left(A\vec{x}_{s+L} - \vec{x}_s\right) \right] \\ &= \frac{1}{2} \frac{\partial}{\partial \vec{x}_{s+L}} \left[\left(\vec{x}_{s+L}^\top A^\top - \vec{x}_s^\top\right) \left(A\vec{x}_{s+L} - \vec{x}_s\right) \right] \\ &= \frac{1}{2} \frac{\partial}{\partial \vec{x}_{s+L}} \left[\vec{x}_{s+L}^\top A^\top A \vec{x}_{s+L} - \vec{x}_{s+L}^\top A^\top \vec{x}_s - \vec{x}_s^\top A \vec{x}_{s+L} + \vec{x}_s^\top \vec{x}_s \right] \\ &= \frac{1}{2} \left[2A^\top A \vec{x}_{s+L} - 2A^\top \vec{x}_s \right] \\ &= A^\top A \vec{x}_{s+L} - A^\top \vec{x}_s.\end{aligned}$$

The second term ② with $\vec{\lambda} = (\lambda_0, \lambda_1, \lambda_2)^\top$ and (7.5) ($w = x, y, z$) yields

$$\begin{aligned}\frac{\partial}{\partial \vec{x}_{s+L}} \left(\vec{\lambda}^\top \vec{g}\left(\vec{x}_{s+L}\right) \right) &= \frac{\partial}{\partial \vec{x}_{s+L}} \left(\lambda_0 g_x(\vec{x}_{s+L}) + \lambda_1 g_y(\vec{x}_{s+L}) + \lambda_2 g_z(\vec{x}_{s+L}) \right) \\ &= \lambda_0 \nabla_{\vec{x}_{s+L}} g_x(\vec{x}_{s+L}) + \lambda_1 \nabla_{\vec{x}_{s+L}} g_y(\vec{x}_{s+L}) + \lambda_2 \nabla_{\vec{x}_{s+L}} g_z(\vec{x}_{s+L}) \\ &= \begin{pmatrix} \nabla_{\vec{x}_{s+L}} g_x(\vec{x}_{s+L}) \\ \nabla_{\vec{x}_{s+L}} g_y(\vec{x}_{s+L}) \\ \nabla_{\vec{x}_{s+L}} g_z(\vec{x}_{s+L}) \end{pmatrix}^\top \begin{pmatrix} \lambda_0 \\ \lambda_1 \\ \lambda_2 \end{pmatrix} \\ &= J_g^\top \vec{\lambda}.\end{aligned}$$

Hence, combining both calculations results in

$$\frac{\partial \mathcal{L}}{\partial \vec{x}_{s+L}} = A^\top A \vec{x}_{s+L} - A^\top \vec{x}_s + J_g^\top \vec{\lambda}.$$

The solution of the derivative of the Lagrangian with respect to $\vec{\lambda}$ is trivially given by

$$\frac{\partial \mathcal{L}}{\partial \vec{\lambda}} = \frac{1}{2} \underbrace{\frac{\partial}{\partial \vec{\lambda}} ||A\vec{x}_{s+L} - \vec{x}_s||_2^2}_{=0} + \frac{\partial}{\partial \vec{\lambda}} \vec{\lambda}^\top \vec{g}\left(\vec{x}_{s+L}\right) = \vec{g}(\vec{x}_{s+L}).$$

The derivatives of (7.5) are only non-zero for the moments of the form $\langle w^2 \rangle$, $\langle w p_w \rangle$ and $\langle p_w^2 \rangle$ with $w \in \{x, y, z\}$. Thus,

$$\frac{\partial g_w}{\partial \langle w^2 \rangle_{s+L}} = \frac{\langle p_w^2 \rangle}{2h_w}, \qquad \frac{\partial g_w}{\partial \langle w p_w \rangle_{s+L}} = \frac{-2 \langle w p_w \rangle}{2h_w} = \frac{-\langle w p_w \rangle}{h_w}, \qquad \frac{\partial g_w}{\partial \langle p_w^2 \rangle_{s+L}} = \frac{\langle w^2 \rangle}{2h_w},$$

with

$$h_w = \sqrt{\langle w^2 \rangle \langle p_w^2 \rangle - \langle w p_w \rangle^2}. \tag{F.1}$$

By taking the second derivative of (7.5) with respect to $\vec{x}_{s+L}$ we obtain the non-zero entries — while omitting the Lagrange multipliers — of the Hessian $H_g(\vec{x}_{s+L}, \vec{\lambda})$ in (7.12):

$$\frac{\partial^2 g_w}{\partial \langle w^2 \rangle^2} = -\frac{\langle p_w^2 \rangle^2}{4h_w^3}, \qquad \frac{\partial^2 g_w}{\partial \langle p_w^2 \rangle \partial \langle w^2 \rangle} = \frac{1}{2h_w} - \frac{\langle w^2 \rangle \langle p_w^2 \rangle}{4h_w^3}, \qquad \frac{\partial^2 g_w}{\partial \langle w p_w \rangle \partial \langle w^2 \rangle} = \frac{\langle p_w^2 \rangle \langle w p_w \rangle}{2h_w^3},$$

$$\frac{\partial^2 g_w}{\partial \langle p_w^2 \rangle^2} = -\frac{\langle w^2 \rangle^2}{4h_w^3}, \qquad \frac{\partial^2 g_w}{\partial \langle w p_w \rangle^2} = -\frac{1}{h_w} - \frac{\langle w p_w \rangle^2}{h_w^3}, \qquad \frac{\partial^2 g_w}{\partial \langle w p_w \rangle \partial \langle p_w^2 \rangle} = \frac{\langle w^2 \rangle \langle w p_w \rangle}{2h_w^3},$$

where h_w defined by (F.1) was used again. All these derivatives are computed in Appendix G9.

G Scripts and Source Codes

All data, plotting scripts and other programs that are used in this thesis are stored in a repository. It also contains most of the employed literature. In order to get access, please contact Dr. A. Adelmann (andreas.adelmann@psi.ch).
In this section we only itemize some of the programs. In the subsequent list are the filenames of the *Mathematica* [26] scripts on which we refer in the text:

G1 *code/tools/Mathematica-Scripts/GaussianNormalization.nb*

G2 *code/tools/Mathematica-Scripts/Allen.nb*

G3 *code/tools/Mathematica-Scripts/EFieldSphericalGaussian.nb*

G4 *code/tools/Mathematica-Scripts/FieldEnergyUniform.nb*

G5 *code/tools/Mathematica-Scripts/LinearMatchingPolynomials.nb*

G6 *code/tools/Mathematica-scripts/LinearSystemOfEquations.nb*

G7 *code/tools/Mathematica-Scripts/PhysicalSymbolsAndUnits.nb*

G8 *code/tools/Mathematica-Scripts/Carlson.nb*

G9 *code/tools/Mathematica-Scripts/DerivativeLagrangianConstraints.nb*

The full C++ source codes of the shown code fragments and computations for the figures are given in the following files:

G10 *code/tests/testMapGenerator.cpp*

G11 *code/tests/testEllipticIntegral.cpp*

G12 *code/tests/testRuntime.cpp*

G13 *code/tests/testParallelCubature.cpp*

G14 *code/tests/testAllen.cpp*

G15 *code/tests/testChargeDistribution.cpp*

G16 *code/tests/testElectricField.cpp*

G17 *code/tests/testFieldEnergy.cpp*

G18 *code/tests/testTracking.cpp*

G19 *code/tests/testDrift.cpp*

G20 *code/include/SigmaGenerator.h*

The scripts of Fig. 2.1 and Fig. 4.3 are

G21 *code/tools/R-Scripts/NumberOfMoments.R*

G22 *code/tools/R-Scripts/GaussianDistribution.R*

Bibliography

[1] R. D. Ryne. Finding matched rms envelopes in rf linacs: A hamiltonian approach. 1995. Submitted on 12.02.1995, http://arxiv.org/abs/acc-phys/9502001.

[2] M. Venturini and M. Reiser. Rms envelope equations in the presence of space charge and dispersion. *Phys. Rev. Lett.*, **81**:96–99, July 1998.

[3] C. Baumgarten. Transverse-longitudinal coupling by space charge in cyclotrons. *Phys. Rev. ST Accel. Beams*, **14**:114201, Nov 2011.

[4] C. Baumgarten. Geometrical method of decoupling. *Phys. Rev. ST Accel. Beams*, **15**:124001, Dec 2012.

[5] R. L. Gluckstern. Scalar potential for charge distributions with ellipsoidal symmetry. Fermilab Internal Report TM-1402, http://inspirehep.net/record/231017/files/, May 1986.

[6] C. K. Allen. *Image Effects and Optimal Control of Space-Charge Dominated Particle Beams*. PhD thesis, University of Maryland, 1996. Order of copy at http://wwwlib.umi.com/dissertations/fullcit?p9707562.

[7] M. Frey. Matched distributions in cyclotrons, 2015. ETH Zurich Semester thesis, http://amas.web.psi.ch/people/aadelmann/ETH-Accel-Lecture-1/projectscompleted/cse/frey-semester_thesis.pdf.

[8] F. Hinterberger. *Physik der Teilchenbeschleuniger und Ionenoptik*. Springer-Verlag Berlin Heidelberg, 2. edition, 2008. ISBN: 978-3-540-75281-3.

[9] M. Berz. Differential algebraic description of beam dynamics to very high orders. *Part. Accel.*, **24**:109–124, 1989. http://inspirehep.net/record/260823/files/.

[10] M. Berz. *Modern Map Methods in Particle Beam Physics*. Academic Press, 1999. ISBN: 0-12-014750-5, http://bt.pa.msu.edu/pub/papers/AIEP108book/AIEP108book.pdf.

[11] A. J. Dragt. Lie methods for nonlinear dynamics with applications to accelerator physics. Version of 26th July 2012, Current version at http://www.physics.umd.edu/dsat/dsatliemethods.html.

[12] A. J. Draft, F. Neri, G. Rangarajan, D. R. Douglas, L. M. Healy, and R. D. Ryne. Lie algebraic treatment of linear and nonlinear beam dynamics. *Annual Review of Nuclear and Particle Science*, **38**(1):455–496, 1988. http://www.annualreviews.org/doi/abs/10.1146/annurev.ns.38.120188.002323.

[13] J. D. Jackson. *Classical Electrodynamics*. Wiley, 3. edition, 1999. ISBN: 9971-512-50-5.

[14] L. Greengard and V. Rokhlin. A fast algorithm for particle simulations. *Journal of Computational Physics*, **73**(2):325–348, 1987. http://www.sciencedirect.com/science/article/pii/0021999187901409.

[15] L. Greengard and V. Rokhlin. A new version of the fast multipole method for the laplace equation in three dimensions. *Acta Numerica*, **6**:229–269, January 1997. http://journals.cambridge.org/article_S0962492900002725.

[16] H. Zhang and M. Berz. The fast multipole method in the differential algebra framework. *Nuclear Instruments and Methods in Physics Research Section A: Accelerators, Spectrometers, Detectors and Associated Equipment*, **645**(1):338–344, 2011. The Eighth International Conference on Charged Particle Optics, http://www.sciencedirect.com/science/article/pii/S0168900211001318.

[17] O. D. Kellogg. *Foundations of Potential Theory*. Springer-Verlag, 1967. ISBN-13: 978-3-642-86750-7, Reprint from the first edition of 1929.

[18] M. Abramowitz and I. A. Stegun. *Handbook of Mathematical Functions With Formulas, Graphs, and Mathematical Tables*. National Bureau of Standards - U.S. Government Printing Office, 1972. Tenth Printing.

[19] B. C. Carlson. A table of elliptic integrals of the second kind. *Mathematics of Computation*, **49**(180):595–606, October 1987. http://www.ams.org/journals/mcom/1987-49-180/S0025-5718-1987-0906192-1/.

[20] The Boost C++ Libraries, May 2015. http://www.boost.org/.

[21] GSL GNU Scientific Library, May 2015. http://www.gnu.org/software/gsl/gsl.html.

[22] A. Adelmann. Particle accelerator physics & modeling 1. In *Lecture 8: Distributions and Linear Space Charge 2*, November 2013. Lecture at ETH Zurich, Contact: andreas.adelmann@psi.ch.

[23] F. J. Sacherer. Rms envelope equations with space charge. *Nuclear Science, IEEE Transactions on*, **18**(3):1105–1107, June 1971.

[24] S. G. Johnson. Cubature (multi-dimensional integration), May 2015. http://ab-initio.mit.edu/wiki/index.php/Cubature, Last revised: 07.11.2014.

[25] V. Markushin. Local hpc user guide for merlin4 cluster. PSI Intranet, September 2015. https://intranet.psi.ch/PSI_HPC/LocalHpcUserGuide, Last revised: 22.09.2015, Version 118, Contact: valeri.markushin@psi.ch.

[26] Inc. Wolfram Research. *Mathematica*. Wolfram Research, Inc., Champaign, Illinois, 2012. Version 9.0.

[27] H. Stöcker. *Taschenbuch mathematischer Formeln und moderner Verfahren*. Verlag Harri Deutsch, 2. edition, 1993. ISBN: 3-8171-1256-4.

[28] M. F. Reusch and D. L. Bruhwiler. High-order space charge effects using automatic differentiation. *AIP Conference Proceedings*, **391**(1):179–184, 1997. http://scitation.aip.org/content/aip/proceeding/aipcp/10.1063/1.52340.

[29] S. B. Provost. Moment-based density approximants. *The Mathematica Journal*, **9**, 2005. http://www.mathematica-journal.com/issue/v9i4/DensityApproximants.html.

[30] C++ reference, September 2015. http://en.cppreference.com/w/cpp/language/lambda, Last revised: 03.09.2015.

[31] A. Adelmann. Particle accelerator physics & modeling 1. In *Lecture 4: Basic Building Blocks of an Accelerator in the linear Approximation*, October 2013. Lecture at ETH Zurich, Contact: andreas.adelmann@psi.ch.

[32] C. Blatter. *Ingenieur Analysis*, chapter 4-6. ETH Zurich, 2004. Studiengänge Informationstechnologie, Elektrotechnik und Informatik, Download version of 2002 at `https://people.math.ethz.ch/~blatter/dlp.html`.